Spontaneously active networks in the outer and inner degenerated *rd10* retina

Dissertation

Zur Erlangung des Grades eines

Doktors der Naturwissenschaften

der Mathematisch-Naturwissenschaftlichen Fakultät

und

der Medizinischen Fakultät

der Eberhard-Karls-Universität Tübingen

vorgelegt

von

Prerna Srivastava

Aus Mankapur, India

February 2020

Tag der mündlichen Prüfung: July 13th, 2020

Dekan der Math.-Nat. Fakultät: Prof. Dr. W. Rosenstiel

Dekan der Medizinischen Fakultät: Prof. Dr. I. B. Autenrieth

1. Berichterstatter: Prof. Dr. Thomas Euler

2. Berichterstatter: Prof. Dr. Aristides Arrenberg

Prüfungskommission: Prof. Dr. Thomas Euler

Prof. Dr. Aristides Arrenberg

Prof. Dr. Bernd Wissinger

Dr. Günther Zeck

Erklärung / Declaration:

Ich erkläre, dass ich die zur Promotion eingereichte Arbeit mit dem Titel:

"**Spontaneously active networks in the outer and inner degenerated *rd10* retina**"

selbständig verfasst, nur die angegebenen Quellen und Hilfsmittel benutzt und wörtlich oder inhaltlich übernommene Stellen als solche gekennzeichnet habe. Ich versichere an Eides statt, dass diese Angaben wahr sind und dass ich nichts verschwiegen habe. Mir ist bekannt, dass die falsche Abgabe einer Versicherung an Eides statt mit Freiheitsstrafe bis zu drei Jahren oder mit Geldstrafe bestraft wird.

*I hereby declare that I have produced the work entitled "**Spontaneously active networks in the outer and inner degenerated rd10 retina**", submitted for the award of a doctorate, on my own (without external help), have used only the sources and aids indicated and have marked passages included from other works, whether verbatim or in content, as such. I swear upon oath that these statements are true and that I have not concealed anything. I am aware that making a false declaration under oath is punishable by a term of imprisonment of up to three years or by a fine.*

Tübingen, den 07.09.2020 ..... Prerna. .....

Datum / Date Unterschrift /Signature

Contents

1. List of figures

2. Tables

3. Abbreviations

AAV	adeno-associated virus
Aβ	amyloid-β
AC	amacrine cell
ACF	autocorrelation function
AD	Alzheimer's disease
AMPA	α-amino-3-hydroxy-5-methyl-4-isoxazolepropionic acid
AP5	2-amino-5-phosphonopentanoic acid
AP4	L-2-amino-4-posphonobutyric acid
BC	bipolar cell
BP	band pass
Ca^{2+}	calcium ion
CBC	cone bipolar cell
cGMP	cyclic guanosine monophosphate
Cl^-	chloride ion
CMOS	complementary metal-oxide semiconductor
CNS	central nervous system
CRISPR	clustered regularly interspaced short palindromic repeats
DAC	dopaminergic amacrine cell
DMSO	dimethyl sulfoxide
DTFT	discrete time Fourier transform
EAAT	excitatory amino acid transporter
EEG	electroencephalography
EM	electron microscopy
ETL	electrically tunable lens
fMRI	functional magnetic resonance imaging
GABA	gamma-aminobutyric acid
GAM	generalized additive model
GCL	ganglion cell layer
HC	horizontal cell

iAC	interplexiform amacrine cell
iGluSnFR	intensity-based glutamate sensing fluorescent reporter
I_h	hyperpolarization-activated current
I_{NaP}	persistent sodium current
INL	inner nuclear layer
IPL	inner plexiform layer
K^+	potassium ion
KS test	Kolmogorov-Smirnov test
LGN	lateral geniculate nucleus
MEA	micro-electrode array
MEG	magnetoencephalography
mGluR	metabotropic glutamate receptor
Na^+	sodium ion
NBQX	2,3-dioxo-6-nitro-1,2,3,4-tetrahydrobenzo[f]quinoxaline-7-sulfonamide
NFL	nerve fiber layer
NMDA	N-methyl-D-aspartate
OGB-1	Oregon green 488 BAPTA-1
ONL	outer nuclear layer
OPL	outer plexiform layer
P	postnatal day
PD	Parkinson's disease
PDE	phosphodiesterase
PKC	protein kinase C
PMT	photomultiplier tube
PSD	power spectral density
RBC	rod bipolar cell
RCS	Royal College of Surgeons rat model
rd	retinal degeneration
rd1	retinal degeneration 1 mouse model
rd10	retinal degeneration 10 mouse model
RGC	retinal ganglion cell

ROI	regions of interest
RP	retinitis pigmentosa
sd	standard deviation
SAC	starburst amacrine cell
SARFIA	semi-automated routines for functional image analysis
SC	superior colliculus
SNR	signal-to-noise ratio
SR101	sulforhodamine 101
TRPM	transient receptor potential receptor M subfamily
TTX	tetrodotoxin
UBP-310	(S)-1-(2-amino-2-carboxyethyl)-3-(2-carboxy-thiophene-3-yl-methyl)-5-methylpyrimidine-2,4-dione
VGCC	voltage-gated Ca^{2+} channels
VGluT1	vesicular glutamate transporter 1
WM	whole-mount

4. Abstract

Interaction between spontaneously active networks is prominently present in the central nervous system (CNS). Network interaction at both local and global levels mediates communication across different regions and thus, plays a crucial role in the brain's physiology (Andrews-Hanna et al., 2010; Oswald et al., 2017). Alterations in the network dynamics have been designated as a hallmark of neuronal dysfunction in various neurodegenerative diseases (Palop et al., 2007; Xu et al., 2015; Wang et al., 2017), signifying their relevance in clinical applications. However, these network activities that seem to be a suitable therapeutic target require a complete understanding towards it at a cellular level, which is still lacking.

Similar to other neurological diseases, in a majority of retinal diseases, such as Retinitis Pigmentosa (RP), the degeneration and subsequent loss of photoreceptors generates enhanced spontaneous signals in several retinal neurons (Trenholm et al., 2012; Biswas et al., 2014; Haq et al., 2014). The degenerated retina is thought to form spontaneously active networks in the outer and inner retina (reviewed in Euler and Schubert, 2015). Because these networks were studied only in isolation, it is still unclear whether and how these interact. But since the networks are structurally connected via bipolar cells (BCs), they may modulate each other.

Here, we used the primary rod degeneration *rd10* mouse model, to investigate the interaction between spontaneously active networks at both somatic and synaptic levels. We established a method of dual recordings to record somatic calcium (Ca^{2+}) signals from the neuronal population in the outer and inner retina using two-photon microscopy. Signal dynamics between the networks displayed spatio-temporal variability, however, the signals became similar in the later degeneration phase. We further assessed the interaction at the synaptic level and examined the role of BCs as potential linking neurons by implementing a vertical imaging technique. This allowed us to record near-simultaneous spontaneous glutamate release at the BC dendrites and axon terminals at the outer (OPL) and inner plexiform layers (IPL), respectively. Disconnecting outer and inner retinal networks by blocking glutamatergic input at the BC dendrites, drastically affected inner retinal signals suggesting that the inner retinal network is largely modulated by the outer retinal signals, most likely via BCs. Finally, our data also revealed the existence of multiple correlated active clusters which might reflect the presence of parallel pathways involved in the generation and propagation of spontaneously active networks in the degenerated retina.

5. Introduction

5.1 Spontaneous activity in the CNS

One of the characteristic features of the CNS is the presence of spontaneous activity in the neuronal population. Unlike evoked activity, which is generated in response to an external task or stimulus, spontaneous activity is the property displayed by neurons in the absence of any stimulus. In the past, scientists have largely focused on studying task-evoked responses. However, currently, many studies have turned their attention towards understanding the physiological significance of the spontaneous activity. It has always been controversial to consider this activity either as a source of 'noise' or connect it with some functional relevance. But the fact that the activity is conserved across species even after utilizing a higher intake of energy as compared to task-related responses (reviewed in Raichle and Mintun, 2006) suggests it's importance in the brain's physiology. Recently, it was revealed that the activity of the brain present during its resting state actually reflects its functional architecture (Biswal et al., 2010). Raichle and colleagues (2001) also defined this resting state activity of the brain as its 'default mode'. The role of spontaneous activity has also been widely described over different developing nervous systems such as the retina, cortex, hippocampus and spinal cord where it plays a crucial role in synapse formation, maturation, and wiring of the neuronal circuits (Milner and Landmesser, 1999; Leinekugel et al., 2002; Khazipov et al., 2004; Sun and Luhmann, 2007; Soto et al., 2012). Interestingly, the spontaneous activity even persists after the development but here it is involved in the brain's important functions such as memory and cognition (Wang et al., 2008; Andrews-Hanna et al., 2010; Oswald et al., 2017).

5.1.1 Generation of spontaneous activity in neurons

At the single cell level, neurons can exhibit different temporal patterns of spontaneous activities. These activities can either be generated in the form of fast spontaneous firing of action potentials which sometimes can appear as bursts or in the form of slow frequency oscillations. The spontaneous activity of a neuron actually reflects its intrinsic ability due to its inherent membrane properties. The generation of the activity requires interaction between ionic currents that could

depolarize and hyperpolarize the membrane at subthreshold potentials (reviewed in Llinás, 1988). In general, any instability in the neuron that might result in its hyperpolarization could activate ionic currents like hyperpolarization-activated current (I_h). This could, in turn, lead to the activation of low-threshold Ca^{2+} currents that further depolarizes the membrane and generates a low-threshold Ca^{2+} spike. This could activate voltage-gated sodium (Na^+) channels resulting in an inward current triggering spontaneous bursts of spikes. Further influx of Ca^{2+} could activate an outward Ca^{2+} mediated potassium (K^+) current due to the opening of voltage-gated K^+ channels and thus, leading to membrane repolarization. Many neurons, such as pacemaker neurons, exhibit an interplay between voltage-dependent ionic currents such as persistent Na^+ current (I_{NaP}), I_h, Ca^{2+} or K^+ currents that allows generation of oscillatory activity between them (reviewed in (Perez-Reyes, 2003; Harris-Warrick, 2002)). For example, oscillations can arise in neurons such as AII amacrine cells (ACs) as a result of interaction between fast depolarizing Na^+ current and slow hyperpolarizing K^+ current (Choi et al., 2014). Hyperpolarization could also induce oscillations in some neurons such as OFF retinal ganglion cells (RGCs) due to the activation of I_{NaP} current (Margolis and Detwiler, 2007). These changes in the membrane potential that arise as a result of interaction between different currents can be recorded either as large membrane fluctuations using various electrophysiological techniques or as small Ca^{2+} transients through Ca^{2+} imaging.

5.1.2 Spontaneously active networks in developing and mature nervous systems

As already mentioned at the beginning of this introduction, spontaneous activity is not restricted to the level of an individual neuron. Instead, many neurons synchronize their activity, forming networks. This has been well described in the developing visual system and particularly in the retina, where, for example, during a specific phase in retinal development, RGCs display bursts of action potentials and can also synchronize their activity with other neighboring neurons (Meister et al., 1991). Correlated network activities in retinal neurons can interact at a large-scale, forming a wave-like pattern and thus can travel across the retina (Feller et al., 1996), promoting synaptogenesis (Soto et al., 2012) (see also 5.1.3). The retinal waves can also propagate to the higher visual centers of the brain like superior colliculus (SC), primary visual cortex and lateral geniculate nucleus (LGN), where they are involved in the organization of retinotopic maps and

eye-specific segregation (reviewed in Torborg and Feller, 2005; Xu et al., 2011; Ackman et al., 2012; Zhang et al., 2012; Akrouh and Kerschensteiner, 2013). Similar to the visual system, spontaneous network activity in the developing hippocampus, cortex, and spinal cord have also been inferred to contribute in the development and maturation of circuitry (Corlew et al., 2004; Khazipov et al., 2004; reviewed in Hanson et al., 2008; Winnubst et al., 2015).

Spontaneous network activity also exists in the mature (healthy) nervous system. Synchronized network activity has been reported in both mature cortical and hippocampal neurons (Mazzoni et al., 2007; Takahashi et al., 2010, Penn et al., 2016). Interestingly, the activity generated at a local area can interact with other networks across different brain regions, mediating large-scale communication. This became, for instance, evident in a study where network interactions have been demonstrated by strong coupling between CA1 and CA3 hippocampal neurons (Both et al., 2008). Slow spontaneous oscillations in cortical neurons present during sleep have also been shown to be correlated with the oscillations present in the thalamic region (Steriade et al., 1993; Rothschild et al., 2017). Similarly, interactions among network associated with developed primary visual areas have also been reported (Wang et al., 2008). The coordinated activity of the mature neuronal population can give rise to specific patterns with specific frequencies. Hence, it can be classified based on the dominant frequency band, namely: delta, theta, alpha, beta, and gamma. These activity patterns are easily detectable in humans and can be measured using various diagnostic tools like electroencephalography (EEG) and magnetoencephalography (MEG). Another neuroimaging technique called functional magnetic resonance imaging (fMRI) overcomes the restriction of poor spatial resolution in EEG and MEG, thereby allowing investigation of long-range networks with more structural information. Using these techniques, slow oscillations developed during sleep have been shown to be involved in memory processing (Wei et al., 2018). In addition to this, correlated spontaneous activity recorded from distinct brain regions has been demonstrated to be linked with working memory, learning, and other cognitive tasks (Andrews-Hanna et al., 2010; Oswald et al., 2017).

5.1.3 Mechanisms underlying network interactions

As mentioned earlier, spontaneous activity of a particular neuron underlies its intrinsic property (see 5.1.1). The generation of spontaneous network activity, on the other hand, relies on the interaction between intrinsic membrane properties and synaptic mechanisms. In the developing visual system, where spontaneous network activity propagates across the retina in the form of waves (see 5.1.2), this wave-like activity actually exhibits three different phases. Each phase is mediated by different synaptic mechanisms, serving specific functions for the organization of the visual circuitry (reviewed in (Wong, 1999; Firth et al., 2005)). During embryonic development until postnatal day (P) 1, spontaneous bursts of activity generated in the RGCs propagate among neighboring neurons through the gap-junction coupling. However, between P1 and P10, cholinergic retinal waves emerge when the connections develop between cholinergic ACs for e.g., starburst amacrine cells (SACs) with other SACs or RGCs. These waves can be initiated as spontaneous depolarizations of SACs, which can then spread across the retina through excitatory synaptic connections, probably due to the volume release of acetylcholine (Ford et al., 2012). Later in the development, between P10 and P14, glutamatergic waves come into play and contribute to the development of the synapses between BCs and RGCs (reviewed in Kerschensteiner, 2016). These glutamatergic waves are thought to be generated in the BCs and propagated across the retina through glutamate release (Wong et al., 2000; Firl et al., 2013). The initiation of the activity in the BCs as a result of spontaneous depolarization can further lead to the depolarization of AII ACs which could subsequently generate anti-correlated activity between ON and OFF-RGCs through synaptic inhibition (Akrouh and Kerschensteiner, 2013; Firl et al., 2015). Additionally, glutamatergic waves can also recruit ON and OFF segregation at the higher visual centers (Kerschensteiner and Wong, 2008).

Similar to the visual system, wave-like correlated activity can also be found in the developing cerebellum which relies on depolarizing GABA mediated synaptic transmission (Watt et al., 2009). In mature neurons, GABA is an inhibitory neurotransmitter that inhibits the excitability of the neuron by activating chloride ion (Cl^-) channels. As the concentration of the Cl^- is lower inside the cell, activation of these channels causes an influx of Cl^- leading to membrane hyperpolarization. However, during neuronal development, the immature neurons exhibit a higher intracellular concentration of Cl^- due to undergoing changes in the Cl^- transporter expression. The activation of

GABA receptors, in this case, causes diffusion of Cl^- outside the cell further leading to membrane depolarization. Therefore, during the development stage, GABA exhibits excitatory properties. Depolarizing GABA mediated oscillations are also involved in the network activity present in the developing hippocampus (Garaschuk et al., 1998). However, unlike hippocampal neurons, network activity in the developing cortical neurons depends mainly on glutamatergic synapses (Garaschuk et al., 2000).

In mature CNS, spontaneous network interactions rely on the combination of intrinsic and synaptic mechanisms. This has been demonstrated, for example, in the cortical neurons, where synchronization among the neuronal population can be mediated by both intrinsic mechanisms via I_h/I_{NaP} current, and through glutamatergic synaptic transmission (Mao et al., 2001). Moreover, a precise balance between synaptic excitation and inhibition as mediated by glutamate and GABA receptors, respectively, is required for the interactions between spontaneously active networks (Haider et al., 2006; Mazzoni et al., 2007). A stable balance between recurrent excitations that leads to membrane depolarization followed by rapid feedback inhibition via GABAergic neurons causing hyperpolarization of the membrane underlies the mechanism of spontaneous activity. Finally, gap junction coupling can also contribute to the synchronization and spread of the activity in the network (Draguhn et al., 1998; Maier et al., 2003). Taken together, a dynamic interaction between intrinsic and synaptic mechanisms is required for the initiation, maintenance, and propagation of spontaneous network activity.

5.1.4 Alterations in the spontaneous activity during neurodegenerative diseases

Neurodegenerative diseases result in the disruption of various cellular and molecular pathways and changes in the synaptic connectivity, thus affecting normal physiology and functional connectivity of the brain. As spontaneous activity plays a key role in the brain's crucial function, it is to be expected that they are also severely altered during various pathological conditions such as Parkinson's disease (PD), Alzheimer's disease (AD), epilepsy and Schizophrenia.

Alterations in Parkinson's disease

PD is marked by the death of dopaminergic neurons of the substantia nigra of the basal ganglia in the brain. The dopaminergic neurons release dopamine that plays a role in transmitting signals to the brain regions controlling movement and coordination (Panigrahi et al., 2015, Dodson et al., 2016). Therefore, the degeneration of these neurons also causes a decrease in overall dopamine release (Bernheimer et al., 1973), which then leads to movement disorders in the patients. Interestingly, these neurons also fire spontaneously even in the absence of any synaptic input, which is thought to be associated with the release of the dopamine (Gonon, 1988). In many PD patients, the slow frequency spontaneous activities have been shown to be altered in the basal ganglia and other associated brain areas such as globus pallidus (Hou et al., 2014; Xiang et al., 2016). Several primate models of PD also show aberrant spontaneous activities in the regions of basal ganglia, thalamus and cortex (Filion and Tremblay, 1991; Magnin et al., 2000; Wang et al., 2017; Du et al., 2018). The dopaminergic neurons of the substantia nigra receive GABAergic inputs from different parts of the basal ganglia including globus pallidus (reviewed in Bergman et al., 1998). As a result, a decrease in dopamine release leads to reduced activity of the globus pallidal neurons and thus, reduced GABAergic output to its respective targets. Deafferentation of dopaminergic neurons also leads to enhanced synchronized activity in the globus pallidus further contributing to the tremor symptom in the disease (Nini et al., 1995; Raz et al., 2005). Additionally, PD pathophysiology has also been found to be associated with an increase in the synchronization of spontaneous firing among neurons in the subthalamic nuclei (Levy et al., 2000).

Alterations in Alzheimer's disease

Another common neurodegenerative disease is AD, which is characterized by neuronal degeneration and accumulation of amyloid-β (Aβ) peptides in the brain, resulting in memory and cognition deficit. Alterations in oscillation frequencies have been reported in AD patients (Czigler et al., 2008). Specifically, it was found that the neurons which are particularly present near Aβ plaque deposits display enhanced spontaneous activity (Busche et al., 2008; Busche et al., 2012). Aβ peptides can also cause an imbalance between synaptic excitation and inhibition which could, in turn, induce elevated synchronization (hypersynchronization) in the hippocampal and cortical neuronal network, making functional connectivity of the system highly unstable (Palop et al., 2007). Furthermore, dysfunction of GABAergic inhibition probably due to synaptic remodeling of

GABAergic neurons also underlies abnormal spontaneous firing patterns in the network (Palop et al., 2007; Busche et al., 2008).

Alterations in Epilepsy

Epilepsy is also a commonly studied neurological disorder associated with abnormal brain activity. Often epileptic activity is associated with other neurodegenerative diseases. The epileptic condition typically represents elevated synchronization between the activities in the neuronal population that generates seizure like activity (reviewed in Margineanu, 2010; Jiang et al., 2016). Consistent with other neurological diseases, any disparity in the proportion of excitation and inhibition could generate this condition. For example, in neocortical slices obtained from epileptic patients, it was demonstrated that the enhanced synchrony among the neuronal networks can be an outcome of overexcitation, possibly due to an increase in the number of excitatory synapses (Tóth et al., 2018). GABAergic inhibition also contributes to hypersynchrony, in this case, was mostly mediated by glutamatergic signaling (Tóth et al., 2018). In addition to this, gap junction coupling may also underlie neural synchronization in epileptic neurons (Ross et al., 2000).

Alterations in other pathological disorders

Alterations in spontaneous network activities are also present in various brain regions of schizophrenic patients (Xu et al., 2015) and have been shown to be associated with reduced GABAergic inhibition (Gisabella et al., 2005). Interestingly, these changes in the correlation of the network activities have been linked with hallucinations reported by the patients (Gao et al., 2015; reviewed in Northoff and Duncan, 2016). Also, in Huntington's disease, abnormal spontaneous spiking generated due to disrupted GABAergic signaling was demonstrated in hippocampal neurons (Dargaei et al., 2018).

Alterations in spontaneous activity is also a characteristic feature of diseased sensory systems such as auditory and visual system. Hearing disorders are often accompanied by a discomforting symptom called tinnitus which is a perception of sound even in the absence of any stimulus. Abnormal frequency fluctuations in the auditory cortex and other linked brain areas are found in the tinnitus patients (Leaver et al., 2011; Chen et al., 2014; Chen et al., 2015). This phenomenon is also associated with alterations in the organization of tonotopic maps in the auditory cortex (Rajan et al., 1993; Mühlnickel et al. 1998). Even at the cellular level, auditory nerve fibers display

an increased rate of spontaneous firing following acoustic injury (Liberman, 1978; Noreña and Eggermont, 2003). Similar hyperactivity was also reported in auditory cochlear nuclei in a tinnitus mouse model, where it was demonstrated that the down-regulation in GABAergic inhibition underlies this enhanced activity (Middleton et al., 2011). Hallucinations related to visual perceptions are also common in patients suffering from retinal degeneration. Recently, direct evidence has been provided confirming the role of hyperactivity in triggering this symptom in patients of age-related macular degeneration (Painter et al., 2018). Even in many retinal degenerated (*rd*) animal models, aberrant activity has been prominently reported in several retinal neurons (reviewed in Euler and Schubert, 2015) (see 5.4.4) and in the primary visual cortex (V1) and SC (Dräger and Hubel, 1978; Ivanova et al., 2016a; Wang et al., 2018a) (see 5.4.9). Altogether, it can be concluded that any discrepancy in the spatio-temporal properties of the spontaneous network dynamics could affect brain function, thus making it a very relevant field for further investigation in neurodegenerative diseases.

5.1.5 Strengths and limitations of the non-invasive studies

Based on the fact that the abnormalities in spontaneously active networks are associated with a majority of neurodegenerative diseases, studies have been made to use them for diagnostic purposes. Changes in the dynamics of these network activities have been widely used now as a potential marker for detecting signs of the diseases (reviewed in (Buckner et al., 2008; Fox and Greicius, 2010; Zhou et al., 2010)). Until now, aberrant network activities have mostly been used as a biomarker for the diseases although they could also be one of the possible targets for therapeutic treatment. Several drugs are being developed for the suppression of the hyperactivity to improve cognition in patients (Bakker et al., 2012; Plata et al., 2013). Currently, several modifications are being made in a variety of techniques like EEG, MEG, and fMRI to make them more efficient and informative, to enable earlier disease detection, and to render them more comfortable for the patients (Al-Jumeily et al., 2015; Wang et al., 2015; Wang et al., 2018b). Even though most of these neuroimaging methods are non-invasive and very reliable way of assessing neurological diseases in the patients, they usually can only detect the sum activity of whole circuits. As a result, while they can be used to interpret the changes in the functional connectivity over

different regions of the brain, they do not provide detailed information regarding the anatomical or functional changes at a cellular level. However, the successful implementation of any pharmacological therapy requires a better understanding of the interaction between the networks at both the cellular level and synaptic level, which is still lacking.

These limitations may be overcome by exploiting various electrophysiological techniques such as single or multi-unit recordings, that have high spatial resolution and thus could help in deciphering the functional connectivity at the cellular level. However, these techniques have their drawbacks too. First, these are invasive and require complicated surgical procedures as compared to the non-invasive imaging tools like fMRI and EEG. And, second, due to the limited size of the recorded field, these techniques can only help in identifying the interactions among local circuits but would fail to unravel the interaction between large-scale networks over vast regions of the brain.

5.2 Looking into the brain through the retina

The retina is considered as a “window to the brain” not only because it is an extended part of the brain, but as many findings in the retina can be directly linked to the function of the other regions of the CNS (reviewed in London et al., 2013). This is also evident from the fact that several neurodegenerative diseases can have a component that leads to retinal dysfunction. The anatomy and functional connectivity of the retina is comparable to the brain. However, the less intricate structure of the retina makes it a feasible model to directly investigate neurodegenerative diseases. The retina is a well-studied and easily accessible model for manipulations; therefore, it can contribute a lot in understanding structural and functional connectivity of the CNS under normal and diseased conditions. Above that, the laminar arrangement of the retinal neurons makes it an attractive model to study interactions between laterally organized networks. Hence, in the present study, the retina was used as a model system to explore how spontaneously active networks interact with each other at the synaptic level.

5.2.1 Structural organization of the mammalian retina

The retina, an integral part of the CNS, is a light-sensitive tissue at the back of the eye (reviewed in Erskine and Herrera, 2014). The mammalian retina is a well-organized laminar structure that consists of a feedforward pathway from rod and cone photoreceptors (rods and cones), through the BCs to the RGCs, which are modulated laterally by horizontal cells (HCs) and ACs (Fig. 1). The RGCs are the retina's output neurons. The five major neuronal cell classes in the retina are structured into three nuclear layers, namely, outer (ONL), inner nuclear layer (INL) and ganglion cell layer (GCL) which form their synapses at the two synaptic layers, i.e., OPL and IPL (Fig. 1). While in the OPL, BCs synapse with the photoreceptors and the HCs, in the IPL they make connections with the ACs and the RGCs (reviewed in (Hoon et al., 2014; Baden et al., 2018)).

The light-sensitive neurons in the outer retina, i.e., photoreceptors, convert light signals into electrical signals through a series of processes in the phototransduction cascade that leads to cell hyperpolarization (Grossniklaus et al., 2015). The signal is then relayed to the BCs which transmit signals through multiple parallel channels to the RGCs (Baden et al., 2016; Franke et al., 2017). The excitatory synaptic transmission is modulated by two classes of inhibitory interneurons: HCs in the outer retina and ACs in the inner retina (reviewed in Diamond, 2017). As a result, the vertebrate retina exhibits many distinct circuits that operate in parallel to generate visual output. This involves a complex organization of synaptic connectivity both in the outer and inner retina. This retinal network can perform complex computations, decomposing the visual stimulus and sending the resulting feature representations to the brain.

All the axons of the RGCs collectively form a bundle-like structure called the optic nerve (Fig. 1). The visual information is then transferred via the optic nerve to more than 50 regions of the brain for further processing (Martersteck et al., 2017). The two major targets of the RGCs are the SC of the midbrain and LGN of the thalamus. The visual information from the LGN is passed to the primary visual cortex (V1) (Fig. 1, top). However, depending on the species one of the two pathways can be more pronounced for e.g., in mice, majority (~ 80%) of the RGCs project their axons to the SC (Ellis et al., 2016) while in primates, ~ 90% of the RGCs project to the LGN (Perry et al., 1984).

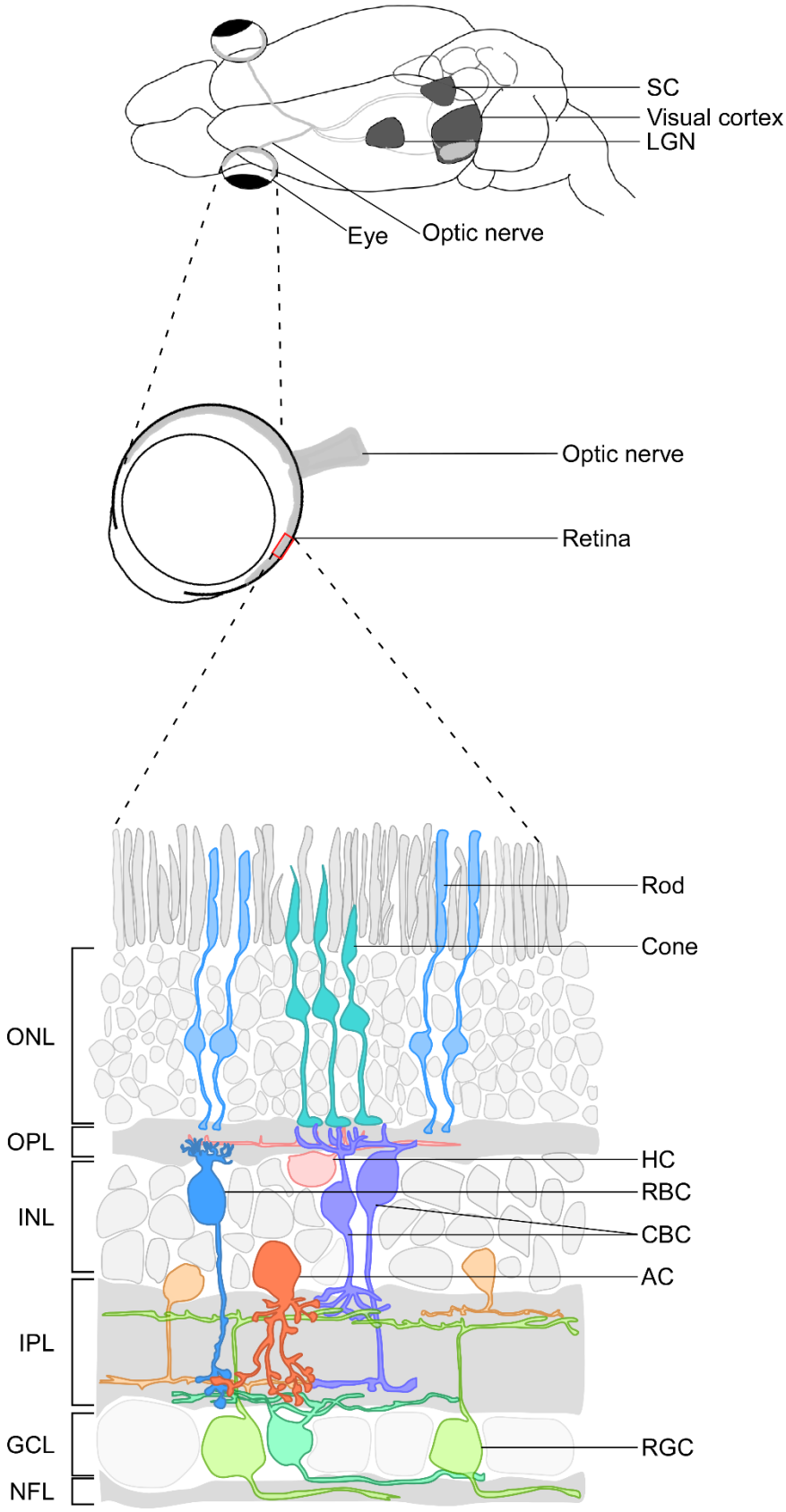
SC
Visual cortex
LGN
Eye
Optic nerve
Optic nerve
Retina
Rod
Cone
ONL
OPL
HC
INL
RBC
CBC
AC
IPL
GCL
RGC
NFL

Figure 1. Illustrative representation of a mouse retina as an extension to the brain.

Top: A simplified schematic representing higher visual centers in the mouse brain, i.e., visual cortex, lateral geniculate nucleus (LGN) and superior colliculus (SC). Note not all the visual pathways are shown here (Adapted from Wilks et al., 2013). Middle: Simplified schematic of a mouse eye as an extension of the central nervous system (CNS). The retina is located at the back of the eye and sends visual information to the brain via the optic nerve (Adapted from an image from Thomas Euler (http://www.vision-research.eu/index.php?id=925)). Bottom: Schematic showing an enlarged view of a vertical section of a mouse retina (Adapted from Euler and Schubert, 2015). The retina is composed of five neuronal cell classes; namely photoreceptors (rods and cones), horizontal cells (HCs), rod (RBCs) and cone bipolar cells (CBCs), amacrine cells (ACs) and retinal ganglion cells (RGCs). These neurons are organized in different nuclear and synaptic layers: outer nuclear layer (ONL), outer plexiform layer (OPL), inner nuclear layer (INL), inner plexiform layer (IPL) and ganglion cell layer (GCL). Nerve fiber layer (NFL) comprises all the RGC axons that form the optic nerve.

5.2.2 Stratification of the synapses in the plexiform layers

While OPL mainly consists of synapses between photoreceptor terminals (rod spherules and cone pedicles) and dendrites of HCs and BCs, the IPL consists of connections between BC axon terminals, AC processes, and RGC dendrites. The IPL can be traditionally divided into five strata (1-5) of the same width depending on the BC axonal stratification. There are at least 15 types of BCs (reviewed in Euler et al., 2014; Tsukamoto and Omi, 2017) that receive input from photoreceptors. Based on their response polarity to a flash of light, they can be subdivided into ON- and OFF-BCs; ON-BCs respond to light increments with depolarization, while OFF-BCs become hyperpolarized to increments of light. Further, depending on whether they make contacts with rods or cones, ON-BCs can further be categorized into rod BCs (RBCs) and ON- cone BCs (CBCs), respectively. However, RBCs can also make synapses with cone pedicles and a few OFF-CBC types such as type 3 and 4 also receive inputs from rods (Behrens et al., 2016). Strikingly, different types of BCs segment themselves across the whole IPL depth in a specified manner; while OFF-BCs extend their terminals in strata 1 and 2, ON-BC types predominantly stratify in strata 3 to 5. This results in a separation of the IPL into two distinct sublamina known as OFF (strata 1 and 2) and ON sublamina (strata 3 to 5) (reviewed in Euler et al., 2014). Besides, ON and OFF division, the systematic stratification of the BC axon terminals generates finer subdivisions in the IPL such

as segregation (broadly) into transient (IPL centre) and sustained channels (IPL borders) (Franke et al., 2017). Thus, the highly organized IPL structure functions as the retina's 'switchboard' receiving input from parallel BC channels and sending information to different ACs and RGCs (reviewed in Euler et al., 2014).

5.2.3 Synapses in the outer retina

In the OPL, the connectivity between photoreceptor terminals and their postsynaptic neurons represent a unique synaptic organization. Photoreceptor terminals contain specialized synaptic release structures known as ribbons which are surrounded by glutamate containing vesicles. Presynaptic HC and postsynaptic ON-BC dendrites make invaginating contacts with photoreceptor terminals, whereas OFF-BCs make non-invaginating synaptic contacts (Fig. 2). However, an exception to this norm are type X ON-BCs, which primarily make non-invaginating contacts with cone terminals (Behrens et al., 2016).

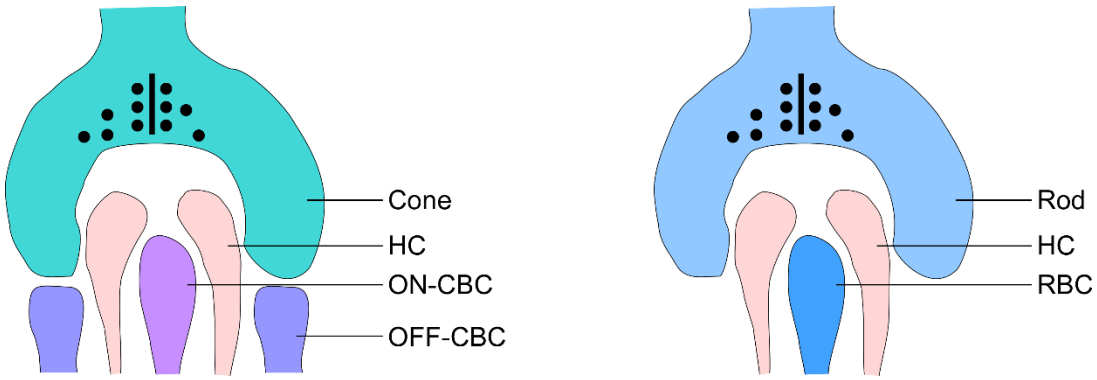

Figure 2. Schematic representation of typical synaptic connectivity at the OPL.

Photoreceptor (rod and cone) terminals contain synaptic ribbons (black line) that are surrounded by glutamate containing synaptic vesicles (black circles). At each synaptic ribbon, the cone axon terminal (left) makes invaginating connections with HC dendritic tips and ON-CBC dendrite, while it makes non-invaginating contacts with OFF-CBC dendrites. Invaginating connections between rod spherule (right) and HC processes and RBC dendrites are also present at the OPL. OFF-CBC connections to rod spherules are not shown here (Adapted from Euler et al., 2014).

Signal transduction in rods and cones triggers a change in their membrane potentials resulting in neurotransmitter release. Photoreceptor terminals through their specialized ribbon synapses enable graded release of glutamate (reviewed in Sterling and Matthews, 2005), which is then transmitted downstream to the HCs and BCs. For the binding of glutamate, HCs express AMPA (α-amino-3-hydroxy-5-methyl-4-isoxazolepropionic acid) and kainate type ionotropic glutamate receptors (Haverkamp et al., 2001; Schubert et al., 2006; Feigenspan and Babai, 2015; Ströh et al., 2013). The binding of the glutamate onto the receptors of HCs leads to their hyperpolarization (Haverkamp et al., 2000; Cueva et al., 2002). This feedforward synaptic transmission from the cones to the HCs is in turn modulated through different feedback mechanisms by the HCs, namely, ephaptic, proton mediated and GABAergic mediated feedback (reviewed in Chapot et al., 2017). In general, ephaptic feedback is faster than the other two processes and is mediated by the entry of cations into the dendritic tips of the HCs following hyperpolarization. Both ephaptic and proton mediated feedback mechanisms can regulate the glutamate release from the cone axon terminals by acting on voltage-gated Ca^{2+} channels (VGCC) present on them (Nachman-Clewner et al., 1999; reviewed in Kamermans and Fahrenfort, 2004). On the other hand, GABAergic mediated feedback does not contribute directly, instead, the GABA receptors present on the HCs can act on themselves (autoreceptors), further modulating the GABA release from the HCs (Haverkamp et al., 2000; Cueva et al., 2002; Liu et al., 2013). Thus, the GABAergic feedback is thought to be an indirect mechanism that could modulate the other two feedback mechanisms (Kemmler et al., 2014).

OFF-BCs also express AMPA and kainate type glutamate receptors forming ‘sign conserving’ synapses with photoreceptor terminals and thus, exhibiting the same response polarity to the light (Puller et al., 2013). Recently, it was reported that the cone-driven glutamate release from the OFF-CBCs in response to light stimulus appears to be mainly mediated by kainate receptors and not AMPA receptors (Borghuis et al., 2014). Contrary to the OFF-CBCs, ON-CBCs express metabotropic glutamate receptors (mGluRs) at their dendritic tips making ‘sign-inverting’ synapses with the photoreceptors and thus, responding with opposite polarity to the photoreceptors on the light onset. While different types of mGluRs are found to be expressed in the retina, group III type mGluR6 is predominantly expressed on the dendritic tips of ON-BCs (reviewed in Dhingra and Vardi, 2012). Besides mGluR6, another crucial component involved in the ON-BC signaling cascade is a transient receptor potential M1 (TRPM1) protein, which is negatively regulated by

mGluR6 activation. The interaction between mGluR6 and TRPM1 is facilitated by another essential protein called nyctalopin (Gregg et al., 2003; Gregg et al., 2007). Upon glutamate binding on to the mGluR6 receptor, the activation of mGluR6 leads to the closure of the TRPM1 channel further resulting in membrane hyperpolarization (Morgans et al., 2009; Koike et al., 2010). Additionally, the BCs also express GABA receptors on to their dendrites and their signals may be modulated by the GABAergic feedforward inhibition from the HCs (Haverkamp et al., 2000; Behrens et al., 2019).

5.2.4 Synapses in the inner retina

The glutamatergic signals from the BCs are relayed to the RGCs and this vertical signal transmission is modulated by the inhibitory activity of the ACs. Similar to the photoreceptor terminals, BCs also contain ribbons with synaptic vesicles at their terminals and make non-invaginating synapses with their postsynaptic neurons, i.e., ACs and RGCs (Fig. 3). CBCs contact both RGCs and ACs, however, RBCs instead of contacting RGCs directly synapse with two ACs which further relay the signals to the RGCs via CBCs (Fig. 3) (see below; the rod pathway).

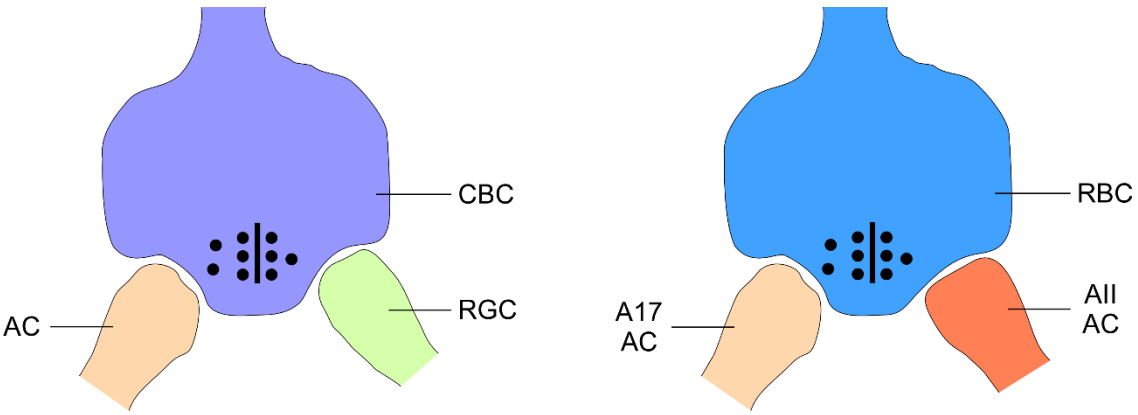

Figure 3. Schematic representation of the synaptic connectivity in the IPL.

Both CBC and RBC terminals contain synaptic ribbons (black line) surrounded by glutamate filled vesicles (black circles) at the synaptic site. A typical synaptic connection between a CBC terminal and its postsynaptic elements; RGC and AC at a single synaptic site is shown on the left while a

simplified representation of the connectivity between an RBC bouton and AII and A17 ACs is shown on the right (Adapted from Baden and Euler, 2016). Note not all connections are shown here.

The excitatory signal transmitted by the BCs to the ACs and RGCs is mainly mediated by ionotropic glutamate receptors via both AMPA/kainate type and NMDA type receptors resulting in a '*sign-conserving*' response (Lukasiewicz et al., 1997; reviewed in (Yang, 2004; Shen et al., 2006)). While the majority of the ACs express both AMPA and kainate type receptors, a few of them express either only AMPA or kainate receptors (Dumitrescu et al., 2006). In addition, recent evidence suggests the presence of NMDA receptors on ACs (Zhou et al., 2016; Veruki et al., 2019). Moreover, a few ACs also express different mGluR receptor types such as mGluR4, 7 or 8, which are localized mainly on their processes and somata (Brandstatter et al., 1996; Koulen and Brandstatter, 2002; Quraishi et al., 2007; reviewed in Dhingra and Vardi, 2012). Also, a few RGCs express mGluRs (reviewed in Dhingra and Vardi, 2012).

The signal flow from the BCs to the RGCs can be shaped by ACs in different ways: either they can provide feedback inhibition to the BCs upon receiving glutamatergic input or could directly inhibit RGCs in a feedforward fashion. In addition, ACs can also regulate the activity of other ACs by forming synapses with them (reviewed in (Zhang and McCall, 2012; Hoon et al., 2014; Diamond, 2017)). The inhibitory signal modulation by the ACs can be either GABAergic or glycinergic. Along with this, many ACs also release an additional neurotransmitter, for example, SACs release both GABA and acetylcholine onto direction selective RGCs (O'Malley et al., 1992), shaping their responses. Similarly, dopaminergic amacrine cells (DACs) co-release GABA and dopamine to their postsynaptic neurons (Contini and Raviola, 2003).

The rod pathway or RBC-AII AC circuitry

The rod pathway involved in scotopic vision displays a unique synaptic organization between RBCs and ACs. Rods predominantly make invaginating synapses with the RBC dendrites in the OPL. However, unlike other BCs, RBCs do not directly provide input to RGCs. Instead, they form output synapses with two types of ACs, namely, AII and A17 ACs (reviewed in Bloomfield and Dacheux, 2001) (Fig. 3, right). This synaptic connectivity also represents a special arrangement in the IPL. RBCs extend their bouton-like terminals deep into the inner sublamina of the IPL reaching

down to strata 4 and 5. AII ACs, on the other hand, are narrow-field bistratified neurons that have their processes distributed at different strata in the IPL. In strata 4 and 5, the distal dendrites of the AII ACs contact RBC terminals; this is where they receive glutamatergic input from RBCs, whereas in strata 1 and 2, lobular appendages of the AII ACs make glycinergic inhibitory synapses with OFF-CBCs. In addition, AII ACs also form gap junctions with ON-CBCs stratifying in strata 3 to 5. ON- and OFF-CBCs, in turn, make synapses with ON- and OFF-RGCs, respectively. This enables well-segregated information flow between both ON and OFF channels (Strettoi et al., 1992; reviewed in Bloomfield and Dacheux, 2001; Ghosh et al., 2001; Wässle et al., 2009) (Fig. 4).

Contrary to AII cells, A17 ACs which are wide-field ACs also make synapses with the RBCs in the inner strata of the IPL (Fig. 4). The glutamatergic input received by the A17 ACs is modulated by GABAergic reciprocal synapses with RBCs (Hartveit, 1999; Ghosh et al., 2001). The incoming glutamatergic signals collected by both AII and A17 ACs are mainly mediated by AMPA/kainate type receptors (Ghosh et al., 2001). However, recent studies revealed an extrasynaptic localization of NMDA receptors on both AII and A17 ACs, which may point at a role for these synapses in signal modulation and plasticity (Zhou et al., 2016; Veruki et al., 2019).

Interestingly, AII ACs are coupled via gap junctions to other AII ACs (homotypic coupling) and ON-CBCs (heterotypic coupling). The coupling between these networks is influenced by light levels. At dark-adapted conditions, the network remains uncoupled and with the increase in background illumination to a mesopic range, the coupling between the networks increases. Any further increase in light level that falls into the photopic range leads to a reduction in the coupling, a process that is mainly regulated by enhanced dopamine signaling (Hampson et al., 1992). It has been suggested that the extrasynaptic NMDA receptors present on the AII ACs play a crucial role in modulating the coupling between the networks (Kothmann et al., 2012; Veruki et al., 2019). Altogether, rod signals from the RBCs are transmitted to the AII ACs, which leads to their depolarization. The depolarized signal is then relayed to the ON-CBCs through gap junctions while OFF-CBCs receive glycinergic inhibition via AII ACs. The antagonistic signals received by ON- and OFF-CBCs is further conveyed to the ON- and OFF-RGCs, thus establishing parallel, rod-driven ON and OFF channels along the pathway (Fig. 4).

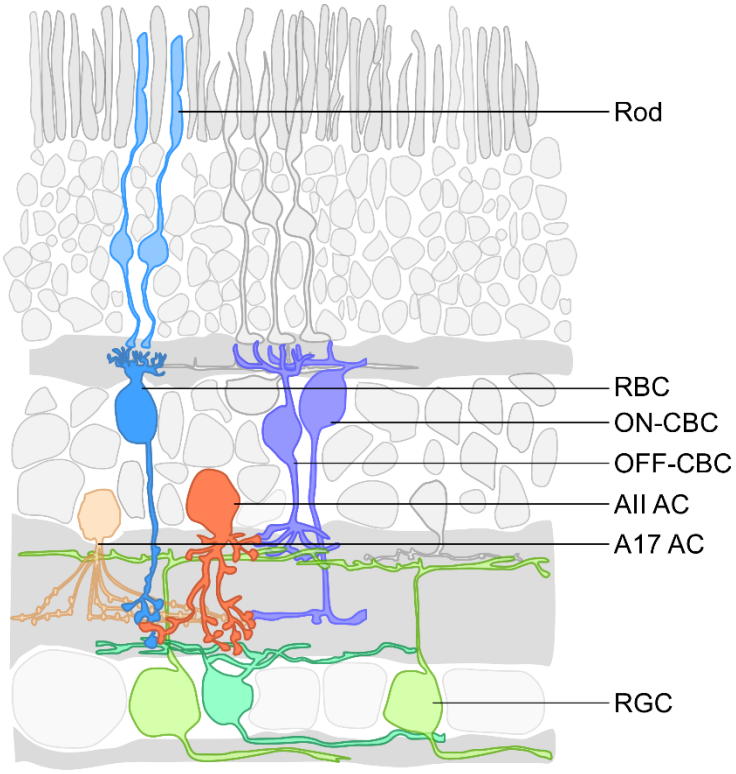

Figure 4. Schematic illustrating rod pathway circuitry.

In a classical rod pathway, many rods converge onto a single RBC which then sends excitatory output to AII and A17 ACs. The signals received by AII ACs are then relayed to ON- and OFF-CBCs through gap junctions and glycinergic synapses, respectively which in turn relay signals to ON- and OFF-RGCs. The A17 ACs, on the other hand, modulate the glutamate release from the RBCs by forming GABAergic reciprocal synapses with them (Adapted from Euler and Schubert, 2015).

5.3 Spontaneous activity in the retina

As spontaneous activity is a characteristic feature of the neural system (see also 5.1.1 and 5.1.2), it is also displayed by some mature retinal neurons. For example, OFF- but not ON-RGCs usually exhibit spontaneous activity due to their intrinsic pacemaker properties; this activity is driven mainly by I_{Nap} leading to subthreshold oscillations (Margolis and Detwiler, 2007). Spontaneous oscillatory activity has also been reported in SACs as a result of Ca^{2+} dependent glutamate release by the BC axon terminals (Petit-Jacques et al., 2005). Another neuron type in the retina which is known to fire spontaneously is the DAC. Spontaneous rhythmic activity or bursts of spikes have been reported for DACs in both isolated and intact retina (Feigenspan et al., 1998; Zhang et al., 2007). The activity in these neurons is mainly mediated by subthreshold Na^+ currents that rely on tetrodotoxin (TTX)-sensitive voltage gated Na^+ channels (Feigenspan et al., 1998).

Compared to the adult retina, spontaneous network activity can be distinctively observed in the developing retina in the form of so-called retinal waves (see 5.1.2 and 5.1.3). However, these

waves disappear with the emergence of light-evoked activity. The wave-like activity is suppressed by the maturation of the inhibitory network due to switching of the GABA and glycine receptor-mediated activity from excitatory to inhibitory, particularly due to change in the intracellular concentration of Cl^- (Toychiev et al., 2013) (see also 5.1.3). Strikingly, degeneration of photoreceptors and thus loss of light-evoked input in many retinal diseases trigger spontaneous activity in several types of retinal neurons (see 5.4.4). Unlike in the healthy adult retina, spontaneous activity in the degenerated retina forms networks (reviewed in Euler and Schubert, 2015), representing a unique model to study network interactions in a diseased condition.

5.4 Retinal degeneration

A vast variety of genetic mutations in the rods, cones or retinal pigmented epithelium can cause severe retinal dystrophies. These mutations can lead to dysfunction or progressive death of the photoreceptors and are known to be the primary cause of blindness in the world. RP is one of the major characterized inherited retinal disorders resulting from a diverse range of mutations in different genes (reviewed in (Wang et al., 2005; Daiger et al., 2013)). This leads to the degeneration of photoreceptors where for the majority of the cases, rod cell death is followed by the secondary degeneration of cones. This consequently leads to a deficit in photoreceptor function and ultimately blindness in the late stages of the disease. Depending on the extent and location of the mutation, the rate of RP progression varies from person to person (Sandberg et al., 1995). One of the early clinical signs of RP is night blindness due to loss of rod photoreceptors which eventually converts into large-scale cell deaths at the periphery leaving the patient with only tunnel vision. As in RP, cone cell death follows rod degeneration, loss of visual acuity and defects in color perception is also seen in the patients. The advancement of the disease subsequently leads to a complete loss of vision.

The clinical manifestations of RP are a result of severe morphological and functional remodeling in the retina resulting from the degeneration. The deafferented retina undergoes an intense remodeling process which can be broadly divided into three different phases (reviewed in (Marc et al., 2003; Jones et al., 2005; Kalloniatis et al., 2016)) (Fig. 5):

Phase 1/Neuronal stress – This phase depicts 'photoreceptor stress' and is marked by the truncation of the outer segments of the photoreceptors, initiation of the photoreceptor death and extension of rod neurites. Alterations in expression and function of neurotransmitter receptors can also be observed.

Phase 2/Photoreceptor death – This phase is mainly characterized by massive rod death followed by cone degeneration. RBCs and HCs start retracting their dendrites, which also causes changes in the inner retina.

Phase 3/Comprehensive remodeling – This phase represents extensive remodeling in the neuronal circuitry and is characterized by severe structural changes in both outer and inner retina. Sprouting of neurite processes and the formation of ectopic synapses is also prominent at this stage.

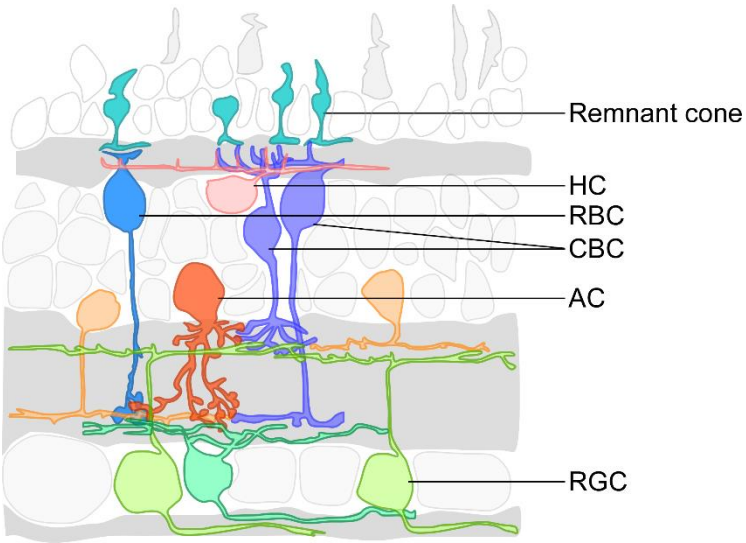

Figure 5. Schematic representation of a vertical section of a degenerated mouse retina.

In retinal degenerative diseases, the degeneration of photoreceptors starts with the loss of light-sensitive outer segments followed by dendritic retraction leaving behind only remnant cone somata. This further leads to retraction and loss of dendrites of HCs and BCs. Ectopic synapse formation between RBC and remnant cone somata can also be seen. Some minor changes in the inner retina such as the reduction in density of RBC boutons can also be observed (Adapted from Euler and Schubert, 2015).

These changes in the retina have been thoroughly studied in rodent models of RP. Patients with autosomal recessive RP disorders are known to exhibit mutations in the gene encoding for the β – subunit of the rod cyclic guanosine monophosphate (cGMP) phosphodiesterase (PDE) 6, *Pde6b* (McLaughlin et al., 1993). Being an essential player in the signaling cascade, any defect in the *Pde6b* gene results in an increase in cGMP concentration that can induce photoreceptor

degeneration (Lolley et al., 1977). Two mouse models, namely, retinal degeneration 1 *(rd1)* and retinal degeneration 10 *(rd10)*, carrying mutations similar to the human autosomal recessive forms of RP have been identified (Pittler and Baehr, 1991; reviewed in Chang et al., 2002; Chang et al., 2007). These models are being employed widely to investigate alterations in mechanisms underlying the disease to provide insights to the development of therapeutic strategies.

Pde6b^{rd1} or *rd1* mouse has a nonsense mutation in exon 7 of the *Pde6b* gene (Pittler and Baehr, 1991; reviewed in Chang et al., 2002) that makes the protein non-functional, resulting in rapid degeneration of rods (Carter-Dawson et al., 1978). Another mouse model, *Pde6b*^{rd10} or *rd10,* which has a missense mutation in exon 13 of the *Pde6b* gene, show a milder phenotype (reviewed in Chang et al., 2002). The onset of photoreceptor degeneration in *rd10* is around P18 (Gargini et al., 2007; Barhoum et al., 2008), which is slightly delayed as compared to *rd1,* where the degeneration begins around P10 (Strettoi et al., 2002). Although the two lines of the RP model have their own benefits, the late onset of degeneration in *rd10* provides a wider window for investigating general principles underlying degeneration. Moreover, cell death in *rd1* precedes eye-opening at ~ P14, leaving no doubt that the degeneration process would also interfere with neuronal differentiation and development.

As the focus of the present work was to study spontaneous network interactions in a degenerated retina with the advancement of the disease, we, therefore, used the *rd10* as our model system. Being a slowly progressive disease model and with few remnant cones still remaining until later stages of life (Gargini et al., 2007), it closely resembles human RP. Besides, as the developing retina also exhibits spontaneous waves of activity (Meister et al., 1991; Feller et al., 1996) (see 5.1.2 and 5.1.3), it is important for this study to choose a model where these activities are distinguished between both the developing and developed system. This makes the *rd10* the more suitable model than *rd1* for the purpose of our study.

5.4.1 Photoreceptor degeneration timeline in the rd10 mouse

The degeneration of photoreceptors in the *rd10* retina starts at around P18, displaying disrupted morphology of the outer and inner segments. Maximal degeneration reaches a peak at P25, with

only two or three layers of photoreceptor somata left in the ONL (Gargini et al., 2007). Between P40 and P45, only one or two layers of photoreceptor somata are remaining and the cells have no outer nor inner segments (Barhoum et al., 2008). At this time point, the ONL mainly constitutes cones, with a very few sparsely located rods. Although most of the cones are also lost by P60, some remnant cone cell bodies can be still found even until 9 months of age (Gargini et al., 2007). Additionally, a center-to-periphery degeneration pattern can also be observed in the *rd10* retina as the degeneration appears to be more pronounced in the central region at P30 as compared to the periphery (Gargini et al., 2007; Barhoum et al., 2008). However, this has been contradicted by a recent study, where the authors did not find any significant change in the degeneration of the neurons with respect to its spatial location between P24 and P30 (Power et al., 2019). The loss of rods leads to severe anatomical and functional remodeling of downstream retinal neurons and circuits. While the remodeling is severe in the outer retina and starts early, the inner retina is usually morphologically more stable but is thought to undergo some (minor) structural changes during later phases of the disease.

5.4.2 Alterations in the synaptic connections in the outer rd10 retina

Photoreceptor degeneration triggers massive alterations of synaptic connections between postsynaptic neurons. Alterations in glutamatergic transmission from the photoreceptor terminals are clearly apparent from the reduction in vesicular glutamate transporter 1 (VGluT1) immunoreactivity as early as P30, with VGluT1 labeling continuing to decrease further until later stages of degeneration (Phillips et al., 2010). As rods are the first retinal neurons to degenerate, RBCs are the most affected neurons after photoreceptors (Fig. 6A). Following photoreceptor loss, severe morphological defects can be observed in the RBC dendrites. Changes in protein kinase C (PKC) immunoreactivity are visible from P20, which progressively decreases with the advancement of the disease (Barhoum et al., 2008). This is followed by the shortening and retraction of the dendrites around P30, which gradually leads to a total loss of dendrites after P40 (Gargini et al., 2007; Puthussery et al., 2009; Phillips et al., 2010). Strikingly, at this time point retracted processes of surviving RBCs show a tendency to make transient flat ectopic contacts with cone pedicles (Puthussery et al., 2009) (Fig. 6B). Unlike *rd10* retina, in *rd1* retina, during the late

degeneration phase around P35, remnant cones develop bulbar neurites to make synapses with RBC somata (Haq et al., 2014). In *rd10* mouse, later after 3 months, remaining RBCs mostly cluster together, and their dendrites have been shown to associate with the remnant cones (Phillips et al., 2010). In addition, similar to photoreceptors, RBCs also display a center-to-periphery gradient of degeneration (Gargini et al., 2007; Puthussery et al., 2009). ON-CBCs follow a similar degeneration and remodeling trend as RBCs (Puthussery et al., 2009; Phillips et al., 2010). OFF-CBC dendritic morphology and function, on the other hand, are broadly preserved (Puthussery et al., 2009), however, some dendritic retraction can be observed after P60 (Gargini et al., 2007).

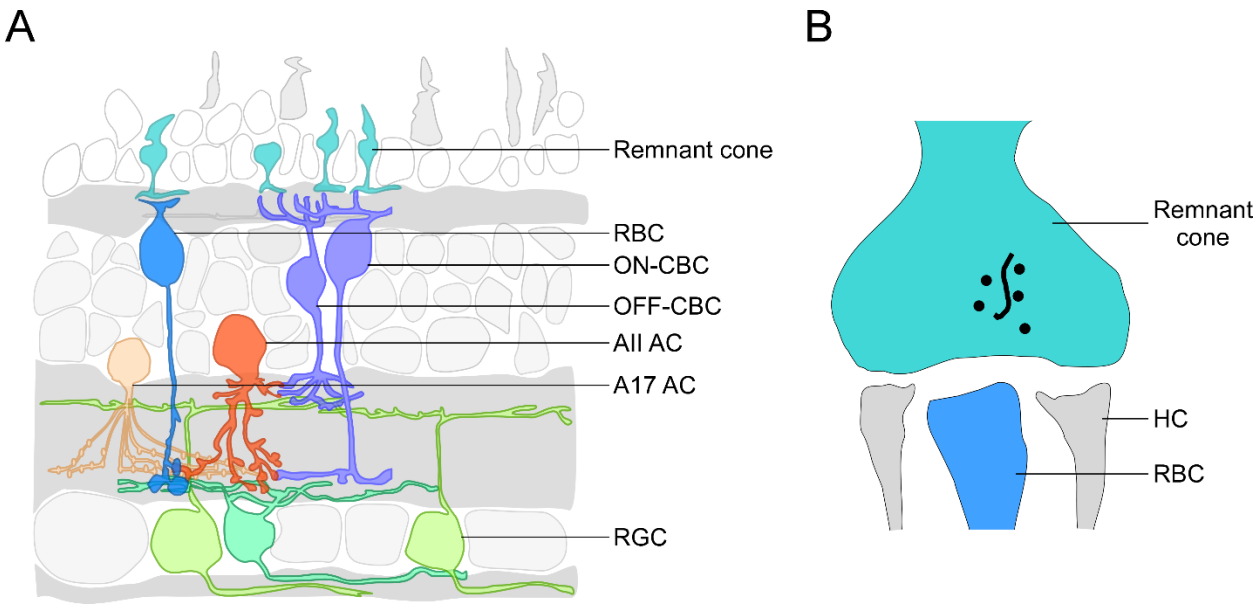

Figure 6. Schematic representation of altered rod pathway circuitry in the degenerated mouse retina.

(A) The degeneration of rod photoreceptors is followed by secondary cone degeneration that starts with the truncation of outer and inner segments leaving behind only remnant cone somata. This further leads to retraction and loss of bushy like dendrites of RBCs. Dendritic retraction can also be seen in CBCs. In the inner retina, while ACs and CBCs synaptic connectivity and organization remain broadly preserved reduction in density and length of bulbar endings of the RBC axon terminals can be observed. During degeneration, ectopic synapses are also formed between remnant cone somata and RBC (Adapted from Euler and Schubert 2015). (B) Simplified schema illustrating non-invaginating ectopic synapse formation between remnant cone somata and RBC during retinal degeneration.

Another cell class that is greatly affected in the outer retina by the degeneration of photoreceptors is the HC. In wild-type retina, HC dendrites make synapses with the cone pedicles, while axon terminals synapse with rod spherules in the OPL (see 5.2.3). Following degeneration, retraction of HC processes can be observed as early as P20; these processes are completely lost until later time points of the degeneration (Gargini et al., 2007; Barhoum et al., 2008). Ectopic sprouting in the ONL and INL can also be detected from P30 (Barhoum et al., 2008; Phillips et al., 2010). Both dendritic and axonal processes of HCs largely disappear after 4 months of age (Gargini et al., 2007). In the healthy retina, HCs modulate cone output predominantly by providing ephaptic feedback to the cone axon terminals while GABA mediated feedback indirectly contributes to the process (Kemmler et al., 2014) (see 5.2.3). The ephaptic feedback mechanism relies on the change in voltage between the inside of the HC and the synaptic cleft between the cone axon terminal and HC dendritic tips. As there is retraction and loss of dendrites of the HCs during degeneration, it is possible that this altered synaptic connectivity also causes reduced feedback through the ephaptic pathway. On the other hand, it has also been shown that the remnant cones in the degenerated retina can express GABA receptors and thus, GABA release from the HCs might directly modulate the signals of the remnant cones in the degenerated retina (Haq et al., 2014). Ultimately, the loss of feedback from the HCs to the photoreceptors could, in turn, also affect the output of the remnant cones and other downstream neurons (Chaya et al., 2017).

The anatomical defects in the degenerated retina are accompanied by remodeling of the postsynaptic receptor proteins. Corresponding to severe structural disruption in the ON-BCs, major defects in the expression and distribution of mGluR6 can be found. Though its expression and localization are largely normal compared to the wild-type at least until P25, reduction in the immunoreactivity of mGluR6 can be detected around P40 (Gargini et al., 2007; Barhoum et al., 2008). Abnormal localization of the receptors on the cell bodies and axon terminals can be observed with degeneration (Gargini et al., 2007; Barhoum et al., 2008; Puthussery et al., 2009). This is also evident as the mGluR6 mediated visual responses are reduced between P20 and P180 (Puthussery et al., 2009). In contrast to this, the expression of AMPA/kainate type glutamate receptors on the dendrites and functional responses of the OFF-CBCs are broadly unaltered (Puthussery et al., 2009).

5.4.3 Alterations in the synaptic connections in the inner rd10 retina

The degeneration of photoreceptors also affects the inner retinal circuitry. Although in comparison to the outer retina, remodeling in the inner retina is delayed and likely small in terms of complexity and severity, it still exhibits significant changes. The degeneration of RBCs is marked by a reduction in PKC immunoreactivity in the axon and axon terminals (Gargini et al., 2007; Barhoum et al., 2008). RBCs show a reduction in the size and density of the bulbar endings of the axonal terminals (Barhoum et al., 2008; Phillips et al., 2010) (Fig. 6A). CBCs on the other hand, seem not to exhibit dramatic changes in their morphology, however, some disorganization can also be found at their terminals (Phillips et al., 2010). Besides these changes, both ON- and OFF-BC axon terminals maintain their stratification profiles in the IPL even until later time points of the disease (Phillips et al., 2010). As severe remodeling occurs in the RBCs, it also affects RBC-AII AC circuitry (Fig. 6). Initially around P30, the lobular appendages of AII ACs in the OFF sublamina of the IPL show reduction in size, indicating imperfect synaptic transmission from the AII ACs to the OFF-CBCs (Barhoum et al., 2008). The dendritic morphology of AII ACs in the ON sublamina of the IPL is mostly unaltered at this stage. However, at P40 substantial loss in disabled-1 (Dab1) immunoreactivity that labels AII ACs denote that these neurons are also severely disrupted (Barhoum et al., 2008). Apart from changes in the AII ACs, the stratification profiles of other types of ACs are largely preserved and do not seem to exhibit any significant differences even in the advanced stage of the disease (Phillips et al., 2010). Together, this implies that the degeneration of photoreceptors leads to a profound change in the rod-pathway while the cone-pathway may experience only minor alterations.

5.4.4 Functional changes in the degenerated retina

In addition to all morphological changes discussed above, the deafferentation of photoreceptors also leads to severe alterations of the functional properties of the retina. One of the characteristic features is the generation or enhancement of spontaneous activity in different retinal neurons. Following degeneration, in the outer retina, remnant cones and RBCs start oscillating spontaneously, forming synchronized clusters (Haq et al., 2014). These spontaneous signals can

also be observed in other postsynaptic neurons such as AII ACs, ON- and OFF-CBCs (Borowska et al., 2011; Trenholm et al., 2012; Choi et al., 2014) and RGCs (Margolis et al., 2008; Goo et al., 2011; Stasheff et al., 2011; Biswas et al., 2014). In addition, degeneration triggered alterations in spontaneous signals have been reported in both ON- and OFF-SACs (Tu et al., 2015) (see 5.4.10) and DACs (Atkinson et al., 2013) (see 5.4.8). Although the functional relevance of this abnormal hyperactivity during degeneration is not completely elucidated, it is known to hamper evoked responses by affecting the signal-to-noise ratio (SNR) (Yee et al., 2012).

Furthermore, the activities in the retinal neurons are not discrete. Rather, like in the brain, they form networks. Previous studies suggest that spontaneous activity in the degenerated retina arises in two individual networks: outer retinal network and inner retinal network (reviewed in Euler and Schubert, 2015). Here, the outer retinal network comprises of remnant cones, RBCs and HCs and the inner retinal network comprises ACs, CBCs, and RGCs (reviewed in Euler and Schubert, 2015) (see also 5.4.7).

5.4.5 Spontaneous activity in the outer rd retina

Outer retinal neurons, i.e., remnant cones, RBCs, and HCs, exhibit spontaneous activity usually up to a frequency of approximately 3 Hz in the degenerating *rd1* retina (Haq et al., 2014). The activity in the outer retina has been suggested to originate in electrically coupled remnant cones (Haq et al., 2014). After rod cell death, due to secondary degeneration, outer segments of the cones are lost mimicking dark condition. Hence, cone membrane potentials are likely more depolarized compared to wild-type retina. This change in membrane potential causes activation of VGCCs present at the cone terminals (Nachman-Clewner et al., 1999) and thereby Ca^{2+} influx, and thus leading to the generation of spontaneous activity in the remnant cones (Haq et al., 2014). Spontaneous cone activity is propagated to the RBCs through sign conserving, glutamatergic synapses mediated by excitatory amino acid transporter 5 (EAAT5) glutamate transporters (Haq et al., 2014). This is also evident as the RBCs form positively synchronized clusters with the remnant cones (Haq et al., 2014). The HCs also reveal network mediated activity which is likely to be driven by the remnant cones and might help in the spreading of the activity laterally in the

outer retina (Haq et al., 2014). The HCs modulate the activity of the remnant cones via GABAergic inhibition, as both the number of spontaneous events in the remnant cones and RBCs and synchronization between them increases after blocking the inhibitory input using GABA receptor antagonists (Haq et al., 2014). Taken together, intense remodeling in the outer retina as a result of photoreceptor death results in the generation of spontaneous rhythmic activity in the surviving cones. The activity is then relayed from the cones to the RBCs and HCs through synaptic interactions.

5.4.6 Spontaneous activity in the inner rd retina

Compared to the outer retinal activity, inner retinal network activity has been widely described in the literature using various electrophysiological and imaging techniques though more in *rd1* than in *rd10* retinae. Inner retinal neurons comprising ACs, CBCs, and RGCs display spontaneous activity at frequencies that range between approximately 4 and 10 Hz (Margolis et al., 2008; Borowska et al., 2011; Goo et al., 2011; Stasheff et al., 2011; Biswas et al., 2014). In contrast to the outer retina, where the activity is triggered mainly due to remodeling in the circuitry, inner retinal activity is thought to be initiated due to a lack of light-driven input after photoreceptor loss (Trenholm et al., 2012). Supporting this idea, a study demonstrated that even partial photobleaching of the photoreceptors in the wild-type retina can induce spontaneous activity in RGCs similar to the activity observed in the *rd10* retina (Menzler et al., 2014).

The origin of inner retinal activity in the network is still controversially discussed. Using *rd1* mice, it has been suggested that the inner retinal oscillations can originate intrinsically due to the pacemaker activity of AII ACs. Particularly, the absence of light-driven source can lead to the hyperpolarization of the AII AC network resulting in fluctuations of the membrane potentials due to the interaction between fast Na^+ and slow K^+ conductances, which is reflected as rhythmic activity in these neurons (Choi et al., 2014) (see also 5.1.1). Another theory suggests that the inner retinal oscillations are initiated within the gap junction coupled AII AC/ON-CBC network as a result of the interaction between voltage gated Na^+ channels present on the AII ACs and I_h current in the ON-CBCs (Trenholm et al., 2012; reviewed in Trenholm and Awatramani, 2015). In any

case, the activity is fed into the cone pathway via electrical synapses to the ON-CBCs (Trenholm et al., 2012) and through the glycinergic synapse to OFF-CBCs (Poria and Dhingra, 2015). This hyperactivity is then relayed from the pre-synaptic neurons (possibly BCs) to the RGCs by the vertical glutamatergic pathways, as the rhythmic activity in the RGCs can be abolished with the application of ionotropic glutamate receptor antagonists (Borowska et al., 2011; reviewed in Margolis and Detwiler, 2011; Biswas et al., 2014). The inhibitory inputs provided by GABAergic and glycinergic neurons rather than taking part in the generation of these activities instead helps in regulating them. Application of GABA or glycine receptor antagonists either alone or together increases the amplitude of slow-wave activity in the RGCs in *rd1* mice (Ye and Goo, 2007). Furthermore, blocking inhibitory synapses also increases the correlation between RGCs (Menzler and Zeck, 2011). Similar experiments when performed in *rd10* mice using a GABA or glycine receptor antagonist did not show any significant effect on the activity of the RGCs. However, when combined, the antagonists caused an increase in the amplitude of the oscillations (Biswas et al., 2014).

Taken together, the inner retinal network developed in the absence of light-evoked input originates in electrically coupled AII ACs or between AII AC/ON-CBC network which is then propagated to the ON-RGCs through the glutamatergic excitatory pathway and OFF-RGCs via glycinergic inhibitory pathway (Trenholm et al., 2012; reviewed in Zeck, 2016). Interestingly, as a result of this synaptic interaction within the inner retinal network, a phase-shifted activity is generated in ON- and OFF-RGCs. Simultaneous recordings from ON- and OFF-RGC pairs in the *rd1* retina show that they are correlated but 180 degrees out of phase (Margolis et al., 2014). Large-scale network oscillations recorded from populations of *rd1* RGCs also revealed synaptically driven phase-shifted rhythmic activity in the neighboring neurons that can spread laterally over wide regions because of the gap junction coupling between the neurons (Menzler and Zeck, 2011; reviewed in Zeck, 2016). The role of gap junctions in the lateral spread of the activity has also been demonstrated by the selective ablation of the *connexin 36* (*Cx36*) gene essential for the electrical coupling between AII ACs in *rd10/Cx36*$^{-/-}$ mice (Ivanova et al., 2015). Knock out of the *Cx36* gene resulted in a reduction in spontaneous activity and enhanced light-evoked responses in both ON- and OFF-RGCs (Ivanova et al., 2015).

5.4.7 Potential interaction between spontaneously active networks

Various differences can be used for the classification of outer and inner networks in the degenerated retina (reviewed in Euler and Schubert, 2015).

1) The dominant frequency of the spontaneous activity differs in both outer (maximum ~ 3 Hz) and inner retinae (between 4 and 10 Hz) (Margolis et al., 2008; Borowska et al., 2011; Goo et al., 2011; Stasheff et al., 2011; Biswas et al., 2014) (see 5.4.5 and 5.4.6). However, it should be noted that these signals were recorded using different methods, recording conditions and mouse models and therefore the reported dominant frequencies have to be considered with some caution.

2) The source of the activities also seems to vary in both outer and inner retinal network; while in the outer retina the activity is an outcome of the remodeling in the circuitry following photoreceptor degeneration (Gargini et al., 2007; Barhoum et al., 2008; Haq et al., 2014) (see 5.4.5), the inner retinal activity is an intrinsic property triggered by the loss of light-driven activity due to the death of photoreceptors that can originate independently to the rewiring of the circuitry (Trenholm et al., 2012; Menzler et al., 2014) (see 5.4.6).

3) The activity generated in the two networks also has different origins; while in the outer retina, network activity originates in the surviving cones (Haq et al., 2014) (see 5.4.5), the inner retinal activity is generated between AII AC/ON-CBC network (Trenholm et al., 2012; Choi et al., 2014; Margolis et al., 2014; reviewed in Trenholm and Awatramani, 2015) (see 5.4.6).

4) There is also difference in the network properties; while the outer retinal network is restricted to a local area involving up to 5-15 cells forming clusters (Haq et al., 2014), the inner retinal activity can propagate laterally over a large area across the retina (Menzler and Zeck, 2011; reviewed in Zeck, 2016) (see 5.4.6).

In view of these dissimilarities, it seems reasonable to conclude that the two networks in the degenerated retina are distinct and largely independent of each other (reviewed in Euler and

Schubert, 2015). However, the networks also represent some commonalities. First, spontaneous activity in both the networks is likely to originate in neurons mainly due to alterations in membrane potentials of voltage gated ion-channels (Trenholm et al., 2012; Choi et al., 2014; Haq et al., 2014). Second, signal propagation to the postsynaptic neurons is mediated via vertical glutamatergic pathways (Borowska et al., 2011; reviewed in Margolis and Detwiler, 2011; Biswas et al., 2014; Haq et al., 2014), while gap junction coupling between neurons supports lateral signal spread (Menzler and Zeck, 2011; Haq et al., 2014). Third, the activity of both networks is shaped by inhibitory input (Ye and Goo, 2007; Menzler and Zeck, 2011; Biswas et al., 2014; Haq et al., 2014) (see 5.4.5 and 5.4.6).

Taken together, while there is evidence pointing at the independence of the networks, there is also data that argue for possible interaction between the two.

5.4.8 Putative pathways of interaction between spontaneously active networks

At least three potential pathways can be postulated regarding how these networks might interact with each other in the degenerated retina (reviewed in Euler and Schubert, 2015) (Fig. 7): (a) neuromodulation by DACs, (b) interplexiform ACs (iACs), and (c) BC-AC glutamatergic pathway.

DACs extrasynaptically release dopamine in response to light that can act distantly on neighboring neurons through volume transmission (Bjelke et al., 1996; reviewed in Hirasawa et al., 2015). These neurons receive glutamatergic input from ON-BCs in IPL stratum 3 and provide reciprocal GABAergic synapses to the BCs (Contini et al., 2010). They make GABAergic synapses with AII AC cell bodies in IPL stratum 1 (Voigt and Wässle, 1987; Contini and Raviola, 2003). In addition, they receive inhibitory GABAergic inputs from a few other ACs and glycinergic inputs from ACs mediated by OFF-CBCs (Newkirk et al., 2013). Besides, DACs are known to be spontaneously active in a healthy retina (Feigenspan et al., 1998; Zhang et al., 2007) (see also 5.3), which may play a role in the synaptic release of the dopamine (Floresco et al., 2003) and thus could modulate the coupling between AII ACs (see 5.2.4; the rod pathway). Under photopic conditions, the release of dopamine from DACs could act on dopamine receptors (D1) present on AII ACs, triggering

their uncoupling (Kothmann et al., 2009). Under scotopic conditions, when the coupling between the AII ACs is strong, spontaneous activity of the DACs has been reported to be reduced probably due to enhanced inhibition from the ACs (Gustincich et al., 1997). The crucial role of DACs in the coupling and decoupling of AII AC network makes them a possible candidate that could relay spontaneous signals from the inner to the outer retina in the degenerated retina. However, recent studies revealed alterations in anatomical and functional characteristics of the DACs during degeneration. Morphological analysis of the DACs during late stages of RP in both *rd10* and *rd1* retinae showed reduction in soma size, dendritic density and length (Ivanova et al., 2016b). These changes in the synaptic properties of the DACs can be associated with the decrease in synaptic transmission and reduced bursting activity of these neurons (Atkinson et al., 2013). This, in turn, could lead to a decrease in the endogenous dopamine release in the retina (reviewed in Djamgoz et al., 1997) probably due to a decrease in expression levels of tyrosine hydroxylase (Ivanova et al., 2016b), which is required for dopamine synthesis. Together, these remodeling induced changes in the DACs argue against the possibility that these cells play a crucial role in the signal transfer between the two networks in the degenerated retina.

Other candidates that could relay signals from the inner to the outer retina are iACs, which extend their processes bidirectionally up to OPL and IPL thus establish release sites throughout the outer and inner retina (Witkovsky et al., 2008; Dedek et al., 2009). iACs project their processes in the IPL strata 4 and 5, where they receive inputs from BCs, most probably type 7 and 8, and provide output to other ACs and RGCs. The processes of iACs also extend up to the OPL; however, no evidence for the direct synaptic contact between them and photoreceptors has been detected (Dedek et al., 2009). Interestingly, iACs are GABAergic, therefore, could modulate the signals at both OPL and IPL (Dedek et al., 2009). In addition to GABA, iACs can also release dopamine or glycine (Gustincich et al., 1997; Haverkamp and Wässle, 2000). What argues against a role for iACs in mediating interactions between the activity networks in the outer and inner retina is that they do not directly synapse onto outer retinal neurons and that GABA/glycinergic input is expected to only shape (but not drive) the spontaneous activity in the degenerated retina (Biswas et al., 2014) (see 5.4.6).

BCs, on the other hand, participate in both spontaneously active networks (Borowska et al., 2011; Trenholm et al., 2012; Haq et al., 2014). BC-AC connectivity in the degenerated retina is

considered not as severely affected as the BC and photoreceptor connectivity, and the stratification of the second order retinal neurons in the IPL is roughly maintained (Gargini et al., 2007; Phillips et al., 2010) (see also 5.4.2 and 5.4.3). Thus, it is conceivable that BCs play a crucial role as linking neurons in relaying spontaneous signals from the outer to the inner retina in a degenerated tissue. Besides, it is also possible that the signal modulation through this pathway is bidirectional where ACs could also modulate the signals in the outer retina.

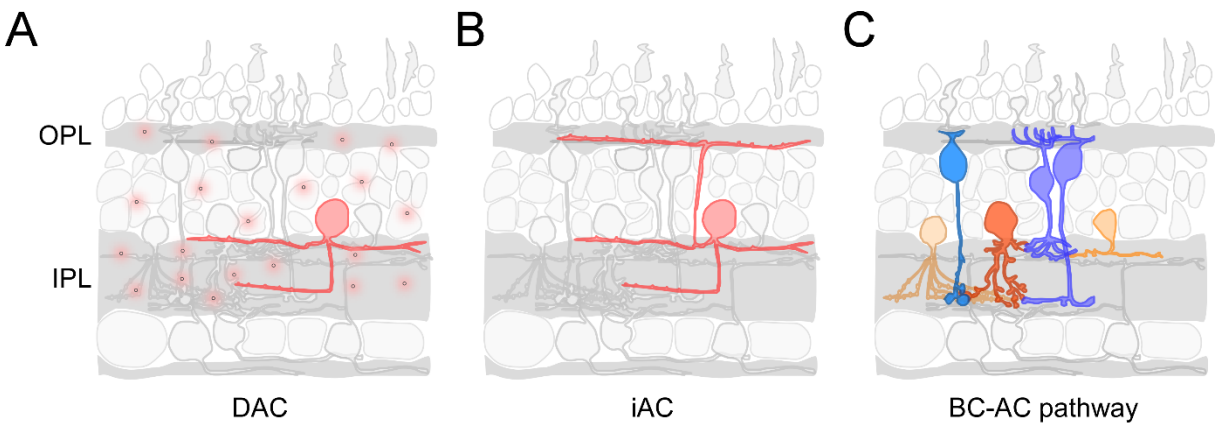

Figure 7. Potential interactive pathways between spontaneously active networks.

Three pathways for interaction between spontaneous networks can be proposed: (A) neuromodulation via dopaminergic amacrine cells (DACs) modulating signals from the inner to the outer retina. (B) GABAergic interplexiform ACs (iACs) that span between OPL and IPL can relay signals from the inner to the outer retina, and (C) signal modulation through BC-AC glutamatergic vertical pathway (Adapted from Euler and Schubert, 2015).

5.4.9 Spontaneous activity at the higher visual centers

Abnormal hyperactivity generated during degeneration is not restricted to the retina, it also spreads further to the higher visual centers of the brain. For example, *in vivo* recordings from the SC of *rd10* mice at P40 revealed spontaneous activity. This hyperactivity was in the range of 4 and 10 Hz, which is comparable to that reported for RGCs (Ivanova et al., 2016a). Similarly, recordings from SC and primary visual cortex in *rd* mice older than 5 months showed spontaneous rhythmic discharges in these regions (Dräger and Hubel, 1978). Interestingly, enucleation or asphyxiation

of the eyes resulted in the disappearance of the activity in the brain (Dräger and Hubel, 1978), confirming its retinal origin. Such degeneration induced spontaneous activity in the retina could further hamper visual perception (Ivanova et al., 2016a). In line with the finding in rodents, a recent study reported altered synchronization of spontaneous activity in the primary visual areas of RP patients as compared to the healthy controls (Dan et al., 2019). Together, it can be concluded that any disruption in the retinal circuitry following photoreceptor degeneration can impair the resting state activity both in the retina and in the higher visual centers of the brain, thus affecting overall visual function.

5.4.10 Spontaneous activity in other diseased animal models

Apart from the study of aberrant activity in *rd10* and *rd1* mice which are autosomal recessive models of RP (see also 5.4), there are various reports in the literature revealing abnormal activity in different models of retinal diseases. In several *rd* models of rats, such as Royal College of Surgeons (RCS) Dystrophic Rats (Pu et al., 2006), P23H rats (Sekirnjak et al., 2011) or S334ter-3 rats (Yu et al., 2017), alterations in spontaneous firing rates in the retinal neurons have been reported. While in the *rd10* and *rd1* mice, spontaneous activity is almost equally affected in different RGC types (Margolis and Detwiler, 2007; Stasheff, 2008; Borowska et al., 2011; Stasheff et al., 2011), in RCS (mutation in retinal pigmented epithelium cells) and P23H (autosomal dominant RP model) rats, spontaneous firing rate is higher in OFF-RGCs compared to ON-RGCs (Pu et al., 2006; Sekirnjak et al., 2011). Cell type-specific alterations in spontaneous activity in RGCs have also been reported in the S334ter-3 rat model of autosomal dominant RP (Yu et al., 2017). Besides, in another mouse model of autosomal dominant RP, rho-ΔCTA, both ON- and OFF-SACs have been shown to display spontaneous activity (Tu et al., 2015). Interestingly, in this model the mechanisms underlying the activity in ON- and OFF-SACs were different. While the AII AC network seems to be involved in the generation of the activity in the ON-SACs, the activity generated in the OFF-SACs appears to be driven by a completely distinct mechanism and thus, may employ an additional generator (Tu et al., 2015). Very likely, the source of the activity in the OFF-SACs relies on periodic glutamate release from the axon terminals of the BCs (Petit-Jacques et al., 2005; Tu et al., 2015).

Mutations in the ON-BC signaling pathway (see 5.2.3) can also lead to the generation of spontaneous activity in retinal neurons. In a TRPM1 knockout mouse model, spontaneous activity has been reported in RGCs (Takeuchi et al., 2018). Here, the activity is probably generated due to structural changes at the axon terminals of RBCs which could result in reduced signal transmission. This could lead to membrane hyperpolarization of the AII ACs further resulting in hyperactivity in the RGCs (Takeuchi et al., 2018). Also, in *nob* (no b-wave) mice, altered ON signaling due to mutation in *nyx* gene (encoding nyctalopin) (Gregg et al., 2003; Gregg et al., 2007) (see also 5.2.3) generates enhanced spontaneous activity in the RGCs (Demas et al., 2006; Winkelman et al., 2019).

Overall, it can be inferred that spontaneous activity is not specific to any mutation, rather it is an outcome of deficit signal transmission which might be accompanied by the remodeling in the synaptic connectivity. Thus, the degeneration induced aberrant activity in retinal neurons is a hallmark across different mutations and rodent models. As RP patients also show acute morphological changes in retinal synapses (reviewed in (Marc et al., 2003; Jones et al., 2012)), it is tempting to argue that such aberrant spontaneous activity is also present in humans.

5.5 Effect of spontaneous activity on the degenerated retinal circuitry

As discussed above, hyperactivity found in retinal neurons or at the higher visual centers can hamper visual processing. Spontaneous activity found at different depths of the retina interferes with the signal transmission, adding more "noise" to the system and thus affecting evoked responses by reducing SNR (Yee et al., 2012). This is evident from altered temporal response properties of the retina with the progression of degeneration (Stasheff, 2008; Stasheff et al., 2011; Yu et al., 2017). It is difficult to link such effects of the aberrant activity observed in animal models of degeneration to symptoms in human patients (i.e. "photopsia", see below). This is because direct evidence showing an increase in spontaneous activity in the neurons of human RP patients is currently not available. People often speculate that "photopsia" found in RP patients is an outcome of the abnormal increase in the activity in the retina (Haq et al., 2014; reviewed in Stasheff, 2018). Photopsia is a discomforting symptom that is often reported by RP patients, who describe this

phenomenon as the perception of bright light flashes or shimmering and flickering lights often in some form of geometric patterns (Bittner et al., 2009). Studies in a large population of patients revealed that photopsia can be present at all phases of the disease (Bittner et al., 2009; Bittner et al., 2011). In general, the patients had photopsia usually in the central retina as compared to the periphery, which often undergoes degeneration at a faster pace. The reduction in visual acuity of the patients with an increase in photopsia suggests that the photopsia indeed interferes with normal vision (Bittner et al., 2011).

Apart from having a significant impact on vision, spontaneous activity has also been predicted to interfere with various visual restoration strategies. Haselier and colleagues (2017) showed that the efficiency of electrical stimulation is significantly decreased in *rd10* retina whenever it is accompanied by spontaneous activity. Moreover, neurons exhibiting rhythmic activity or bursts responded less effectively to the stimulation as compared to non-oscillating neurons (Haselier et al., 2017). Likewise, a study in humans showed that stronger stimulation is required for RP patients as compared to healthy controls (Rizzo et al., 2003). Hence, it is plausible to state that besides technical restrictions, spontaneous activity also contributes to the limitations of the implantation of the electronic retinal chips.

6. Objectives and Contributions

Correlation between spontaneously active networks is one of the prominent features of the (diseased) CNS (see 5.1.2 and 5.1.3). Deviations in the network properties have been designated as a hallmark of neuronal dysfunction in the CNS, depicting them as one of the potential markers for clinical applications (see also 5.1.5). Taking into account the structural and functional complexity of the whole brain, we here used the retina as a model system to investigate the interactions between spontaneously active networks. Thereby, the broad objective of the project was to provide insight into whether and how distinct spontaneously active networks interact with each other.

Unlike healthy retina, the degenerated retina exhibits enhanced spontaneous activity in several retinal neurons (Stasheff et al., 2011; Biswas et al., 2014; Haq et al., 2014) (see 5.4.4). We, therefore, used the *rd10* mouse model of photoreceptor degeneration (reviewed in Chang et al., 2002) for our studies. The degenerated retina comprises of spontaneously active networks in the outer and inner retina (reviewed in Euler and Schubert, 2015) (see also 5.4.5 and 5.4.6). However, being studied only in isolation so far, it is still unclear if and how these two networks interact. Furthermore, as they are structurally connected, they might drive and/or modulate each other (see 5.4.8). Based on their synaptic input and output connections in the outer and inner retina, respectively, BCs are the most likely candidates to relay spontaneous activity from the outer to the inner network in the degenerated retina.

Therefore, the main goals of this study are:

1. Identification and characterization of outer and inner spontaneously active networks at the same location and same tissue in the *rd10* retina.

2. Evaluation of change in activity dynamics of the two networks with the progression of degeneration.

3. Investigation of the role of BCs as potential linking neurons between outer and inner spontaneously active networks in the degenerated *rd10* retina.

4. Understanding the underlying mechanisms of vertical (and lateral) signal transmission of the spontaneous signals in the degenerated *rd10* retina.

In this study, I performed all the experiments (i.e., intravitreal injections, two-photon Ca^{2+} and glutamate imaging), pre-processing and initial analysis of the imaging data. The statistical analysis of these functions and the generation of the respective statistical plots were done by Luke Edward Rogerson (with input from my side).

For the combined two-photon and micro-electrode array (MEA) recordings, I performed intravitreal injections, while all the actual experiments were conducted together with Meng-Jung Lee (PhD student under the supervision of Dr. Günther Zeck, NMI, Reutlingen, Germany). The pre-processing and the analysis of the glutamate imaging data was done by me, while the analysis of the electrical imaging data was performed by Meng-Jung Lee.

7. Methods

7.1 Animals

All experiments were done using the *rd10* (retinal degeneration 10) mouse, a model for autosomal RP (reviewed in Chang et al., 2002). These animals were obtained from The Jackson Laboratory (strain - B6.CXB1-*Pde6b*^{rd10}/J; stock no. - 004297) and bred locally. All animals were maintained under a standard 12 hour light and dark cycle. For experiments, mice between P28 to P92 of either sex were used depending on the experiment type: for the Ca^{2+} imaging experiments, the ages were around P30, 45, 60 and 90, +/- 2 days; for the glutamate imaging experiments, the ages were between P66 and 82. All experiments were performed according to the law on animal protection (Tierschutzgesetz) issued by the German Federal Government and approved by the institutional committee on animal experimentation of the University of Tübingen, Germany.

7.2 Virus injection

For glutamate imaging, an intensity-based glutamate-sensing fluorescent reporter (iGluSnFR) (Marvin et al., 2013) was used to express the biosensor ubiquitously in the retinal neurons of the *rd10* mice through adeno-associated virus (AAV) mediated transduction. The viral construct (AAV2.7m8.hsynapsin.iGluSnFR, obtained from Dr. Deniz Dalkara, Institut de la Vision, INSERM, CNRS, Sorbonne Université, Paris, France) was injected intravitreally in both eyes.

Briefly, animals were first anesthetized with a freshly prepared mixture of 10% ketamine (bela-pharm GmbH & Co. KG) and 2% xylazine (Rompun, Bayer Vital GmbH) in 0.9% NaCl (Fresenius, Germany). Then, with the help of a Hamilton syringe (syringe: 7634-01, needle: 207434, point style 3; length 51 mm, Hamilton, Messtechnik GmbH) mounted on a micromanipulator (M3301, World Precision Instruments, Germany) 1 µl of the viral construct was injected into the vitreous humor of both eyes. All injections were done in 3-5 weeks old *rd10* mice. Imaging experiments were performed 3-4 weeks after the injection.

7.3 Tissue preparation

For all experiments, mice were first dark-adapted for at least one hour and then anesthetized using isoflurane (CP-Pharma, Germany) and sacrificed by cervical dislocation. According to the experiment type, mice were also marked at the ventral position before dissection to trace the orientation while imaging. The dissection was performed under dim red-light conditions (> 650 nm) in carboxygenated (95% O_2 and 5% CO_2) extracellular solution with (in mM): 125 NaCl, 2.5 KCl, 1 $MgCl_2$, 1.25 NaH_2PO_4, 20 glucose, 26 $NaHCO_3$, 2 $CaCl_2$ and 0.5 L-glutamine (pH 7.4). Firstly, the eyes were enucleated and hemisected. After removing cornea and lens, the retina was then subsequently isolated from the eyecup. The vitreous body was carefully removed from the retina. After the dissection, the retina was then flattened and mounted on an Anodisc (#13, 0.2 µm pore size, GE Healthcare) with photoreceptor side facing up as a whole, half or quadrant retina depending on the experiment type.

7.4 Labelling of retinal neurons

For labeling the population of neurons in the retina for Ca^{2+} imaging, a method of bulk electroporation was used (Briggman and Euler, 2011; Baden et al., 2016). The previous parameters were optimized to label somata of neuronal population mostly in the ONL and INL in the degenerated *rd10* retina. To do this, the *rd10* retina was electroporated from the photoreceptor side using a green fluorescent Ca^{2+} indicator, Oregon Green 488 BAPTA-1 (OGB-1). Briefly, a setup with a Petri dish attached with horizontal platinum electrodes of 4 mm in diameter (CUY700P4E/L, Nepagene) was used for the electroporation. The setup consisted of two electrodes: a bottom electrode attached to the Petri dish and a top movable electrode attached to a manipulator. For electroporation, the bottom electrode was first filled with 15 µl of the extracellular solution and the top electrode was loaded with 10 µl of 5 mM OGB-1 dissolved in the extracellular solution. The retina mounted on the Anodisc was then carefully placed on the bottom electrode avoiding any air bubbles. With the help of the manipulator, the top electrode was then brought down until it touches the retina. Next, using a pulse generator and amplifier (TGP 110 and WA301, Thurlby Handar/Farnell), 9-11 pulses were applied (+ 9.5 V, 100 ms pulse width

and 1 Hz pulse frequency) onto the retina. The tissue was then quickly transferred to the recording chamber and kept under continuous perfusion with the extracellular solution at 35-36^{o} C. The recording was started after one hour to allow the tissue to recover.

7.5 Pharmacology

All drugs were prepared as stock solutions in distilled water except UBP-310 which was dissolved in dimethyl sulfoxide (DMSO). The drugs were then aliquoted and stored at -20^{o} C. Before each experiment, the drugs were freshly diluted (Table 1) in a carboxygenated extracellular solution. All drugs were bath applied to the tissue for 10 minutes while continuously being carboxygenated at a maintained temperature between 35-36^{o} C. For the analysis, recordings were performed both before and during drug application at the same location. All drugs were purchased from Tocris Bioscience (Bristol, England). The final concentrations of the drugs applied during the experiments are summarized in Table 1.

Drug	**Target**	**Concentration (µM)**
AP4	mGluR6 receptor agonist	100
AP5	NMDA receptor antagonist	50
NBQX	Unselective AMPA/kainate type glutamate receptor antagonist	100
UBP-310	Selective kainate type glutamate receptor antagonist	50

Table 1. Drugs and their respective targets.

Drugs used with their respective targets and applied final concentrations in micromolar (µM).

7.6 Two-photon imaging

All experiments were performed under dim red-light (> 650 nm) conditions. During recordings, the tissue was always kept under continuous perfusion with carboxygenated extracellular solution

containing 0.5 µM sulforhodamine 101 (SR101; Sigma-Aldrich, Germany) to visualize blood vessels and damaged cells in the red-fluorescence channel.

A custom-designed MOM-type two-photon microscope (Sutter Instruments, Novato, CA and designed by Denk W, MPI for Neurobiology, Martinsried, Germany) (Denk et al., 1990; Euler et al., 2009) was used for imaging. The setup was equipped with a mode-locked Ti:Sapphire laser (MaiTai-HP DeepSEE; Newport Spectra Physics, Germany) tuned to excitation at a wavelength of 927 nm, two fluorescent detection channels and a 20x water-immersion objective lens (XLUMPlanFL, 0.95 NA, Olympus, Germany or W Plan-Apochromat 20x/1.0 DIC M27, Zeiss, Germany). To detect fluorescence emission, photomultiplier tubes (PMTs) with band pass (BP) filters (AHF, Germany) were used; a green channel for OGB-1 (HQ 535/50) or iGluSnFR (HC 510/84) and a red channel for SR101 (HQ 630/60). Data acquisition was done using custom imaging software (ScanM by M. Müller, MPI for Neurobiology, Martinsried, Germany and T. Euler) running under IgorPro 6.3 (Wavemetrics, Lake Oswego, OR, USA) for Windows.

7.6.1 Ca^{2+} imaging

Using two-photon microscopy, spontaneous intracellular changes in the Ca^{2+} levels were measured that arise as a result of subthreshold membrane fluctuations in the retinal neurons. For Ca^{2+} imaging, recordings were done at 64 x 24 pixels (71.5 x 26.8 µm) at a sampling rate of 20.83 Hz. The Ca^{2+} responses were recorded in the dark in the absence of any light stimulus, and from here on are referred to as spontaneous signals. Recordings were focused at the two limiting borders of the INL, referred to as outer and inner retina.

7.6.2 Glutamate imaging

For glutamate imaging, a similar MOM-type setup equipped with an electrically tunable lens (ETL) (EL-16-40-TC, Optotune, Switzerland) was used and customized by Zhao Z, Chagas AM and Euler T (Zhao et al., 2019). The ETL allows rapid change of the focal plane along the z-axis

with the modulation of applied current thus allowing imaging at different depths approximately at the same time (Grewe et al., 2011). The ScanM software was used for scanning. Fast vertical X-Z scanning was done at 64 x 128 pixels (47.6 x 95.3 µm) at a sampling rate of 3.9 Hz to record simultaneously signals from the outer and inner retina.

7.7 Data analysis

7.7.1 Pre-processing

The pre-processing of all the data was done in IgorPro 6 (Wavemetrics, Lake Oswego, USA). For the analysis of the Ca^{2+} imaging data, custom derived scripts from Baden T in IgorPro were used. The data was first detrended by high pass filtering at ~ 0.1 Hz and then normalized by subtracting the mean and dividing by the standard deviation (sd) of the signal. Regions of interests (ROIs) were determined manually corresponding to the somata in the layer using an IgorPro based imaging tool, semi-automated routines for functional image analysis (SARFIA). The resulting ROI mask was also corrected manually in case of any two nearby somata shared one ROI. The Ca^{2+} traces for each ROI were then extracted.

For glutamate imaging, ROIs were determined as described previously (Zhao et al., 2019). Briefly, first, a correlation image was estimated by correlating the trace of each pixel with its eight neighboring pixels and then calculating the mean pixel correlation. A depth specific threshold was then calculated as the 70^{th} percentile of all correlation values along each vertical scan line. This threshold was then used to group neighboring pixels into one ROI. The size of the ROIs was restricted to the size of the cone or BC axon terminals depending on the recording depth at the OPL or IPL, respectively; 4 – 6 µm at the OPL and 2 – 4 µm at the IPL.

7.7.2 Measurement of spontaneous signal dynamics

Spontaneous Ca^{2+} or glutamatergic signals were recorded in the absence of any light stimulus under a two-photon microscope. For quantifying the strength of the spontaneous signals, two methods were evaluated: log cumulative autocorrelation function (log-cACF) and power spectral density (PSD).

The log-cACF was used as a measure of spontaneous signals of our data (also discussed in the Results section, Fig. 10). Autocorrelation is a measure of the linear correlation of the signal with itself over multiple time lags; intuitively, it determines how similar or smooth the signal is over time (Eq. 1).

(1) $$E[(y_t - \mu)(y_{t+n} - \mu)]/\sigma^2 = ACF_n$$

where y_t is a time-varying signal, y_{t+n} denotes time lag, μ and σ are the mean and standard deviation of the signal, respectively.

The ACF computes the sum of the linear correlation coefficients, between a signal at a time *t* and the signal at a lagged time *t+n,* where each lag *n* ranges from 0 to 3 seconds. The cACF is then calculated as the sum of the positive elements of the ACF (Eq. 2).

(2) $$\sum_{n=1}^{N} \begin{cases} ACF_n & if\ sgn(ACF_n) = 1 \\ 0 & if\ sgn(ACF_n) <= 0 \end{cases}$$

As the distribution of the statistic was bounded and skewed, a log transform was used to stabilize the variance.

The PSD was computed using a Discrete Time Fourier Transform (DTFT), to quantify the power spectrum of different frequencies in a signal (Eq. 3).

(3) $$PSD_k = \left|\sum_{t=0}^{T-1} y_t e^{-i2\pi kt/T}\right|^2$$

Where *k* is the frequency of the Fourier basis function.

The Gaussianity of both the ACF and PSD approach was systematically evaluated to identify a suitable approach. This was done by using QQ-plots which was then tested for the goodness of the fit using Kolmogorov-Smirnov (KS) tests. While both the methods were suitable for characterizing

the spontaneous signal dynamics, the log-cACF approach was adopted as a measure of spontaneous signals based on lower KS test statistics.

7.7.3 Statistical modeling

Spatio-temporal modeling

To estimate the linear or non-linear relationship between the variables, we fitted the data to a statistic model, generalized additive model (GAM) optimized to the REML criterion from the *mgcv* package in R (Hastie and Tibshirani, 1986; Wood et al., 2016).

To explain the variability among the signals as a function of age and depth, the log-cACF was modeled as the sum of a linear function for each population (outer/inner retina) and a smooth function for each population, which varied with age (Eq. 4).

$$log\ (cACF) = a\ +\ b_1 x_{population} +\ f_{population}(x_{age}) \quad (4)$$

Eccentricity factor was also sequentially incorporated into the model to examine the effect of retinal location as a function of age on log-cACF (Eq. 5). Eccentricity was defined as the Euclidean distance from the optic disc to the recording field (in μm). The effect of eccentricity was evaluated with additional components, the first encoding for the spatial variation for each population as a smooth function of eccentricity, and the second encoding for a temporal variation estimating a non-linear interaction between age and eccentricity.

$$log(cACF)\ = a\ +\ b_1 x_{population} +\ f_{population}(x_{age}) +\ f_{population}(x_{ecc}) + f_{population}(x_{age},\ x_{ecc}) \quad (5)$$

Each component of the model was also evaluated for significance using Wald tests, whereby the full model fit was compared to alternative models where each component has been excluded. The models were compared using ANOVA, with the improved model fit to be significant ($p < 0.001$).

Drug effects

To analyze the effect of drug application, a mixed effects model was used and optimized with respect to the REML criterion, from the lme4 package in R (Bates et al., 2015) (Eq. 6).

$$(6) \quad log(cACF) = a + b_1 x_{population} + b_2 x_{drug} + b_3 x_{population,drug} + b_{4,id} x_{id}$$

The effect of the drug was modeled as a change from the baseline log-cACF, a, for each population, $x_{population}$ and in each drug condition, x_{drug}. A linear interaction between the population and drug condition was also added to infer the differences in the sensitivities to the two drug conditions between the two populations, $x_{population,drug}$. A parameter, (x_{id}) was incorporated to estimate the baseline level of activity in each recording to control for variability between recordings (Eq. 6).

7.7.4 Clustering method for correlation analysis

Hierarchical clustering

Each ROIs determined in the vertical scans were clustered by Ward hierarchical clustering algorithm and linear correlation as the measure of the distance between each pair of ROIs, from the *scipy.hierarchical* package in Python 3. The dendrogram generated from this algorithm was cut using a distance threshold, which was varied between one and six to evaluate the impact of the parameter on the number of clusters. To measure the cluster quality, a suitable threshold was identified using a clustering metric, the Silhouette coefficient (Rousseeuw, 1987). A threshold of 1.75 was used for our analysis as a compromise between the number of clusters and the cluster quality.

Depth alignment

To account for the variability in the retinal thickness present in the degenerated retina and to control for the vertical jitter during vertical scan imaging, a method of depth alignment was developed. This allowed correction for recording with bands of varying thickness. The alignment was performed for each glutamate imaging field. For each row in a vertical scan recording with *X*

columns and *Y* rows, the mean intensity of each pixel, with the intensity *I* and position *x,y* was calculated (Eq. 7). The cumulative sum of mean intensities was then computed (Eq. 8) and normalized such that it ranged from 0 to 1 (Eq. 9). The normalized cumulative sum $\widetilde{D}_y$ for each row was then treated as a surrogate for the depth of each pixel.

(7) $$\hat{p}_{y,i} = \sum_{x=1}^{X} p_{x,y,I}$$

(8) $$D_y \sum_{y=1}^{k} \hat{p}_{y,i} \ for\ k = 1,2 \dots Y$$

(9) $$D_y / D_Y = \widetilde{D}_y$$

As the fluorescent signals in the recording field are concentrated at the synaptic terminals, the labeling can be seen only at the OPL and IPL. $\widetilde{D}_y$ therefore, it corresponds to the position of a particular ROI with respect to the range of these layers. The operation was implemented in Python 3. An additional smoothing step was incorporated with a Savitzky-Golay filter, from the *scipy.signal* package, which further reduces the variability in each cluster.

Pairwise correlation

To determine the relationship between each pair of clusters identified in the vertical scan imaging, a pairwise linear correlation was quantified where each pair comprised of one ROI from each cluster between OPL and IPL. To examine the effect of drug application and to estimate the statistic for the same, the median, 10^{th} and 90^{th} centile of the pairwise linear correlations between pairs of ROIs from each cluster was done. The 90^{th} centile of the pairwise correlation was found to have the greatest variability between the control and drug condition. This was then further adapted to quantify the strength of the linear correlation between the pair of clusters.

8. Results

The degenerated retina displays enhanced spontaneous activity in several retinal neurons which supposedly form networks in the outer and inner retina (reviewed in Euler and Schubert, 2015) (see 5.4.7). As previous studies on spontaneous activity have largely focused on either outer or inner retinal networks individually, it is still unclear whether the two networks co-exist at the same location and retinal tissue. Furthermore, to which extent the networks interact is also not clear.

Spontaneous activity in the outer and inner network displays diverse spatio-temporal patterns of activity which might be an outcome of a complex interaction between these networks. To assess the interaction between the two networks at both somatic and synaptic levels in the degenerated *rd10* retina, two imaging configurations were used: (1) a population imaging paradigm to record large groups of cell somata, and (2) a vertical imaging configuration to capture near-simultaneous glutamatergic transmission at the synaptic terminals in OPL and IPL.

8.1 Spontaneous Ca^{2+} signals are present in the outer and inner retina at the same location

Our first objective was to establish whether spontaneous signals occurred in both networks at the same location. To this end, we labeled retinal somata with the synthetic Ca^{2+} indicator, Oregon Green 488 BAPTA-1 (OGB-1) by bulk electroporation of the whole-mounted retina from the photoreceptor side (see also 7.4). This allowed labeling in a large population of remnant cones in the ONL, BCs, and ACs in the INL and sparse labeling in the GCL (Fig. 8A, B). We used two-photon microscopy, to record spontaneous Ca^{2+} signals from the somata of the neuronal population (see 7.6.1). We focused our recordings onto two neuronal populations; RBCs and AII ACs. Both neurons have been shown to actively participate in the outer and inner spontaneously active networks; RBCs being strongly active in the degenerated outer retina (Haq et al., 2014), and AII ACs playing an essential role in the generation of the activity in the inner retina (Trenholm et al., 2012; Choi et al., 2014) (see also 5.4.5 and 5.4.6).

In wild-type retina, RBC and AII AC somata usually reside at the two extreme borders of the INL; RBCs at the outermost part of the INL (near OPL border) (Haverkamp and Wässle, 2000) and AII ACs at the innermost part of the INL (near IPL border) (Strettoi et al., 1992; Rice and Curran, 2000). The locations of the somata of these neurons also seem to be consistent in the degenerated retina (Gargini et al., 2007; Barhoum et al., 2008). Therefore, we recorded from the outermost and innermost borders of the INL where the somata of RBCs and AII ACs are expected to be present; these locations from here on referred to as outer and inner retina (Fig. 8C). Though we assumed that the outer retinal recording location contains mostly RBC somata, it is possible that the somata of other neurons such as remnant cones or HCs are also present at this location.

Consecutive somatic population recordings were performed from the outer and inner retinal locations at the same X-Y position which from hereafter referred to as "dual recordings". Dual recordings were performed only at the locations where spontaneous signals were observed in both outer and inner retina. To confirm recording depths, we compared the distribution of the recording locations (recording densities) and somatic distribution profiles of the neurons in the INL obtained from electron microscopy (EM) data published by Helmstaedter et al. (2013) (Fig. 8D). We found that the outer and inner retinal recording densities approximately matched with the somatic densities of the RBCs and AII ACs in the INL as estimated by the EM data from Helmstaedter et al. (2013) (Fig. 8D). Due to sparsity of the labeling and because the spontaneous activity in the RGC population, which we also observed, relies on the glutamatergic input from the presynaptic neurons in the inner retina (Biswas et al., 2014), signals from the GCL were not considered into these experiments.

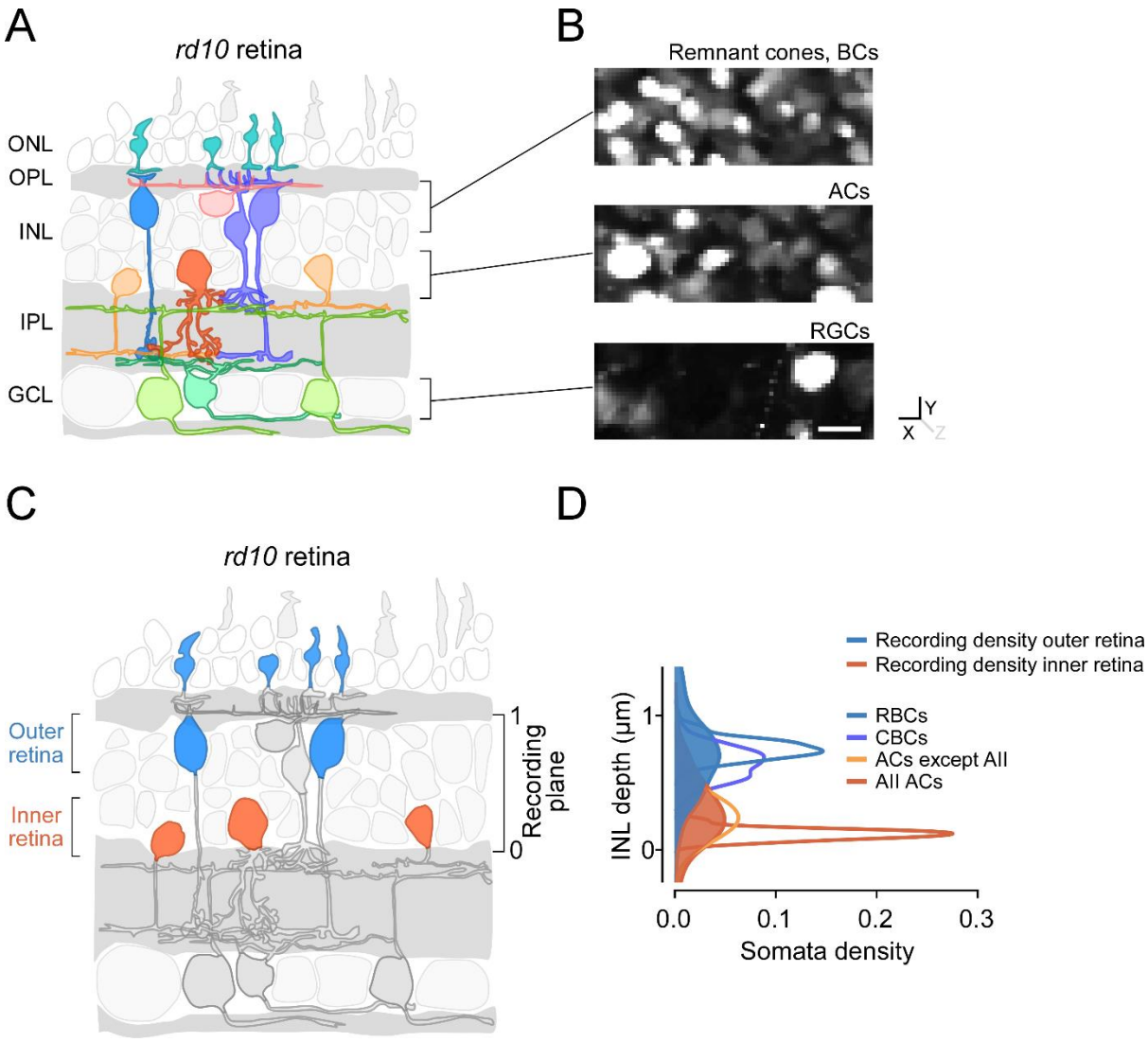

Figure 8. Identification of the spontaneously active networks in the degenerated *rd10* retina.

(A) Schematic representation of the organization of the retinal neurons in the degenerated *rd10* retina (Adapted from Euler and Schubert, 2015). (B) Whole-mounted Oregon Green 488 BAPTA-1 (OGB-1) electroporated retina of a *rd10* mouse at P30 and recorded under the two-photon microscope showing cell somata labeled in the ONL and outer INL (remnant cones/BCs, top), inner INL (ACs, middle) and GCL (RGCs, bottom). Lines from the schematic (front view) in (A) indicates the recording locations (top view) in the same X-Y plane but at varying depths. (C) Schematic representing outer (blue) and inner (orange) retina recording locations. 1 and 0 indicate reference points for the extent of the INL. Recording planes were focused on the extreme borders of the INL. (D) The distribution of recording locations (recording densities) was compared with the distribution of the somatic density profiles of different cell types in the INL from electron microscopy data obtained from Helmstaedter et al. (2013). The dataset was rotated to match the angle of the recordings (Behrens et al., 2016). The distribution of the recording densities and the

somatic density profiles of the retinal neurons in the INL were then aligned to match the reference point in (C). The densities were estimated using Scott's rule. Cell densities of the INL population are indicated by solid lines and differentiated by colors as in (A) while the recording densities color coded as in (C) for outer and inner retina are additionally shaded. Scale bar, 10 μm (B).

To compare the features of the outer and inner retinal spontaneous Ca^{2+} signals at the population level, a series of dual recordings were acquired (Fig. 9A, B) and the time-series of the spontaneous signals of each cell soma was extracted (Fig. 9C). Such recordings were also performed at different time points of degeneration P30, 45, 60 and 90, as major structural remodeling is expected to occur during this timeline (5.4.1).

In total, spontaneous somatic Ca^{2+} signals were measured from both outer and inner retina at 112 retinal locations from 27 experiments (Table 2). Interestingly, the population imaging revealed a high degree of heterogeneity in the signal dynamics in the outer and inner retina (Fig. 9C). The signals usually displayed slow transient non-oscillatory activity (Fig. 9C, example trace 12), but sometimes oscillatory activity was also observed (Fig. 9C, example trace 9). At a given location, there were few cells that did not belong to these two categories and exhibited highly uncorrelated activity (Fig. 9C, example traces 4 and 14). All these activity patterns were included in our analysis.

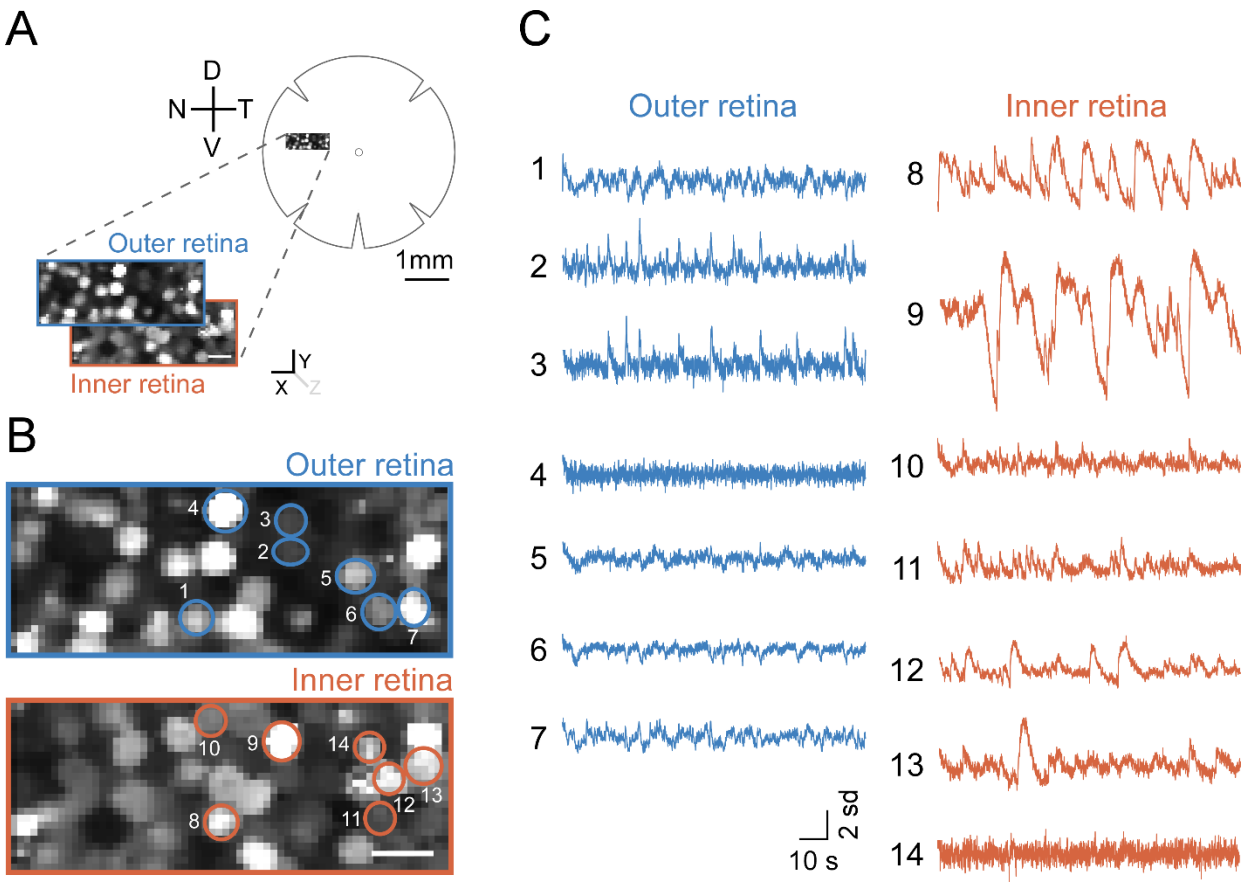

Figure 9. Spontaneous Ca^{2+} signals are present at the same location in both outer and inner retina and exhibit heterogeneity.

(A) Schematic representation of the two-photon Ca^{2+} imaging from the somata of the outer and inner retinal cell population in the degenerated *rd10* retina. In a whole-mounted OGB-1 electroporated retina, dual recordings were made from the soma of both cell populations, at the same X-Y location. (B) Example scan field of a dual recording from the outer and inner retina in a *rd10* mouse at P60. Regions of interests (ROIs) of the cell somata are highlighted in circles and color coded (blue: outer retina; orange: inner retina). (C) Spontaneous Ca^{2+} signals of the corresponding highlighted cells in (B) from both outer (blue) and inner (inner) retina. Only some examples of all active cells are shown. Scale bars, 10 µm (A and B).

8.2 Characterization of spontaneous Ca^{2+} signal dynamics

Next, we wanted to identify a method to quantify the variability we observed in the signal dynamics, and to differentiate the temporal patterns. To this end, we first computed the power spectral densities (PSD) of the signals for all our recordings using the Discrete Time Fourier Transform (DTFT) method (Fig. 10A, B) (see 7.7.2). We found that for a highly uncorrelated activity, periodogram was flat (Fig. 10A, B, top) while for a correlated activity, the periodogram had a high power at low frequency (< 2 Hz) (Fig. 10A, B, bottom). When compared for all the recordings in the outer and inner retina, we only found high power at low frequencies (< 2 Hz) for all the cells (both oscillatory and non-oscillatory) (Fig. 10D). Hence, this method did not enable us to resolve the variability in the signal patterns observed.

Instead, we calculated the log cumulative autocorrelation function (log-cACF) to characterize the temporal features of the signals. Autocorrelation is a measure of the linear correlation of the signal with itself over multiple time lags (Fig. 10A, C) (see 7.7.2). We found that that the correlation curve for a cell showing uncorrelated activity was flat with a value close to 0 (Fig. 10A, C, top) while a cell showing highly correlated activity had a value close to 1 (Fig. 10A, C, bottom). When compared for all recordings in the outer and inner retina, for most of the cells signals were autocorrelated to varying degrees at a given time lag representing variability in the signal dynamics (Fig. 10E). Thus, the log-cACF approach allowed us to distinguish heterogeneity observed in the signal patterns, hence we adapted it for further analysis.

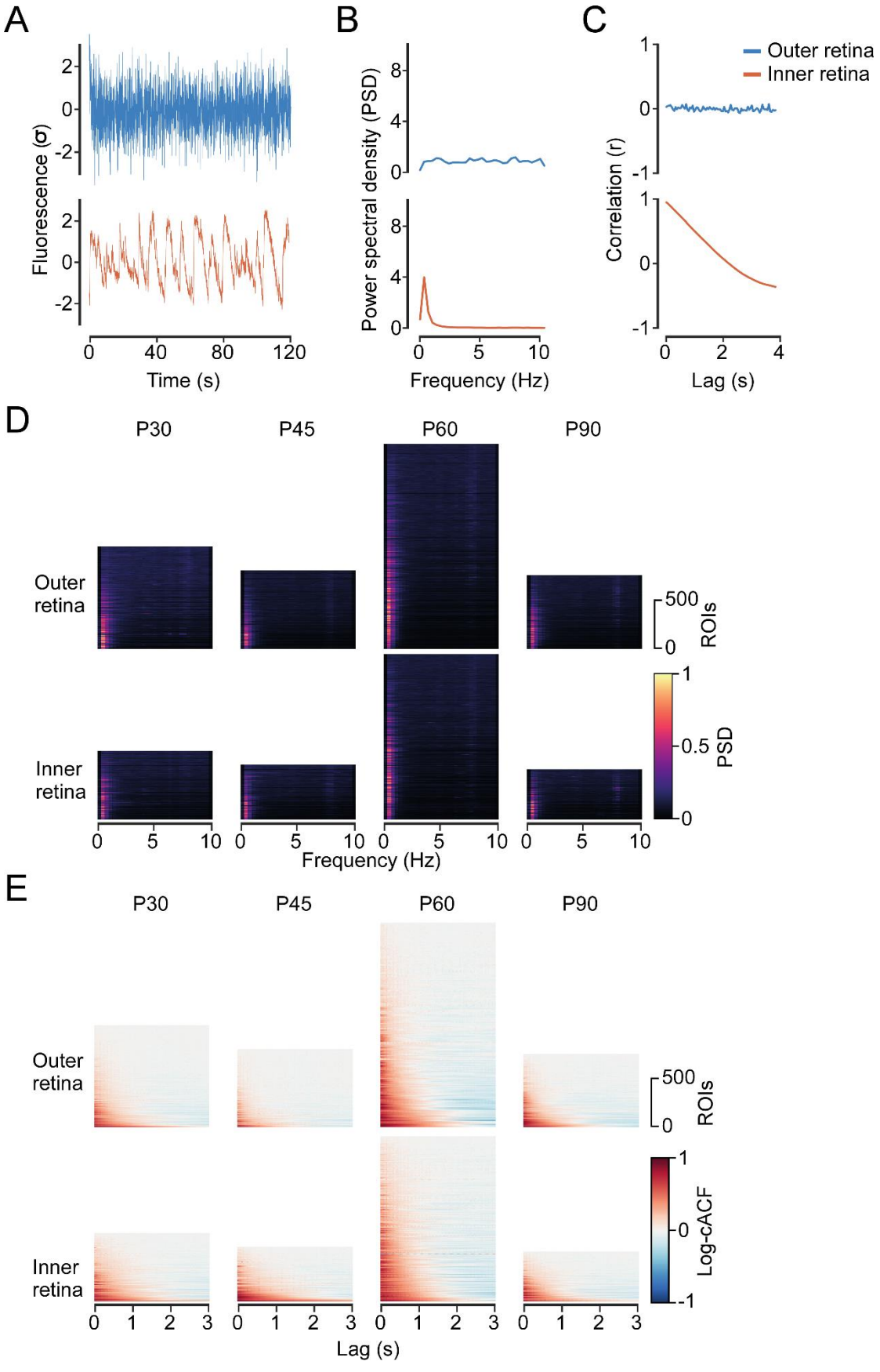
A
Fluorescence (σ)
2
0
-2
2
0
-2
0
40
80
120
Time (s)
B
Power spectral density (PSD)
8
4
0
8
4
0
0
5
10
Frequency (Hz)
C
Outer retina
Inner retina
Correlation (r)
1
0
-1
1
0
-1
0
2
4
Lag (s)
D
P30
P45
P60
P90
Outer retina
Inner retina
500
0
ROIs
1
0.5
0
PSD
0
5
10
Frequency (Hz)
E
P30
P45
P60
P90
Outer retina
Inner retina
500
0
ROIs
1
0
-1
Log-cACF
0
1
2
3
Lag (s)

Figure 10. Characterization of spontaneous Ca^{2+} signals.

(A) Example traces for spontaneous somatic Ca^{2+} signals from both outer and inner retina corresponding to two ROIs in Fig. 9B, C (example traces 4 and 8). Traces are color coded for outer (blue) and inner (orange) retina. Subsequent plots correspond to these ROIs. (B) Periodograms for each ROIs and, (C) plot showing the change in correlation value over time. (D) Heatmaps showing PSDs, and (E) log-cACF for all dual recordings done at different time points. Each row in the heatmaps (D and E) represents a ROI. All ROIs are included and sorted for the outer (#ROIs = 4696) and inner retina (#ROIs = 3322). Height scaled to its relative ROI number at that corresponding age (Table 2). (n = 8/8/24 mice/retinas/scan fields for P30, 4/4/20 for P45, 10/10/48 for P60 and 5/5/20 for P90).

Age	Preparation	Indicator	Sampling rate (Hz)	Number of mice/retina/scan fields	Number of ROIs in outer retina	Number of ROIs in inner retina
P30	full (WM)	OGB-1	20.83	08/08/24	1020	604
P45	full (WM)	OGB-1	20.83	04/04/20	780	518
P60	full (WM)	OGB-1	20.83	10/10/48	2154	1720
P90	full (WM)	OGB-1	20.83	05/05/20	742	480

Table 2: Summary table for dual Ca^{2+} recordings in the outer and inner *rd10* retina

Experimental conditions shown for Ca^{2+} recordings at postnatal day (P) 30, 45, 60 and 90; whole-mount (WM); Oregon Green 488 BAPTA-1 (OGB-1); Regions of interest (ROIs).

8.3 Spatio-temporal changes in the signal dynamics in both outer and inner retina

The degeneration of the retina progresses as a function of age and retinal location. While distinctive structural remodeling occurs between P30 and P90 (Gargini et al., 2007; Barhoum et al., 2008; Phillips et al., 2010) (see 5.4.1 to 5.4.3), it is also believed that the degeneration follows a central to peripheral trend in the disease advancement (Gargini et al., 2007; Barhoum et al., 2008) (see

5.4.1). Hence, if there is an interaction between outer and inner retinal networks, this may be altered by structural remodeling which follows disease progression.

To investigate how spontaneous signal dynamics in the outer and inner retinal populations vary with age and location, dual recordings were performed from the outer and inner retina at different time points of degeneration at P30, 45, 60, and 90, and at varying eccentricities (Fig. 11A). Again, the log-cACF approach was employed to quantify spontaneous signals. To infer how the relationship between the signals changes over time and across the retina, a statistical generalized additive model (GAM) was used (see 7.7.3).

We found a significant difference in the baseline activity between the outer and inner retina ($p < 0.001$; Table 3), which also varied for both with age (both outer retina and inner retina: $p < 0.001$; Fig. 11B; Table 3). We used GAM to quantify the difference in the mean baseline activity between inner and outer retinal populations at different ages. We found that while the difference was larger between P30 and P45, the difference decreased at later time points of degeneration (between P60 and P90) (Fig. 11B; Fig. 12A).

With respect to eccentricity, we found a significant change in the signal dynamics in both outer and inner retina (outer retina: $p < 0.001$; inner retina $p = 0.0002$; Table 3). The GAM identified a significant non-linear relationship between eccentricity and age (both outer and inner retina: $p < 0.001$; Fig. 11C, D; Table 3). Based on our model predictions, we predicted the difference in the mean baseline activity at the central (500 μm) and mid-peripheral (1500 μm) region for both populations at different ages. We found that in both populations, there was a significant difference in the mean activity at these eccentricities (500 and 1500 μm) between P30 and P45 than at later time point (P60 and P90), however, the difference was larger for the outer retina as compared to the inner retina (Fig. 11C, D; Fig. 12B, C). We also observed significant variability in the signal dynamics between the two populations across eccentricity at P30 and P45 which greatly reduced between P60 and P90 (Fig. 11C).

Together, our data suggest that there are spatio-temporal changes in the signal dynamics between the outer and inner retinal populations such that they become more similar with disease progression.

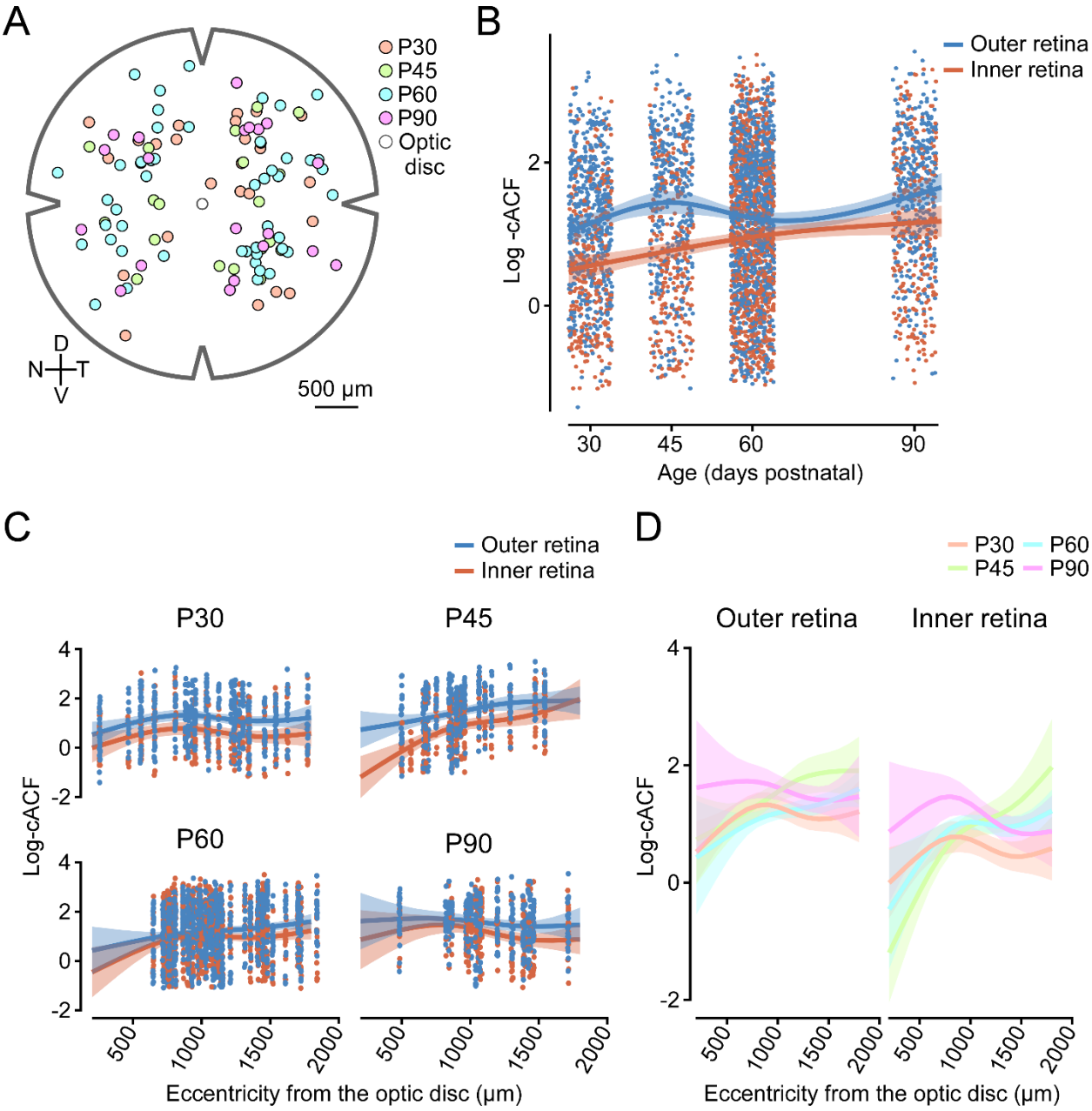

Figure 11. Spatio-temporal changes in the signal dynamics of both outer and inner retina.

(A) Spatial distribution of all dual recordings with respect to the retina at different time points of degeneration (P30, 45, 60 and 90). Each circle represents a dual recording location, at different retinal eccentricities from the optic disc. The circles are color coded for different ages. (B) Plot showing change in log-cACF in the outer and inner retina with age. Each dot represents a ROI at that corresponding age at P30 (1020 ROIs, outer retina; 604 ROIs, inner retina), P45 (780 ROIs, outer retina; 518 ROIs, inner retina), P60 (2154 ROIs, outer retina; 1720 ROIs, inner retina) and P90 (742 ROIs, outer retina; 480 ROIs, inner retina) (Table 2). (C) Change in log-cACF with respect to eccentricity from the optic disc for both outer and inner retina at different time points.

Each dot represents a ROI at that recording location. (B and C) Mean activity is shown in bold; intervals indicate +/- 3 standard errors. Color encodes for outer (blue) and inner (orange) retina. (D) Same as in (C) but representing the change in log-cACF with eccentricity at different time points. (n = 8/24 retinas/scan fields for P30, 4/20 for P45, 10/48 for P60 and 5/20 for P90).

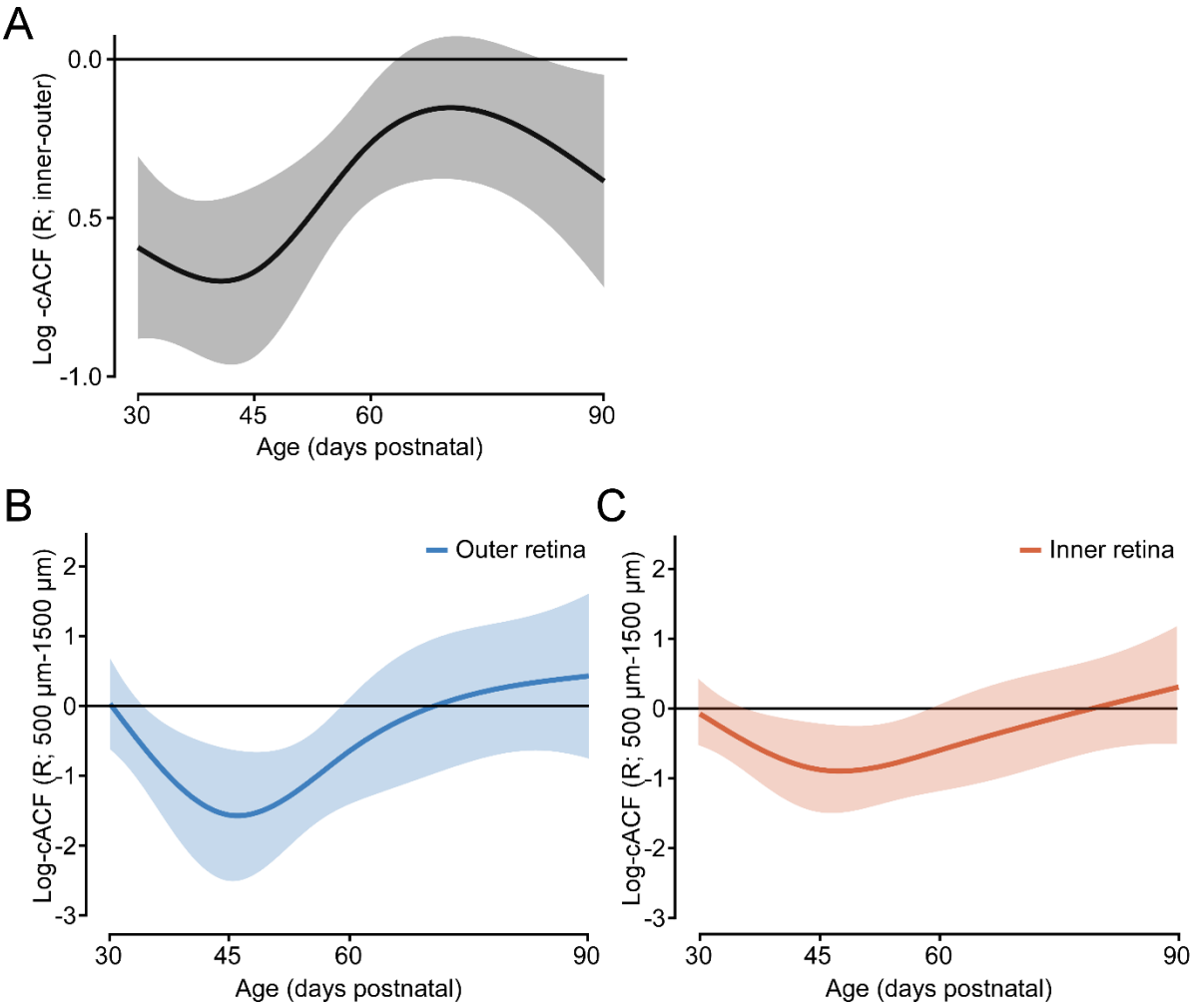

Figure 12. Statistical analysis showing spatio-temporal variation with disease progression

Predictions of the generalized additive models (GAM) corresponding to the plots showing (A) difference in baseline activity measured by log-cACF between inner and outer retinal population with age, and (B, C) difference in the baseline activity at 500 and 1500 µm Euclidean distance from the optic disc at different time points in both outer (B) and inner (C) retinal populations. Mean activity is shown in bold; intervals indicate +/- 3 standard errors. 0 indicates no significant difference between the two populations when it is outside of the intervals (A-C).

Model:

$$log(cACF) = a + b_1 x_{population} + f_{population}(x_{age}) + f_{population}(x_{ecc}) + f_{population}(x_{age}, x_{ecc})$$

Components	**Parameter**	**Significance**	**Interpretation**
a	1.31367	p < 0.0001	Baseline
$b_1 x_{population}$	-0.39643	p < 0.001	Difference in baseline for inner and outer retina
$f_{population}(x_{age})$ (outer)	N/A	p < 0.001	Change with respect to age for outer retina
$f_{population}(x_{age})$ (inner)	N/A	p < 0.001	Change with respect to age for inner retina
$f_{population}(x_{ecc})$ (outer)	N/A	p < 0.001	Change with respect to eccentricity for outer retina
$f_{population}(x_{ecc})$ (inner)	N/A	p = 0.0002	Change with respect to eccentricity for inner retina
$f_{population}(x_{age}, x_{ecc})$ (outer)	N/A	p < 0.001	Interaction between eccentricity and age for outer retina
$f_{population}(x_{age}, x_{ecc})$ (inner)	N/A	p < 0.001	Interaction between eccentricity and age for inner retina

Table 3. Summarized statistics for dual Ca^{2+} recordings in outer and inner *rd10* retina with respect to age and eccentricity.

Cumulative autocorrelation function (cACF); eccentricity (ecc); not applicable (N/A).

8.4 Slow spontaneous Ca^{2+} signals in the inner retina rely on glutamatergic input

We next investigated the possible sources of interaction between the spontaneously active networks of the outer and inner retina. The participation of BCs in both networks (Borowska et al., 2011; Trenholm et al., 2012; Haq et al., 2014) makes them prime candidates for relaying signals from the outer to the inner retina (see also 5.4.8).

To test whether the signals observed in the inner retina were a consequence of the outer retinal activity mediated by the BC's glutamatergic transmission, the input from the BCs to the ACs was pharmacologically blocked by co-applying the ionotropic glutamate receptor antagonists NBQX and AP5 (Fig. 13A). Dual recordings were conducted before and during the drug application. We then used log-cACF as a measure of spontaneous signals and quantified the effect of the drug on the signal dynamics using linear mixed models (see 7.7.3). We analyzed a total of 732 ROIs (441 outer; 291 inner; Table 4) obtained from 10 scan fields and found a significant reduction in slow signal dynamics in both outer and inner retina during the drug application as compared to the control condition ($p < 0.001$; Fig. 13B, C; Table 5).

To examine the change in signal dynamics of the two populations after completely extinguishing the input at the BC dendrites, we supplemented our drug mixture (NBQX + AP5) with a mGluR6 agonist, AP4 (Fig. 13A). This resulted in blocking input at both ON- and OFF-BC dendrites mediated by metabotropic and ionotropic glutamate receptors, respectively (reviewed in Dhingra and Vardi, 2012; Puller et al., 2013) (see 5.2.3). We found a significant reduction in slow signal dynamics in both the outer and inner retinal populations during the drug application as compared to the control condition ($p < 0.001$; Fig. 13B, C; Table 5). However, we did not find any significant difference in the signal dynamics between the two drug conditions (NBQX + AP5 and NBQX + AP5 + AP4) ($p = 0.197$; Table 5). This suggests that AP4 did not have any additional effect, possibly because the slow spontaneous signals have been almost entirely abolished under the first drug condition (NBQX + AP5).

Together, our data indicates that the slow dynamic signals in the inner retina depend on the glutamatergic drive from the outer retina and are primarily mediated by ionotropic glutamate receptors, though certain mGluR types, particularly mGluR4, 7 and 8, expressed on ACs may also

contribute (Brandstätter et al., 1996; Koulen and Brandstätter, 2002; Quraishi et al., 2007; reviewed in Dhingra and Vardi, 2012) (see also 5.2.4). The decrease in slow signal dynamics (and the potential increase in the frequency of events) observed in the outer retina during the application of NBQX and AP5 is consistent with an earlier study, where it was suggested to be a result of reduced inhibition from HCs (Haq et al., 2014). Further, reduction in slow signal dynamics by adding AP4 may result from uncoupling between remnant cone and RBC activity clusters formed during degeneration (Haq et al., 2014) (see 5.4.5).

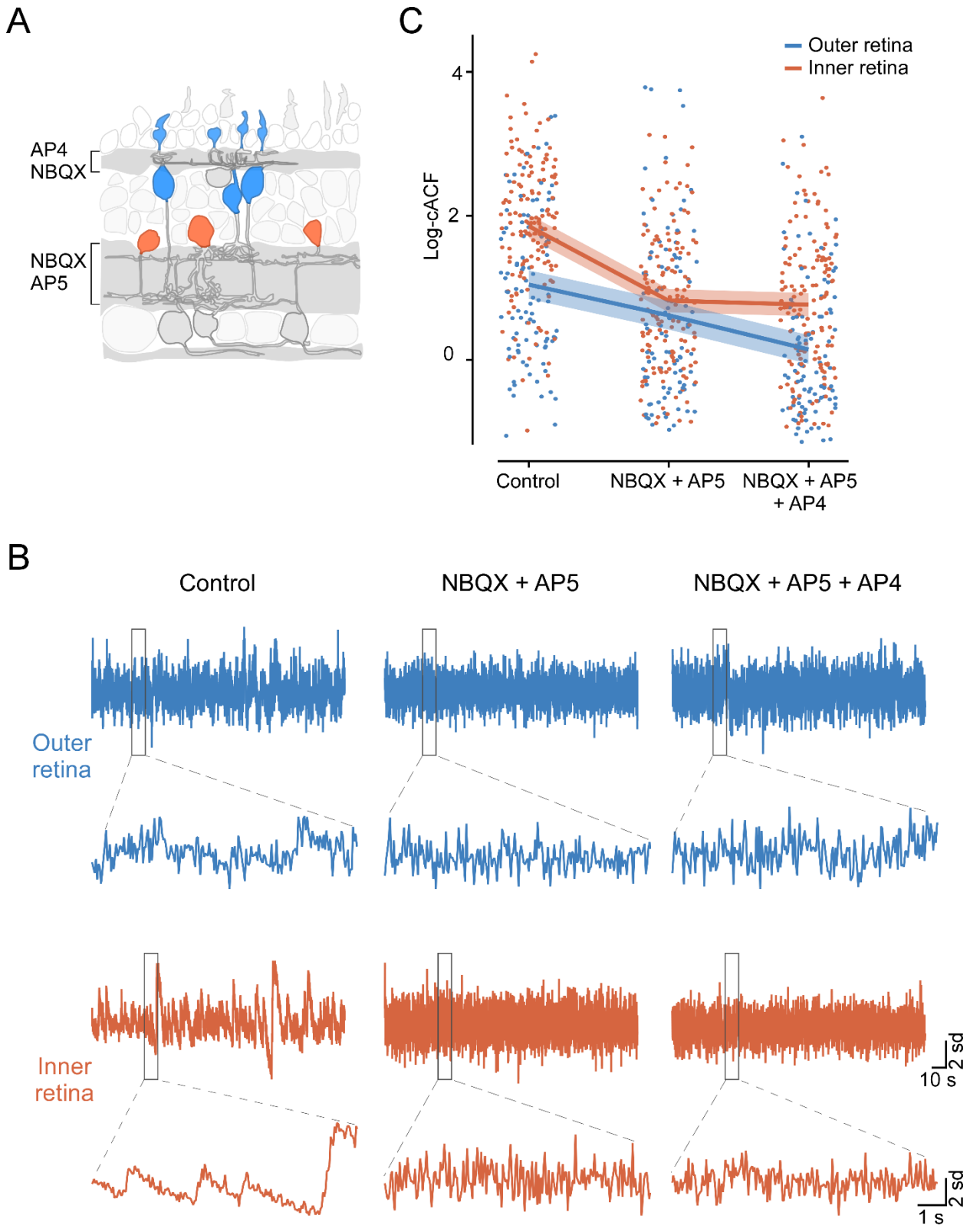
A
AP4
NBQX
NBQX
AP5
C
Outer retina
Inner retina
Log-cACF
4
2
0
Control
NBQX + AP5
NBQX + AP5
+ AP4
B
Control
NBQX + AP5
NBQX + AP5 + AP4
Outer
retina
Inner
retina
2 sd
10 s
2 sd
1 s

Figure 13. Slow spontaneous Ca^{2+} signals in the inner retina rely on glutamatergic input from the outer retina.

(A) Schematic representation of the location of action of NBQX, AP5, and AP4 in the retinal circuitry. (B) Example traces of spontaneous Ca^{2+} signals from a dual recording before and during first (NBQX + AP5) and second drug (NBQX + AP5 + AP4) condition. Each box indicates a snippet of 10 seconds of the corresponding trace with its enlarged view shown below. (C) Quantitative analysis of both drug conditions in the outer and inner retina using log-cACF. Each dot represents a ROI (#ROIs = 441, outer retina; 291, inner retina) in control and drug condition. The ROIs were assigned the same number for control and the two drug conditions. Solid lines indicate mean change with their standard error confidence intervals from the mixed effects model. Color in (B) and (C) corresponds to the outer (blue) and inner (orange) retina. (n = 10 scan fields,10 retina halves from 4 mice; all at P45; Table 4).

Age	**Preparation**	**Sampling rate (Hz)**	**Number of mice/retinas /scan fields**	**Number of ROIs in outer retina**	**Number of ROIs in inner retina**	**Drug condition**
P45	half retinas (WM)	20.83	04/10/10	441	291	NBQX + AP5 + AP4

Table 4. Pharmacological analysis for Ca^{2+} signals in the outer and inner *rd10* retina.

Experimental conditions are shown for *rd10* recordings at postnatal day (P) P45; whole-mount (WM); NBQX, AMPA/kainate type glutamate receptor antagonist; AP5, NMDA receptor antagonist; AP4, mGluR6 receptor agonist.

Model: $log(cACF) = a + b_1 x_{population} + b_2 x_{drug} + b_3 x_{population,drug} + b_{4,id} x_{id}$			
Components	**Parameter**	**Significance**	**Interpretation**
a	1.85525	$p < 0.001$	Baseline
$b_1 x_{population}$	-0.81194	$p < 0.001$	Difference in baseline for inner and outer retina in control condition

$b_2 x_{drug}$ (NBQX + AP5)	N/A	p < 0.001	Change in baseline activity under first drug condition
$b_2 x_{drug}$ (NBQX + AP5 +AP4)	N/A	p < 0.001	Change in baseline activity under second drug condition
$b_3 x_{population,drug}$ (NBQX + AP5)	N/A	p < 0.001	Difference in drug effect (first condition) between outer and inner retina
$b_3 x_{population,drug}$ (NBQX + AP5 + AP4)	N/A	p = 0.197	Difference in drug effect (second condition) between outer and inner retina
$b_{4,id} x_{id}$	N/A	p < 0.001	Variation in baseline activity between recordings

Table 5. Summarized statistics for pharmacological analysis for Ca^{2+} recordings in the outer and inner *rd10* retina.

Cumulative autocorrelation function (cACF); NBQX, AMPA/kainate type glutamate receptor antagonist; AP5, NMDA receptor antagonist; AP4, mGluR6 receptor agonist; not applicable (N/A).

8.5 Simultaneous spontaneous glutamatergic signals are present in the outer and inner retina at the same location

Our finding at the somatic level showed that blocking glutamatergic signal transmission from the BCs to the ACs affects signal dynamics in both populations (Fig. 13). To further investigate the direction of signal transmission along the vertical BC-AC pathway, we next wanted to assess this connectivity at the synaptic level. To this end, we expressed the glutamate biosensor iGluSnFR, ubiquitously in the retina through intravitreal injection of AAVs (see 7.2). We measured the change in glutamate release at both input and output synapses of the BCs, i.e., in the OPL and IPL, respectively, using two-photon microscopy (see 7.6.2).

To determine the direct synaptic interaction between the networks, it is also important that the signals are recorded at the same location and time. We achieved this by using a two-photon

microscope equipped with an electrically tunable lens (ETL) (Zhao et al., 2019) (see also 7.6.2) that allowed us to measure spontaneous glutamatergic signals from BC dendrites at the OPL and axon terminals at the IPL at the same location near-simultaneously using "vertical" scan fields (Fig. 14A, B). The ROIs were then determined by measuring the correlation between the neighboring pixels which were then subsequently used to extract the traces at varying depths (Fig. 14C, D) (see 7.7.1). We observed spontaneous glutamatergic signals at both the outer and inner retinal synapses of the BCs at the same location and time (Fig. 14C, D) which further confirmed our previous finding at the somatic level (Fig. 9B, C).

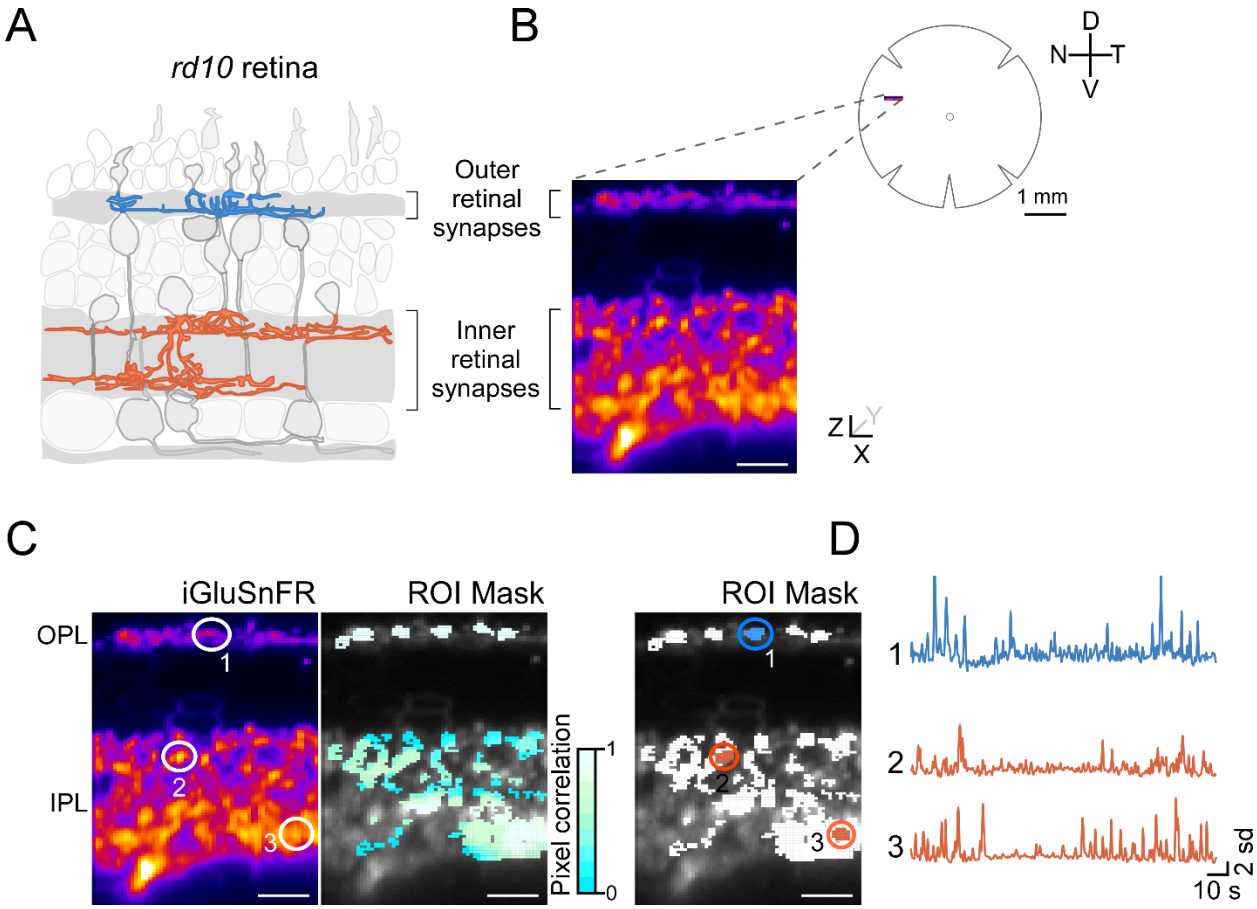

Figure 14. Simultaneous spontaneous glutamatergic signals are present at the OPL and IPL at the same location.

(A, B) Schematic representation of a vertical scan (X-Z) imaging at the outer and inner retinal synapses of the BCs (i.e., OPL and IPL, respectively) in the *rd10* retina. Near-simultaneous two-photon imaging of a *rd10* retina expressing iGluSnFR was achieved with an electrically tunable

lens. (C) Example scan field from a *rd10* retina at P76 on the left with its corresponding ROI mask in the center and on the right. Exemplary ROIs indicated and highlighted in circles (left and right field). Color in the right field represents ROIs at the OPL (blue) and IPL (orange). (D) Spontaneous glutamatergic signals recorded from OPL and IPL in parallel from the same scan field in (C). The color of the traces corresponds to the color of the ROI mask highlighted in (C, right). Scale bars, 10 μm (B and C).

8.6 Multiple correlated active clusters are present in the degenerated *rd10* retina

To evaluate the network interaction between outer and inner retina, a correlation was determined between the ROIs obtained at different depth at the same location. The ROIs were clustered using Ward's hierarchical clustering and a linear correlation metric (see 7.7.4; hierarchical clustering). Between P66 and 82, the degenerated *rd10* retina showed some variability in retinal thickness. This variability was addressed through a depth alignment method, which used the localized glutamate labeling to map the ROIs to their relative position in the OPL and IPL (Fig. 15A) (see 7.7.4; depth alignment). The alignment was performed for each glutamate imaging field. Three distinctive peaks were identified after the alignment, representing mean fluorescent signal at each recording depths; these approximately corresponded to the OPL and, OFF and ON sublaminae of the IPL (Fig. 15B). The clusters exhibited less variation in thickness after the depth alignment (Fig. 15C). The hierarchical clustering algorithm has a single parameter, the distance threshold, which determines the number of clusters. We varied this parameter and investigated its effect on the number and quality of clusters using a clustering metric (the Silhouette coefficient) (Fig. 15E) (see 7.7.4). We adjusted thresholds between 1.5 and 2.5 and found that at a threshold of 1.75 the number of clusters became stable (Fig. 15E). Hence, we decided to use a threshold of 1.75 for all the analyses, which resulted in three to seven clusters per recording (Fig. 15D).

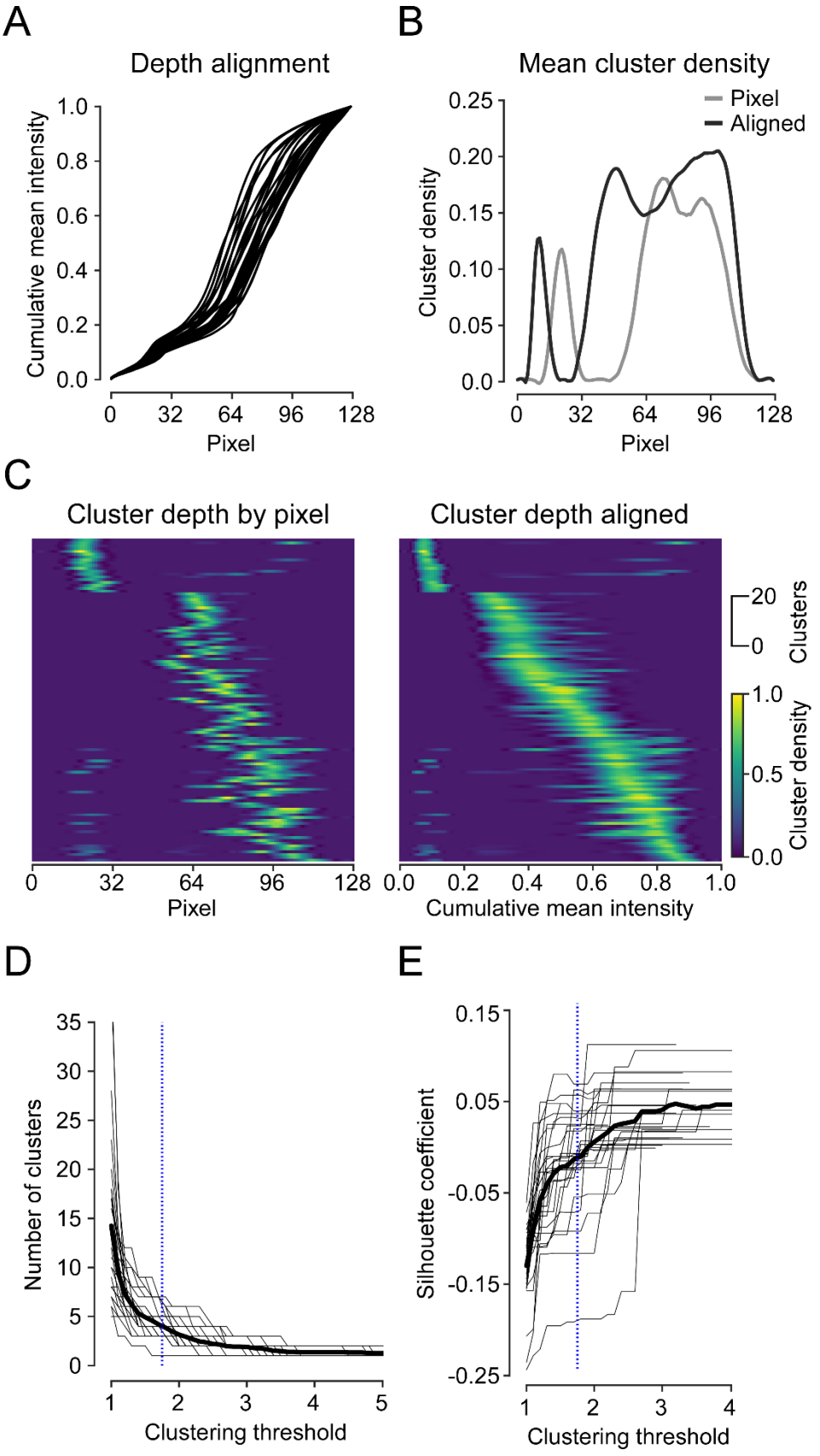
A
Depth alignment
Cumulative mean intensity
1.0
0.8
0.6
0.4
0.2
0.0
0
32
64
96
128
Pixel
B
Mean cluster density
Pixel
Aligned
Cluster density
0.25
0.20
0.15
0.10
0.05
0.0
0
32
64
96
128
Pixel
C
Cluster depth by pixel
Cluster depth aligned
20
0
Clusters
1.0
0.5
0.0
Cluster density
0
32
64
96
128
Pixel
0.0
0.2
0.4
0.6
0.8
1.0
Cumulative mean intensity
D
Number of clusters
35
30
25
20
15
10
5
0
1
2
3
4
5
Clustering threshold
E
Silhouette coefficient
0.15
0.05
-0.05
-0.15
-0.25
1
2
3
4
Clustering threshold

Figure 15. Identification of correlated clusters at varying depth.

(A) Plot indicating mapping from the recording pixel to an aligned depth value. (B) Plot showing mean cluster density at each pixel before and after depth alignment. (C) Heatmaps showing the distribution over depth for each cluster at a selected threshold, for both raw and aligned data. Each row represents a cluster. (D) Plot showing the effect of varying the clustering threshold on the number of clusters, and (E) the Silhouette coefficient. Blue line indicates the threshold used for subsequent analysis, at 1.75. The bold line indicates the mean curve for all recordings, individual recordings are shown in grey.

We located between two and six clusters in the IPL at different depths and one or two clusters in the OPL (Fig. 16). Some of the OPL ROIs also formed a cluster with the ROIs in the IPL (Fig. 16; 18 out of 28 recording fields). We usually found a strong within-cluster correlation between the ROIs (Fig. 16, each bottom row).

Earlier studies revealed phase-shifted activity in ON- and OFF-RGCs (Menzler and Zeck, 2011; Margolis et al., 2014) (see 5.4.6). If this activity was due to synaptic interaction between AII ACs and ON- and OFF-CBCs (reviewed in Zeck, 2016), one would expect a similar pattern in the ON and OFF sublaminae of the IPL. Indeed, we found anti-correlation between groups of clusters in the IPL in some but not all recording fields (Fig. 16; 11 out of 28 recording fields). Taken together, it is evident from our data that the traditional view of the two spontaneously active networks is too simplistic. In contrast, there are seemingly multiple correlated active clusters, possibly representing multiple small interconnected circuits or networks.

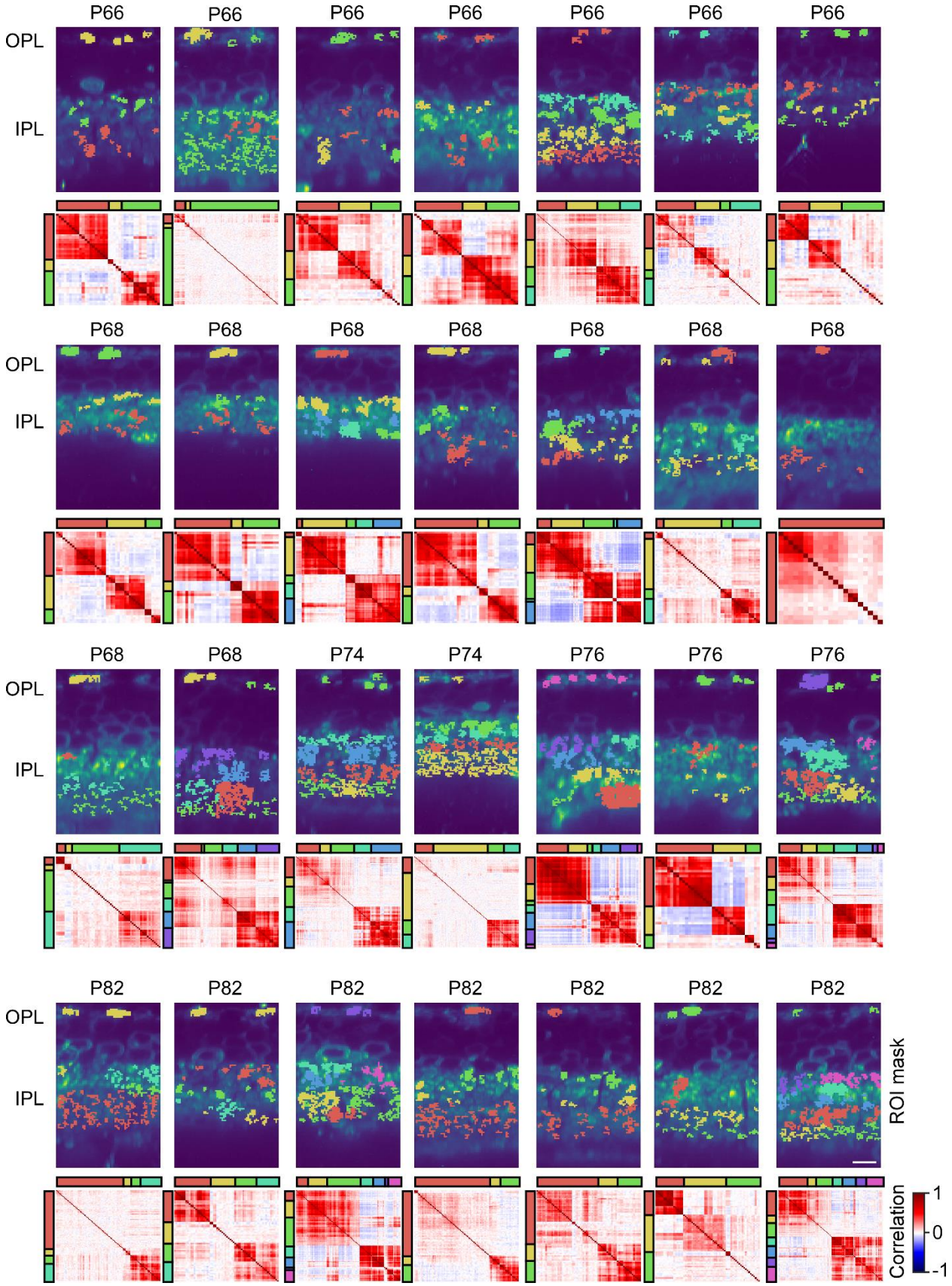
P66
P66
P66
P66
P66
P66
P66
OPL
IPL
P68
P68
P68
P68
P68
P68
P68
OPL
IPL
P68
P68
P74
P74
P76
P76
P76
OPL
IPL
P82
P82
P82
P82
P82
P82
P82
OPL
IPL
ROI mask
Correlation
1
0
-1

Figure 16. Multiple correlated active clusters in the degenerated *rd10* retina.

Different scan fields obtained by recording simultaneous spontaneous glutamatergic signals from the OPL and IPL at the same location with ROI mask (each top row) indicating clusters to which ROIs were assigned for a distance threshold of 1.75. Same color ROIs indicate same cluster. Correlation matrix (each bottom row; red-positive correlation, blue-negative correlation) for the glutamatergic signals for ROIs in the cluster corresponding to their scan field at the top. Colors besides the matrices indicate which matrix columns/rows correspond to the clusters in that recording. (n = 5/11/28 mice/retina quarters/scan fields; all between P66 and 82; Table 6). Scale bar, 10 μm.

8.7 Spontaneous signals in the outer retina modulate the inner retinal network

Next, to confirm the role of BCs as a potential link between the two networks, the synaptic input to the BCs was disrupted pharmacologically with AP4 and the kainate receptor antagonist, UBP-310. The latter antagonist was used because it was previously reported that the light-evoked and cone-driven glutamate release from OFF-CBCs is mainly mediated by kainate and not AMPA receptors (Borghuis et al., 2014) (see also 5.2.3). In addition, using UBP-310 instead of NBQX reduces the unspecific effects on the inner retinal circuitry. We found that the co-application of AP4 and UBP-310 resulted in a reduction of spontaneous glutamatergic signals of the ROIs in both OPL and IPL (Fig. 17B, D) as well as a striking reduction in within-cluster correlation (Fig. 17B, C; Fig. 18, each bottom row; Table 6).

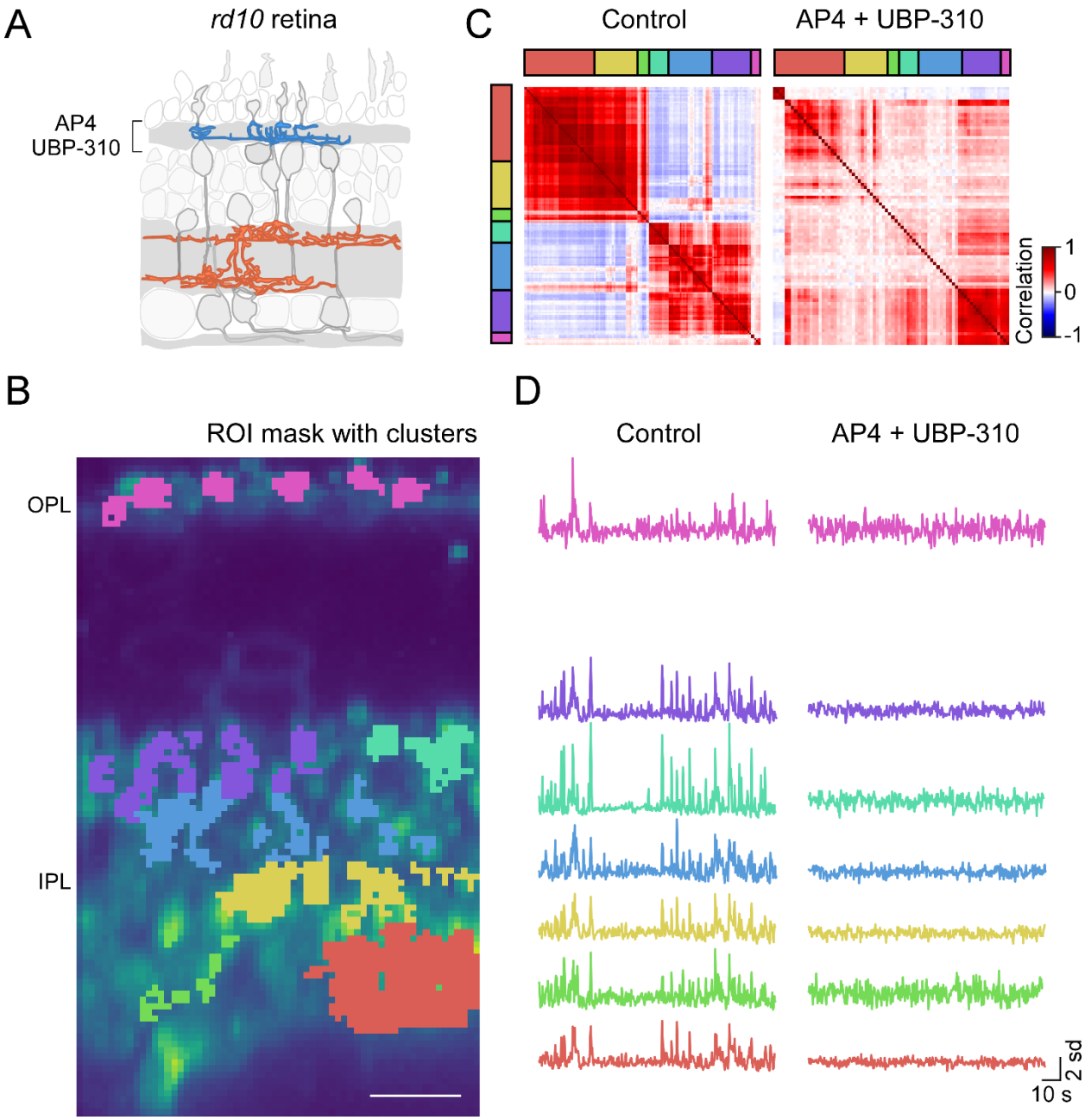

Figure 17. Reduction in spontaneous glutamatergic signals and within-cluster correlation after disrupting connectivity between the outer and inner retina.

(A) Schematic representation of the location of action of AP4 and UBP-310 in the retinal circuitry. (B) Example scan field acquired by vertical scan imaging with ROI mask indicating clusters in OPL and IPL. Same color ROIs represent the same clusters. (C) Correlation matrix for the glutamatergic signals for ROIs in the OPL and IPL corresponding to the scan field in (B) for both control and drug (AP4 + UBP-310) condition. (D) Exemplary spontaneous glutamatergic signals extracted for each cluster before and during drug (AP4 + UBP-310) application. Color in both (C) and (D) corresponds to the color of the clusters indicated in ROI mask in (B). Scale bar, 10 µm.

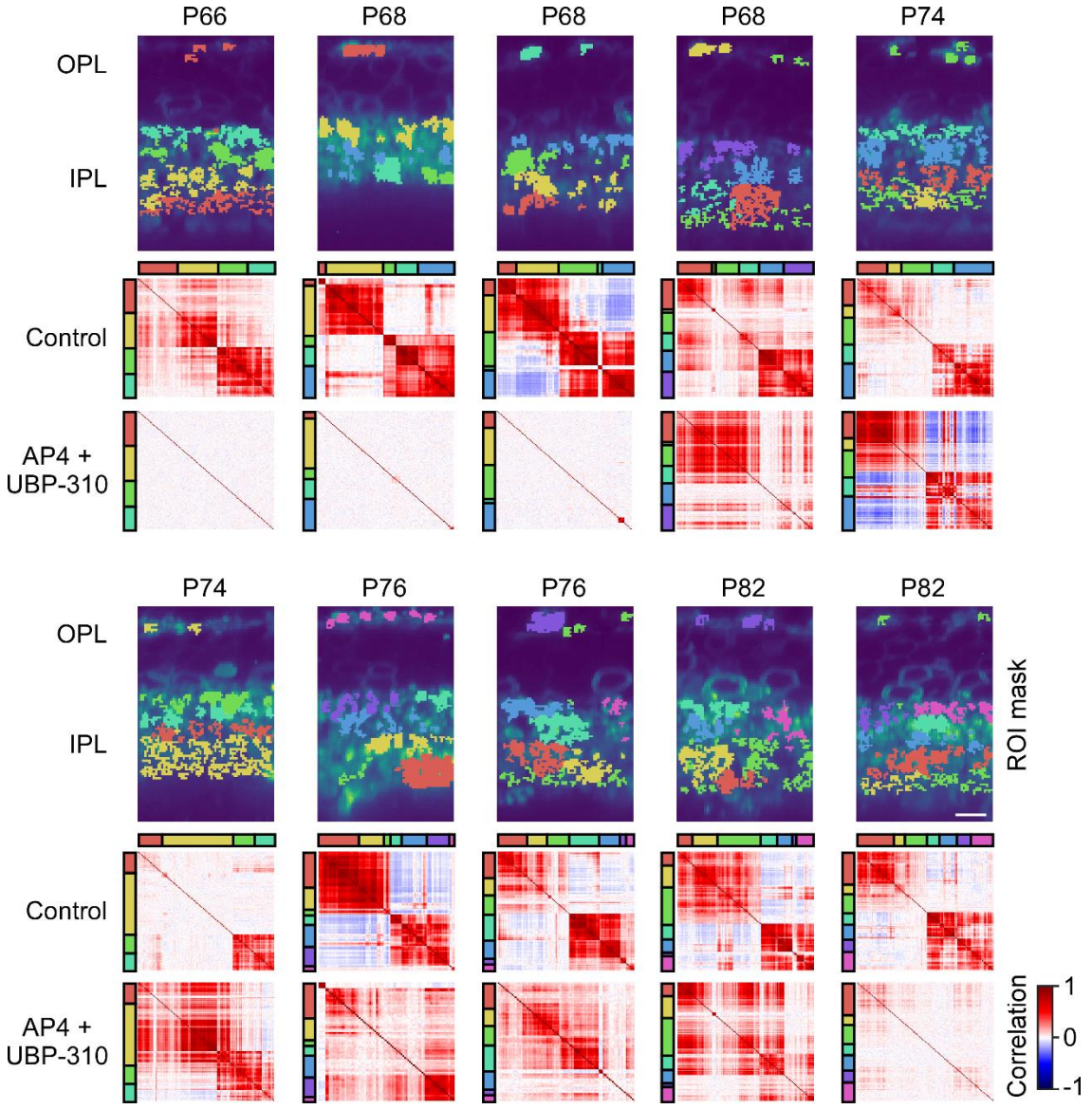

Figure 18. Exemplary scan fields showing reduction in spontaneous glutamatergic signals and within-cluster correlation after application of AP4 and UBP-310.

Different scan fields obtained by recording simultaneous spontaneous glutamatergic signals from the OPL and IPL at the same location with ROI mask (each top row) indicating correlation clusters. Same color ROIs indicate same cluster. Correlation matrix (each bottom row) for the glutamatergic signals for ROIs in the cluster corresponding ROI mask was plotted for control and drug (AP4 + UBP-310) condition. (n = 5/10/10 mice/retina quarters/scan fields; all between P66 and 82; Table 6). Scale bar, 10 µm.

Age	Preparation	Indicator	Sampling rate (Hz)	Number of mice/retina/scan fields	Drug condition
Between P66 and 82	quarter retinas (WM)	iGluSnFR	3.90	05/11/28	No
Between P66 and 82	quarter retinas (WM)	iGluSnFR	3.90	05/10/10	AP4 + UBP-310

Table 6. Summary data table from glutamate imaging in *rd10* retina.

Experimental conditions shown for *rd10* mice between postnatal days (P) 66 and 82; whole-mount (WM); intensity-based glutamate-sensing fluorescent reporter (iGluSnFR); AP4, mGluR6 receptor agonist; UBP-310, kainate receptor antagonist.

Further, to confirm that the change in within-cluster correlation was an effect of the drug and not due to change in the signal dynamics over time, within-cluster correlation was compared between two control recordings done at an interval of 10 minutes but without drugs being applied. No significant change in within-cluster correlation or in the number of clusters in the two control conditions was observed (Fig. 19) suggesting that the effect was primarily due to drug application.

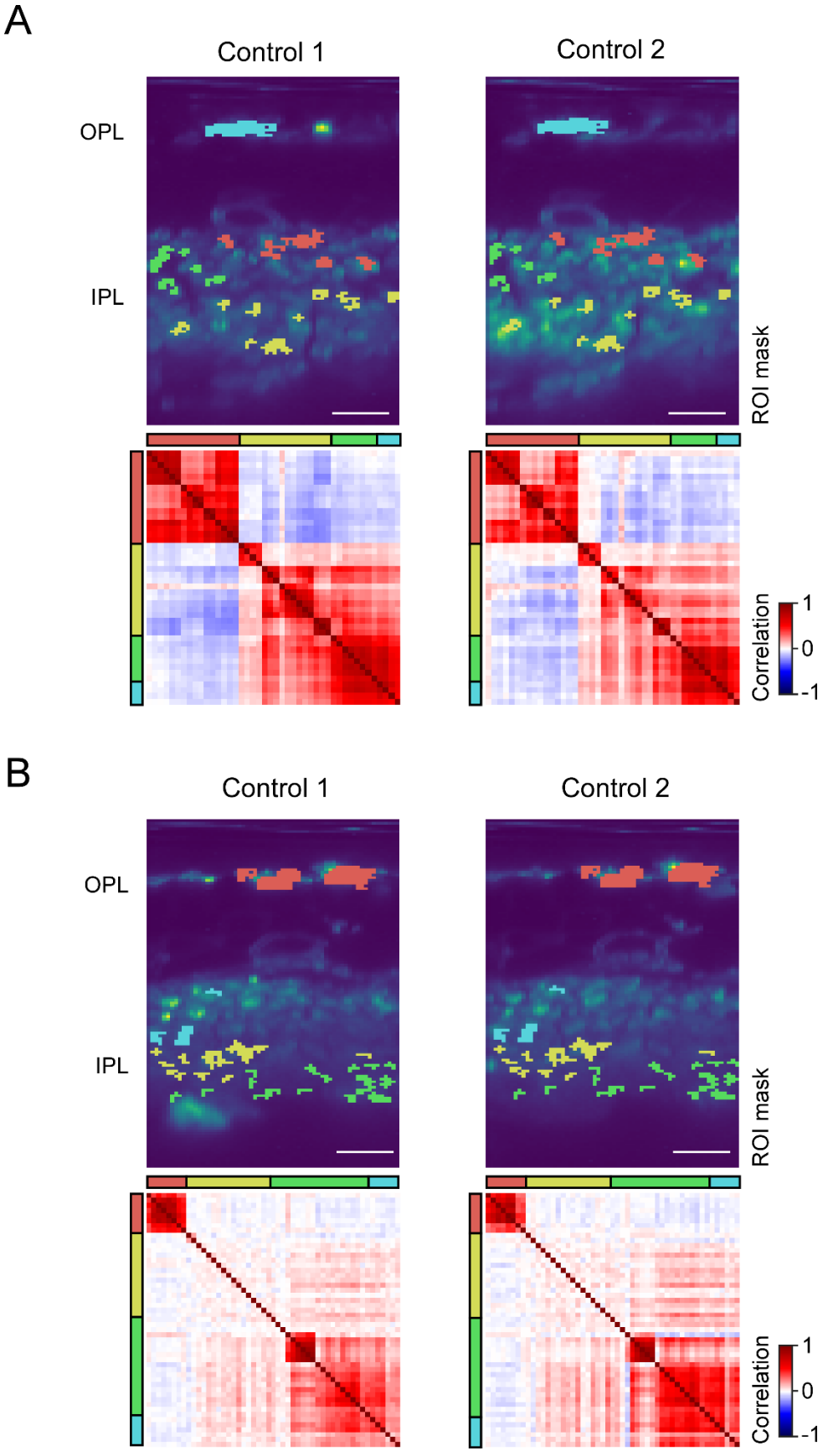
A
Control 1
Control 2
OPL
IPL
ROI mask
Correlation
1
0
-1
B
Control 1
Control 2
OPL
IPL
ROI mask
Correlation
1
0
-1

Figure 19. Within-cluster correlation does not change over time.

(A, B) Exemplary scan fields (top) with their correlation matrix (bottom) for two control conditions (Control 1 and Control 2). Control 1 and 2 represent two consecutive recordings performed at the same location but with an interval of 10 minutes. Scale bars, 10 μm (A and B).

We next, analyzed the drug effects on the relationship between OPL and IPL activity by computing the median, 10^{th} and 90^{th} centile pairwise correlation for each ROI pair between OPL and IPL clusters (see 7.7.4; pairwise correlation). While the OPL-IPL pairwise correlation changed only a little for the median and 10^{th} centile, there was a strong change in the 90^{th} centile pairwise correlation (Fig. 20A). Quantification of the change in the 90^{th} centile OPL-IPL pairwise correlation revealed a significant reduction in the correlation in about 61% of the clusters (Fig. 20B; Table 7). The reduction also varied with the IPL depth (Spearman's $R = 0.24$) and was greater for the ON than for the OFF sublamina of the IPL (Fig. 20C). Notably, there were fewer clusters during the drug application than in the control condition, irrespective of where the clustering threshold was set (Fig. 20D). This might be due to an increase in the within-cluster correlation of some IPL clusters as a result of disruption of cone input at the OPL or due to some clusters becoming inactive. Finally, a small percentage of clusters were also unaffected by the drug application (Fig. 20E).

Overall, our data confirm that the inner retinal signals in the degenerated *rd10* retina are largely modulated by the signals present in the outer retina, relayed particularly by BCs, and thus, indicating a functional interaction between the two networks.

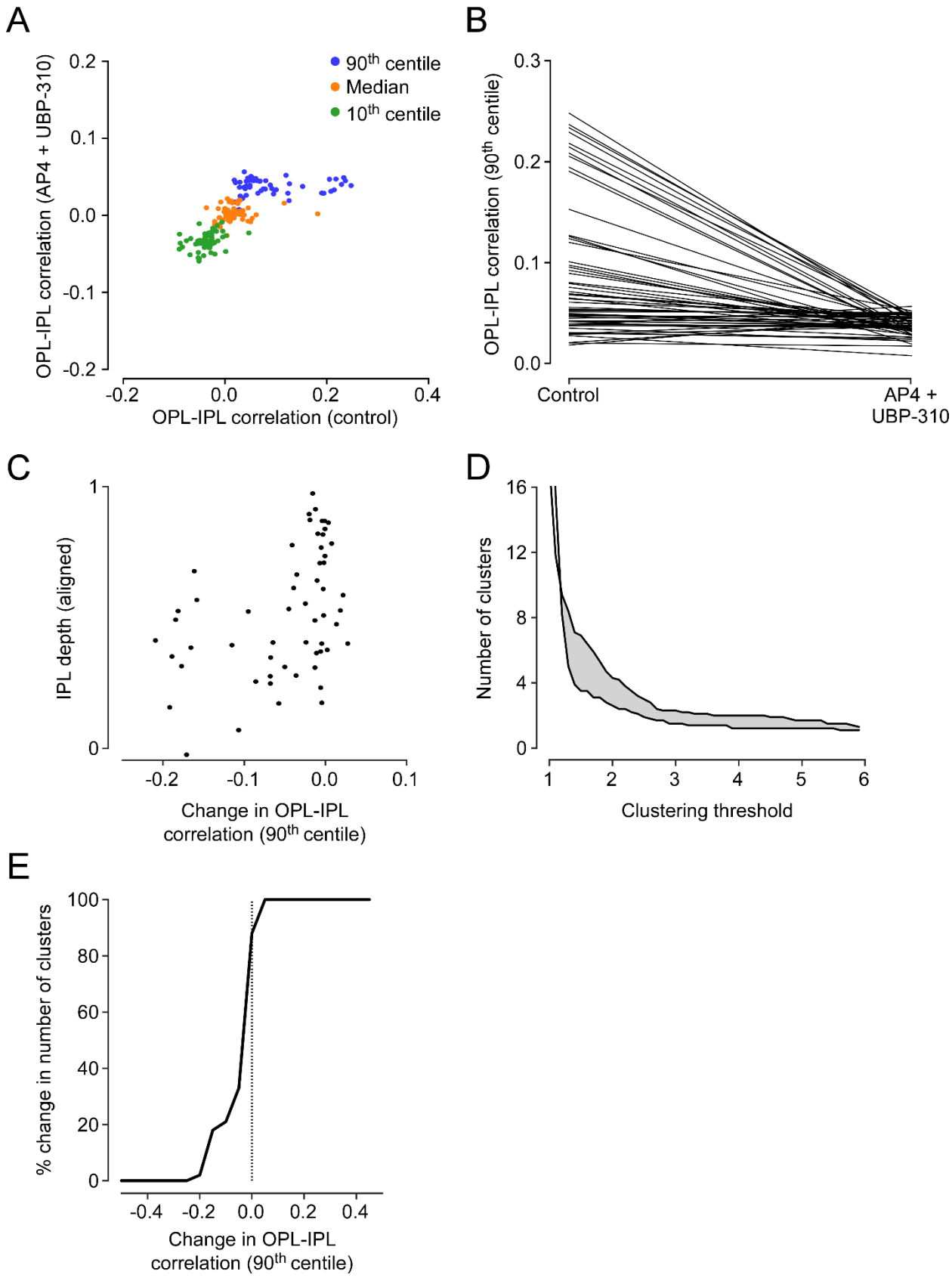
A
90th centile
Median
10th centile
OPL-IPL correlation (AP4 + UBP-310)
OPL-IPL correlation (control)
B
OPL-IPL correlation (90th centile)
Control
AP4 + UBP-310
C
IPL depth (aligned)
Change in OPL-IPL correlation (90th centile)
D
Number of clusters
Clustering threshold
E
% change in number of clusters
Change in OPL-IPL correlation (90th centile)

Figure 20. Spontaneous signals in the outer retina modulate inner retinal signals.

(A) Plot showing change in 10th centile, median and 90th centile OPL-IPL pairwise correlation for each cluster under control and drug (AP4 + UBP-310) conditions. Each dot represents a ROI pair between OPL and IPL clusters. (B) Plot for 90th centile OPL-IPL pairwise correlation before and during drug application (AP4 + UBP-310). Each line represents a ROI pair between OPL and IPL clusters. (C) Change in the 90th centile OPL-IPL pairwise correlation before and during drug application with respect to the aligned depth. Here, 1 indicates start of the OFF sublamina of the IPL and 0 indicates end of the ON sublamina of the IPL (D) Plot showing in change in cluster number during the drug (AP4 + UBP-310) application as compared to the control, for varying cluster thresholds. (E) Plot showing percentage change in the number of clusters after drug application. (n = 10/10 retina quarters/scan fields from 5 mice; all between P66 and 82).

Age	**Scan field number**	**Number of Clusters/ scan field**	**Number of ROIs/clusters**	**90th centile correlation (control)**	**90th centile correlation (AP4 + UBP-310)**
P66	1	1	46	0.056	0.045
P66	1	2	52	0.052	0.050
P66	1	3	38	0.051	0.051
P66	1	4	35	0.053	0.049
P68	2	1	04	0.218	0.047
P68	2	2	29	0.229	0.040
P68	2	3	07	0.208	0.031
P68	2	4	13	0.233	0.049
P68	2	5	21	0.205	0.047
P68	3	1	12	0.021	0.043
P68	3	2	28	0.030	0.025
P68	3	3	24	0.029	0.043
P68	3	4	03	0.018	0.046
P68	3	5	20	0.035	0.022
P68	4	1	38	0.079	0.034
P68	4	2	04	0.042	0.026
P68	4	3	21	0.095	0.028
P68	4	4	21	0.092	0.035
P68	4	5	27	0.042	0.038
P68	4	6	33	0.037	0.036
P74	5	1	38	0.042	0.037
P74	5	2	18	0.048	0.045
P74	5	3	35	0.054	0.048
P74	5	4	28	0.038	0.056
P74	5	5	50	0.047	0.047

P74	6	1	30	0.039	0.037
P74	6	2	89	0.042	0.044
P74	6	3	27	0.040	0.035
P74	6	4	26	0.046	0.037
P76	7	1	43	0.101	0.033
P76	7	2	26	0.089	0.039
P76	7	3	04	0.126	0.019
P76	7	4	12	0.080	0.045
P76	7	5	27	0.127	0.041
P76	7	6	22	0.097	0.033
P76	7	7	06	0.071	0.032
P76	8	1	37	0.248	0.039
P76	8	2	24	0.215	0.033
P76	8	3	18	0.237	0.045
P76	8	4	38	0.075	0.034
P76	8	5	26	0.190	0.029
P76	8	6	08	0.064	0.045
P76	8	7	10	0.194	0.029
P82	9	1	15	0.120	0.052
P82	9	2	26	0.124	0.029
P82	9	3	41	0.153	0.038
P82	9	4	17	0.031	0.024
P82	9	5	16	0.020	0.017
P82	9	6	04	0.028	0.008
P82	9	7	18	0.029	0.036
P82	10	1	46	0.069	0.044
P82	10	2	13	0.068	0.044
P82	10	3	26	0.065	0.029
P82	10	4	16	0.049	0.037
P82	10	5	22	0.045	0.048
P82	10	6	17	0.049	0.039
P82	10	7	28	0.061	0.048

Table 7. Summary table showing change in OPL-IPL pairwise correlation between clusters during control condition and during the application of AP4 and UBP-310.

OPL-IPL pairwise correlation of spontaneous glutamatergic signals in mice at respective postnatal days (P); 90^{th} centile OPL-IPL pairwise correlation in control condition (90^{th} centile correlation (control)); 90^{th} centile OPL-IPL pairwise correlation under drug condition (90^{th} centile correlation (AP4 + UBP-310)).

8.8 Investigating lateral signal transfer in the degenerated *rd10* retina

It is equally important to understand how the signals from the BCs are relayed to the RGCs. Besides, vertical synaptic interaction (Borowska et al., 2011; reviewed in Margolis and Detwiler, 2011; Biswas et al., 2014) (see also 5.4.6), it is conceivable that the activity in the GCL could also be affected by lateral signal transmission. As our two-photon imaging method allowed us to record from only a small field (~ 50 µm wide 'vertical' slice of the retina) laterally, it was not feasible to investigate large-scale interaction using this method.

To analyze the lateral spread of the spontaneous signals in the RGCs, a method that combines two-photon glutamate imaging with electrical imaging using high density complementary metal-oxide semiconductor (CMOS) MEAs was developed (Fig. 21). This method allowed simultaneous recording (locally) of glutamatergic signals at the BC synapses at the OPL and IPL and (globally) electrical activity of the RGCs in the degenerated *rd10* retina. However, for time reasons, we were not able to fully exploit this method for further investigation within the scope of this thesis. Nevertheless, the preliminary data acquired highlights that the method could be a promising tool to dissect both vertical and lateral signal propagation in the degenerated *rd10* retina in the future.

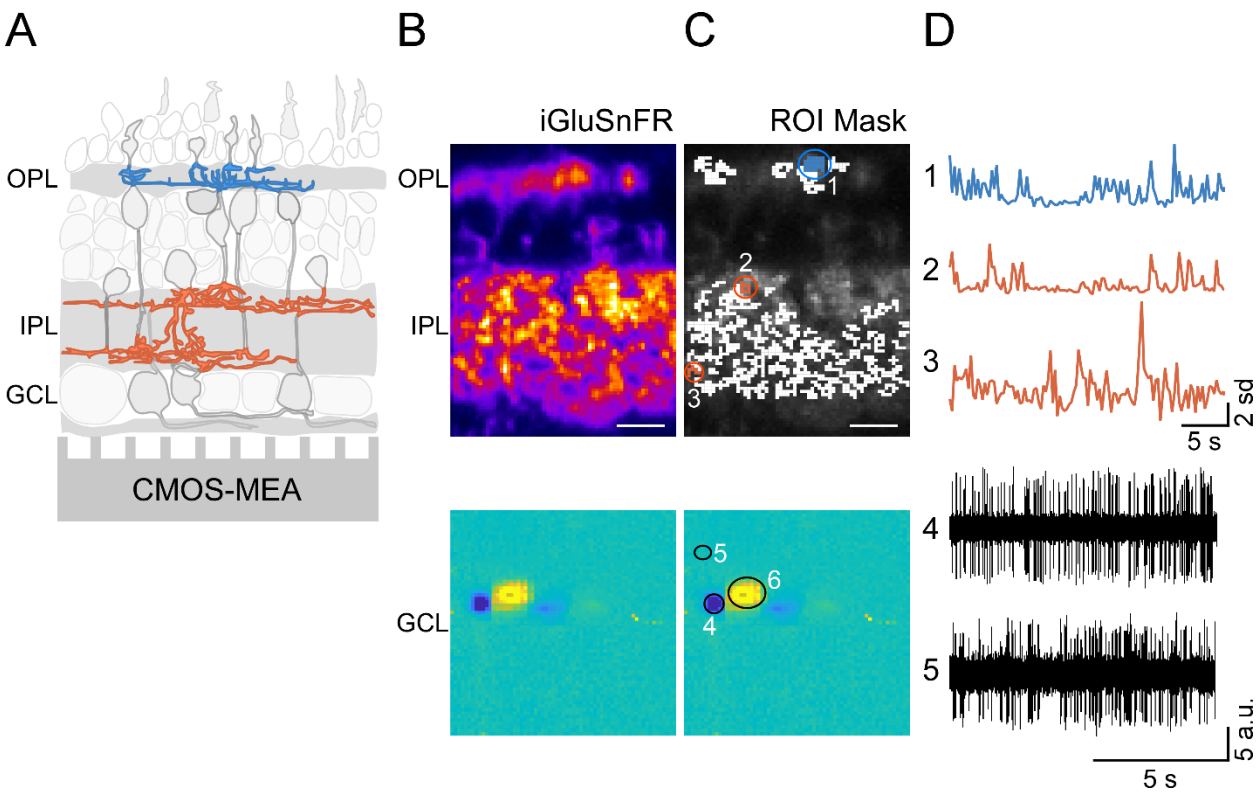

Figure 21. Vertical and lateral signal propagation in the degenerated *rd10* retina.

(A) Schematic illustration of the simultaneous recording of spontaneous glutamatergic signals (using an electrically tunable lens equipped two-photon microscope; top) and spontaneous RGC activity (using a CMOS MEA; bottom). (B) Example of a simultaneous recording from an iGluSnFR expressing *rd10* retina showing vertical scan field (top) and electrical image (bottom) at the same location. (C) ROI masks corresponding to the fields in (B); top – ROI mask vertical scan field, bottom - electrical image with two-photon scanning area (6) and two cells spiking near (4) and far (5) from it. (D) Example traces of the signals obtained by combining the two methods from OPL, IPL, and RGCs at the same location. The color of the traces corresponds to the color of the labeled ROIs in (C).

9. Discussion

Using a rod photoreceptor-deficient *rd10* mouse model system, we investigated the interactions between synaptically connected but independently originated spontaneously active networks in the degenerating retina. We report the co-existence of spontaneously active networks in the outer and inner retinae at the same location in the degenerated retina using two-photon Ca^{2+} and glutamate imaging. The signal dynamics in these active networks displayed spatio-temporal variability. While the networks exhibited mostly independent dynamics during the early degeneration phase (~ P30), the dynamics between them became strikingly similar with the progression of the disease (~ P90). Next, to investigate the source of the observed network interactions, we explored the functional 'footprints' of the synaptic connectivity between the networks. By implementing a near-simultaneous two-photon glutamate imaging at the input and output synapses of BCs, we examined the role of BCs as potential linking neurons between the two networks. We found that the networks do interact with each other and that this interaction is largely mediated by the BCs. We also provided the first evidence for the co-existence of multiple correlated spontaneously active clusters in the inner retina at the same retinal location, suggesting that the origin of spontaneous activity is more complex than anticipated.

9.1 Where do the outer and inner networks interact?

Our major finding from this study is that the outer and inner spontaneously active networks in the degenerated *rd10* retina interact with each other. The interaction between two networks can also be found in other parts of the CNS where the networks could correlate their activities at both local and global levels to mediate communication (Both et al., 2008) (see 5.1.2). However, whether the networks present in the degenerated retina also interact with each other, has not been systematically investigated before. As BCs participate in both the networks, we speculated their role in mediating the interaction between the networks by relaying signals from the outer to the inner retina through the vertical BC-AC pathway (see 5.4.8). In support of our hypothesis, we observed a significant reduction in the spontaneous signals in the inner retina when the glutamatergic inputs from the BCs to the ACs were blocked using NBQX and AP5. However, this

only affected the slow signal dynamics of the inner retina while leaving high frequency signals unchanged. A possible explanation to this is that only the slow dynamics displayed by the ACs in the inner retina are mediated by the signals carried from the outer retina by the BCs. Since the axon terminals of the BCs can act as a low-pass filter (reviewed in Euler et al., 2014), it is conceivable that this allows only the transfer of low frequency signals to postsynaptic neurons. On the other hand, the potential high frequency component in the AC activity was not abolished by glutamate receptor blockers and, hence, might reflect the cells' own intrinsic activity. Together, it is likely that the temporal properties of the signals in the inner retina might be determined by both intrinsic and synaptic mechanisms.

Although BCs relay the outer retinal activity and modulate the signals in the inner retina, it cannot be ruled out that signal modulation can also occur in the opposite way. This seems to be supported by our observation that blocking glutamatergic input to the ACs also modulated activity in the BC somata. Although the ionotropic glutamate receptor antagonists (NBQX + AP5) we applied in these experiments may also reduce photoreceptor input to BC and HC dendrites (see 5.2.3), which should be visible as a modulation in the BC activity as a result of reduced feedforward inhibition from the HCs (Haq et al., 2014) (see also 5.4.2). Reduced inhibition at the BC terminals can also be expected from the ACs in the inner retina, where for e.g., blocking input from the RBCs to A17 ACs could reduce inhibition and modulate the signals of the RBCs (Hartveit, 1999; Chávez et al., 2006) (see 5.2.4; the rod pathway). Thus, ACs might also modulate the signals between the outer and inner networks along the vertical BC-AC pathway. RBCs constitute ~ 38% of the total BC population in the INL (Wässle et al., 2009), and RBCs and AII ACs play an important role in generating activity in the outer and inner retina, respectively (Trenholm et al., 2012; Choi et al., 2014; Haq et al., 2014). Hence, it is possible that the RBC-AII AC pathway plays an essential role in the interaction between the networks. This is also supported by our finding at the synaptic level, whereby blocking (selectively) the glutamatergic photoreceptor input at the BC dendrites using AP4 and UBP-310 resulted in a large reduction in correlation in the clusters present in the ON sublamina of the IPL as compared to the OFF sublamina. Besides this, the AII-CBC network which is involved in the generation of activity in the inner retina (Trenholm et al., 2012; Choi et al., 2014) can also be a connecting link between the networks.

In addition to RBC-AII AC and AII-CBC pathway, there can be other pathways that may relay signals from the inner to the outer retina, such as the ones involving DACs or iACs (see 5.4.8). However, in the light of the synaptic alterations in the degenerated retina, we consider it unlikely that the DAC and iAC pathways predominantly modulate the signals in the network (see 5.4.8). Taken together, our data suggest that though the unidirectional interaction between the networks via BCs appears to be dominating, it is conceivable that the interaction is not strictly in one direction but bidirectional, where ACs also modulate the signal dynamics of the network.

9.2 Spatio-temporal interaction between the networks

The progress of retinal degeneration in the *rd10* retina varies as a function of age and retinal location and differs between retinal circuits (Gargini et al., 2007; Phillips et al., 2010) (see 5.4.1). Also, an increase in spontaneous activity in the RGC population with the advancement of the disease has been reported earlier (Stasheff et al., 2011; Goo et al., 2011). However, how the network interaction changes with the disease progression have not been examined earlier. Our timeline population imaging revealed that there is a spatio-temporal variability in the spontaneous signal dynamics in the outer and inner retina that become more similar with the disease progression. A possible explanation for this observation may be that if spontaneous activity was an outcome of the synaptic remodeling, higher variability in the signal dynamics would be expected in the earlier degeneration phase, when the remodeling has started, as compared to the later phase, when remodeling (i.e. synaptic rewiring or formation of ectopic synapses) is largely concluded (see also 5.4.2 and 5.4.3).

Furthermore, the variability in the spatio-temporal properties of the network can be a consequence of the interaction between the networks at a local as well as at a global level. Our data mainly revealed network interaction and signal propagation at a local area along the vertical pathway. However, the networks can also interact at a large scale, allowing the propagation of the activity over larger distances across the retina (Menzler and Zeck, 2011) (see 5.4.6). Future studies are needed to investigate the role of network interactions between the outer and inner retina for aberrant retinal activity at the global level.

9.3 Co-existence of multiple active networks in the degenerated retina

Previous studies demonstrated the role of only two principal sources that give rise to the network activity in the degenerated retina: remnant cones in the outer retina (Haq et al., 2014) and the AII AC-CBC network in the inner retina (Trenholm et al., 2012) (see also 5.4.5 and 5.4.6). However, our study provided evidence for the presence of multiple active correlated clusters in the inner retina, possibly representing multiple small interconnected circuits or networks. As RBCs form correlated active clusters with remnant cones in the outer retina (Haq et al., 2014), clusters in the ON sublamina of the IPL (with OPL ROIs) might represent the downstream network of the RBCs. However, since we also observed separate clusters in the OFF sublamina of the IPL, it suggests that the activity in the degenerated retina can be driven by more than one parallel mechanisms. Several additional mechanisms have been postulated that can act as an independent source of generating activity in the inner retina such as a parallel OFF-BC pathway (Tu et al., 2016) (see also 5.4.10) or through dystrophic ACs (Yee et al., 2012). This can also be anticipated from the diverse signal characteristics displayed by different RGC types during degeneration (Yee et al., 2012; Yee et al., 2014; Yu et al., 2017). Besides, it is also reasonable to think that the active neurons could modulate and/or drive the activity of other synaptically connected neurons forming individual sub-networks at a local level. However, whether or not distinct neuronal types can form multiple sub-networks can be determined by population imaging at the same retinal locations. We broadened the perspective of previous studies by taking advantage of our vertical imaging at synaptic terminals which allowed us to investigate more than one circuit simultaneously active at the same retinal location. We suggest the existence of parallel mechanisms at the same retinal location based on the following findings: First, at somatic levels, a high degree of heterogeneity in the pattern of spontaneous signals in both outer and inner retina can be observed, which is not expected if the activity was driven by only a single mechanism. Second, at synaptic levels, two to six correlated active clusters were present in the IPL. Third, disrupting outer retinal activity from the inner retina only modulates inner retinal activity but does not abolish them. Taken together, our data demonstrating multiple spontaneously active synaptic clusters in the degenerated retina possibly suggests that the activity is driven by interactions between multiple mechanisms at both local and global levels.

9.4 Physiological relevance of the interactive networks

The generation of spontaneous activity in the diseased retina may be disadvantageous in terms of energy requirement (reviewed in Raichle and Mintun, 2006). But then, what is the purpose of gaining this function during degeneration? One possible explanation could be for the preservation and restoration of the synapses. It is well known that in developing nervous system, spontaneous activity plays a crucial role in the precise wiring of the circuitry, organization of retinotopic maps and eye-specific segregation (reviewed in Blankenship and Feller, 2010; Ackman et al., 2012; Akrouh and Kerschensteiner, 2013 reviewed in Kirkby et al., 2013) (see 5.1.2 and 5.1.3). However, with the maturation of the synapses, these waves get suppressed (Toychiev et al., 2013) (see 5.3). As the degeneration is marked by severe remodeling in the synaptic connectivity, it is possible that the retina regains its spontaneous activity for a similar purpose. Therefore, the degeneration induced spontaneous activity may be advantageous in at least two ways: First, as outer retinal neurons undergo severe remodeling such as dendritic retraction and formation of ectopic synapses between RBCs and remnant cones (Haq et al., 2014) (see also 5.4.2), the generation of spontaneous activity, in this case, might be crucial for maintaining and/or rewiring of such synapses at the local level. This is also consistent with the finding that the remnant cones and RBCs form clusters of correlated activity in the outer retina (Haq et al., 2014). Second, as the hyperactivity present in the inner retinal neurons is further relayed from the RGCs to the higher visual centers (Dräger and Hubel, 1978; Ivanova et al., 2016a), the spontaneous activity may be involved in the maintenance of the retinotopic maps in the brain (Xie et al., 2012) and, hence, help in preserving connectivity at the global level. Based on the studies done in other parts of the CNS (see also 5.1.2), the interaction between the spontaneously active networks in the *rd10* retina is not too surprising. However, the question arises why both networks correlate their activity in the degenerated retina. One possible reason is to maintain connectivity between outer and inner retina – following the Hebbian plasticity hypothesis, that “neurons that fire together wire together”. In addition, correlated activity exhibited by the networks might also promote synaptic stability between the rewired synapses (Kerschensteiner et al., 2009).

9.5 Implications for the visual restoration strategies

As discussed above, the spontaneous activity generated in the degenerated retina may contribute to the preservation and potential restoration of the synapses. At the same time, such aberrant activity has also been suggested as a source of noise that could reduce SNR ratio and affect remaining light stimulus or evoked responses (Yee et al., 2012; Haselier et al., 2017). This could interfere with various retinal prosthetic approaches that aim to restore visual function in the degenerated retina through electrical stimulation of the surviving neurons (Zrenner et al., 2011; reviewed in Weiland et al., 2016). Though being widely approved clinical treatment for RP, retinal implants only provide poor vision and low visual acuity to the patients (reviewed in Zrenner, 2013). This might be due to some limitations such as the size of the stimulating array is relatively small compared to the whole human retina, and thus, can only activate a small area of the whole retina. We showed from our study that the spontaneously active networks do interact with each other, therefore, it is possible that the activity initiated in the non-stimulated area can dampen the efficiency of the evoked signals in the stimulated area. Indeed, it has been reported that the electrical stimulation in human RP eyes requires a stronger threshold as compared to the normal-sighted control (Rizzo et al., 2003). Through our timeline population imaging, we also showed that the signals dynamics between the outer and inner retinal population varies both spatially and temporally during early degeneration but become more similar at later time points. Therefore, to preserve the synaptic connectivity and visual function, it is reasonable to consider an early time point of intervention when still the two neuronal population exhibit differences in their signal dynamics and might have the capability of restoring old synapses (Beier et al., 2017), rather at later degeneration phase when the signals in the networks are already functionally correlated. Although ethical constraints limit the treatment in the patients at an early stage of degeneration when still visual function is present, nevertheless, it is still promising to implement therapeutic approaches during early phase for the preservation and restoration of near to normal visual function.

An interesting approach aiming at preserving photoreceptor function at an early degeneration phase could be gene replacement therapy (Millington-Ward et al., 2011; reviewed in Scholl et al., 2016), clustered regularly interspaced short palindromic repeats (CRISPR)/Cas9 mediated targeted genome editing (Cai et al., 2019) or various neuroprotective approaches such as using possible

candidates for neurotrophic factors for e.g., rod-derived cone viability factor (RdVCF) (Byrne et al., 2015). Besides, various stem cell therapies focusing on photoreceptor transplantation also seem to be promising as they could serve the purpose of restoring visual function with reducing spontaneous activity in the neuronal population (Singh et al., 2013; Foik et al., 2018). The implementation of photoreceptor replacement therapies is usually done at the late stage of the disease (reviewed in Scholl et al., 2016), however, it can prove to be more effective when performed during the early degeneration phase when few photoreceptors are still intact. Taken together, with the advent of new technologies focusing on preservation of both connectivity and function of the retinal neurons during degeneration, our study contributes more towards the understanding of the functional remodeling in the degenerated retina that would help towards a better therapeutic approach.

9.6 Functional relevance to the spontaneous network activity in the CNS

Spontaneous activity displayed by several neurons has been often considered insignificant that contributes nothing but noise to the system. However, if this activity was useless for the CNS, one would expect a loss of this property during the evolutionary process. But since this is not the case, it suggests this function has some relevance in the brain's physiology. Though the role of spontaneous network activity has been very well demonstrated in the developing systems (Milner and Landmesser, 1999; Khazipov et al., 2004; Soto et al., 2012) (see 5.1.2 and 5.1.3), its purpose in the developed CNS is still under investigation. While some neurons such as dopaminergic neurons in the brain and the retina exhibit this function to modulate dopamine release (Gonon, 1988; Feigenspan et al., 1998), for others such as OFF-RGCs this property might be crucial for the generation of maintained activity during the resting state (Margolis and Detwiler, 2007). On the other hand, correlated network activity across different regions might play an important role in introducing variability in neural responses by adding random noise in the system and thus enabling complex brain operations. Network activity also seems to be altered during various neurodegenerative diseases (see 5.1.4). However, it would be interesting to understand how the network interaction changes with the advancement of the disease which might be useful for the early detection of the disease. Using the retina as a model system, we here showed that not only

the distinctly originated networks can interact with each other at a local level but also show spatio-temporal changes with the advancement of the disease. This might indicate that the interaction between the networks is a dynamic process and may vary with the disease progression. Overall, our study broadens the perspective of the previous studies in the CNS by providing more insight into how the networks can functionally interact with each other at both somatic and synaptic levels in a diseased condition.

10. Outlook

Both developing and mature nervous systems exhibit spontaneous neuronal activity (see also 5.1). Recently, a lot of studies have focused on understanding the network dynamics of these activities in the CNS to develop a better therapeutic approach. We here used the retina as a feasible and easily accessible model to study the interaction between the spontaneously active networks in a diseased condition. In the study, we showed that even at a local level, the networks interact with each other and show spatio-temporal variability in the signal dynamics with the advancement of the disease.

As our study mainly focused on deciphering interaction at a local level along the vertical pathway, it cannot be denied that the network dynamics also experience lateral modulation at large-scale. Both local interaction along the vertical pathway and global interaction through lateral signal transmission might be involved in the spread of signal across the retina. Hence, a continuation of this study could be to explore how signal dynamics change at a large-scale in the output neurons, i.e., RGCs, by simultaneously looking at the signal characteristics at the outer and inner retina (see also 8.8). Additionally, it is equally important to understand how the interaction among the signals during different degeneration phases at the retinal level affects the synchronization among the networks at the higher visual centers of the brain (Dan et al., 2019). Together, a complete exploration of the local and global interaction of the network dynamics from the retina to the brain could help in enhancing the compatibility of the visual restoration strategies. This would also shed light on how different retinopathies or visual hallucinations (phosphenes) are associated with several neurological dysfunctions.

11. References

Ackman JB, Burbridge TJ, Crair MC (2012) Retinal waves coordinate patterned activity throughout the developing visual system. Nature 490:219-225.

Akrouh A, Kerschensteiner D (2013) Intersecting circuits generate precisely patterned retinal waves. Neuron 79:322-334.

Al-Jumeily D, Iram S, Vialatte FB, Fergus P, Hussain A (2015) A novel method of early diagnosis of Alzheimer's disease based on EEG signals. ScientificWorldJournal 2015:931387.

Andrews-Hanna JR, Reidler JS, Huang C, Buckner RL (2010) Evidence for the default network's role in spontaneous cognition. J Neurophysiol 104:322-335.

Atkinson CL, Feng J, Zhang DQ (2013) Functional integrity and modification of retinal dopaminergic neurons in the *rd1* mutant mouse: roles of melanopsin and GABA. J Neurophysiol 109:1589-1599.

Baden T, Schubert T, Berens P, Euler T (2018) The functional organization of vertebrate retinal circuits for vision. In: Oxford Research Encyclopedia of Neuroscience.

Baden T, Berens P, Franke K, Román Rosón M, Bethge M, Euler T (2016) The functional diversity of retinal ganglion cells in the mouse. Nature 529:345-350.

Baden T, Euler T (2016) Dispatches retinal physiology: non-bipolar-cell excitatory drive in the inner retina. Curr Biol 26:706– 708.

Bakker A, Krauss GL, Albert MS, Speck CL, Jones LR, Stark CE, Yassa MA, Bassett SS, Shelton AL, Gallagher M (2012) Reduction of hippocampal hyperactivity improves cognition in amnestic mild cognitive impairment. Neuron 74:467-474.

Barhoum R, Martinez-Navarrete G, Corrochano S, Germain F, Fernandez-Sanchez L, de la Rosa EJ, de la Villa P, Cuenca N (2008) Functional and structural modifications during retinal degeneration in the *rd10* mouse. Neuroscience 155:698-713.

Bates D, Mächler M, Bolker BM, Walker SC (2015) Fitting linear mixed-effects models using lme4. J Stat Softw 67.

Behrens C, Schubert T, Haverkamp S, Euler T, Berens P (2016) Connectivity map of bipolar cells and photoreceptors in the mouse retina. Elife 5:e20041.

Behrens C, Zhang Y, Yadav SC, Haverkamp S, Irsen S, Korympidou MM, Schaedler A, Dedek K, Smith R, Euler T, Berens P, Schubert T (2019) Retinal horizontal cells use different synaptic sites for global feedforward and local feedback signaling. bioRxiv 780031. doi:10.1101/780031.

Beier C, Hovhannisyan A, Weiser S, Kung J, Lee S, Lee DY, Huie P, Dalal R, Palanker D, Sher A (2017) Deafferented adult rod bipolar cells create new synapses with photoreceptors to restore vision. J Neurosci 37:4635-4644.

Bergman H, Feingold A, Nini A, Raz A, Slovin H, Abeles M, Vaadia E (1998) Physiological aspects of information processing in the basal ganglia of normal and Parkinsonian primates. Trends Neurosci 21:32–38.

Bernheimer H, Hornykiewicz O, Jellinger K, Seitelberger F (1973) Brain dopamine and the syndromes of Parkinson and Huntington. Clinical, morphological and neurochemical correlations. J Neurol Sci 20:415-455.

Biswal BB et al. (2010) Toward discovery science of human brain function. Proc Natl Acad Sci U S A 107:4734-4739.

Biswas S, Haselier C, Mataruga A, Thumann G, Walter P, Muller F (2014) Pharmacological analysis of intrinsic neuronal oscillations in *rd10* retina. PLoS One 9:e99075.

Bittner AK, Diener-West M, Dagnelie G (2009) A survey of photopsias in self-reported retinitis pigmentosa: location of photopsias is related to disease severity. Retina 29:1513-1521.

Bittner AK, Diener-West M, Dagnelie G (2011) Characteristics and possible visual consequences of photopsias as vision measures are reduced in retinitis pigmentosa. Invest Opthalmol Vis Sci 52:6370-6376.

Bjelke B, Goldstein M, Tinner B, Andersson C, Sesack SR, Steinbusch HW, Lew JY, He X, Watson S, Tengroth B, Fuxe K (1996) Dopaminergic transmission in the rat retina: evidence for volume transmission. J Chem Neuroanat 12:37-50.

Blankenship AG, Feller MB (2010) Mechanisms underlying spontaneous patterned activity in developing neural circuits. Nat Rev Neurosci 11:18-29.

Bloomfield SA, Dacheux RF (2001) Rod vision: pathways and processing in the mammalian retina. Prog Retin Eye Res 20:351-384.

Borghuis BG, Looger LL, Tomita S, Demb JB (2014) Kainate receptors mediate signaling in both transient and sustained OFF bipolar cell pathways in mouse retina. J Neurosci 34:6128-6139.

Borowska J, Trenholm S, Awatramani GB (2011) An intrinsic neural oscillator in the degenerating mouse retina. J Neurosci 31:5000-5012.

Both M, Bahner F, von Bohlen und Halbach O, Draguhn A (2008) Propagation of specific network patterns through the mouse hippocampus. Hippocampus 18:899-908.

Brandstätter JH, Koulen P, Kuhn R, van der Putten H, Wässle H (1996) Compartmental localization of a metabotropic glutamate receptor (mGluR7): two different active sites at a retinal synapse. J Neurosci 16:4749-4756.

Briggman KL, Euler T (2011) Bulk electroporation and population calcium imaging in the adult mammalian retina. J Neurophysiol 105:2601-2609.

Buckner RL, Andrews-Hanna JR, Schacter DL (2008) The brain's default network: anatomy, function, and relevance to disease. Ann N Y Acad Sci 1124:1-38.

Busche MA, Chen X, Henning HA, Reichwald J, Staufenbiel M, Sakmann B, Konnerth A (2012) Critical role of soluble amyloid-beta for early hippocampal hyperactivity in a mouse model of Alzheimer's disease. Proc Natl Acad Sci U S A 109:8740-8745.

Busche MA, Eichhoff G, Adelsberger H, Abramowski D, Wiederhold KH, Haass C, Staufenbiel M, Konnerth A, Garaschuk O (2008) Clusters of hyperactive neurons near amyloid plaques in a mouse model of Alzheimer's disease. Science 321:1686-1689.

Byrne LC, Dalkara D, Luna G, Fisher SK, Clerin E, Sahel JA, Leveillard T, Flannery JG (2015) Viral-mediated RdCVF and RdCVFL expression protects cone and rod photoreceptors in retinal degeneration. J Clin Invest 125:105-116.

Cai Y, Cheng T, Yao Y, Li X, Ma Y, Li L, Zhao H, Bao J, Zhang M, Qiu Z, Xue T (2019) In vivo genome editing rescues photoreceptor degeneration via a Cas9/RecA-mediated homology-directed repair pathway. Sci Adv 5:eaav3335.

Carter-Dawson LD, LaVail MM, Sidman RL (1978) Differential effect of the rd mutation on rods and cones in the mouse retina. Invest Ophthalmol Vis Sci 17:489-498.

Chang B, Hawes NL, Hurd RE, Davisson MT, Nusinowitz S, Heckenlively JR (2002) Retinal degeneration mutants in the mouse. Vision Res 42:517-525.

Chang B, Hawes NL, Pardue MT, German AM, Hurd RE, Davisson MT, Nusinowitz S, Rengarajan K, Boyd AP, Sidney SS, Phillips MJ, Stewart RE, Chaudhury R, Nickerson JM, Heckenlively JR, Boatright JH (2007) Two mouse retinal degenerations caused by missense mutations in the beta-subunit of rod cGMP phosphodiesterase gene. Vision Res 47:624-633.

Chapot CA, Euler T, Schubert T (2017) How do horizontal cells 'talk' to cone photoreceptors? Different levels of complexity at the cone-horizontal cell synapse. J Physiol 595:5495-5506.

Chávez AE, Singer JH, Diamond JS (2006) Fast neurotransmitter release triggered by Ca influx through AMPA-type glutamate receptors. Nature 443:705-708.

Chaya T, Matsumoto A, Sugita Y, Watanabe S, Kuwahara R, Tachibana M, Furukawa T (2017) Versatile functional roles of horizontal cells in the retinal circuit. Sci Rep 7:5540.

Chen YC, Xia W, Luo B, Muthaiah VP, Xiong Z, Zhang J, Wang J, Salvi R, Teng GJ (2015) Frequency-specific alternations in the amplitude of low-frequency fluctuations in chronic tinnitus. Front Neural Circuits 9:67.

Chen YC, Zhang J, Li XW, Xia W, Feng X, Gao B, Ju SH, Wang J, Salvi R, Teng GJ (2014) Aberrant spontaneous brain activity in chronic tinnitus patients revealed by resting-state functional MRI. Neuroimage Clin 6:222-228.

Choi H, Zhang L, Cembrowski MS, Sabottke CF, Markowitz AL, Butts DA, Kath WL, Singer JH, Riecke H (2014) Intrinsic bursting of AII amacrine cells underlies oscillations in the *rd1* mouse retina. J Neurophysiol 112:1491-1504.

Contini M, Raviola E (2003) GABAergic synapses made by a retinal dopaminergic neuron. Proc Natl Acad Sci U S A 100:1358-1363.

Contini M, Lin B, Kobayashi K, Okano H, Masland RH, Raviola E (2010) Synaptic input of ON-bipolar cells onto the dopaminergic neurons of the mouse retina. J Comp Neurol 518:2035-2050.

Corlew R, Bosma MM, Moody WJ (2004) Spontaneous, synchronous electrical activity in neonatal mouse cortical neurons. J Physiol 560:377-390.

Cueva JG, Haverkamp S, Reimer RJ, Edwards R, Wässle H, Brecha NC (2002) Vesicular gamma-aminobutyric acid transporter expression in amacrine and horizontal cells. J Comp Neurol 445:227-237.

Czigler B, Csikos D, Hidasi Z, Anna Gaal Z, Csibri E, Kiss E, Salacz P, Molnar M (2008) Quantitative EEG in early Alzheimer's disease patients - power spectrum and complexity features. Int J Psychophysiol 68:75-80.

Daiger SP, Sullivan LS, Bowne SJ (2013) Genes and mutations causing retinitis pigmentosa. Clin Genet 84:132-141.

Dan HD, Zhou FQ, Huang X, Xing YQ, Shen Y (2019) Altered intra- and inter-regional functional connectivity of the visual cortex in individuals with peripheral vision loss due to retinitis pigmentosa. Vision Res 159:68-75.

Dargaei Z, Bang JY, Mahadevan V, Khademullah CS, Bedard S, Parfitt GM, Kim JC, Woodin MA (2018) Restoring GABAergic inhibition rescues memory deficits in a Huntington's disease mouse model. Proc Natl Acad Sci U S A 115:E1618-E1626.

Dedek K, Breuninger T, de Sevilla Müller LP, Maxeiner S, Schultz K, Janssen-Bienhold U, Willecke K, Euler T, Weiler R (2009) A novel type of interplexiform amacrine cell in the mouse retina. Eur J Neurosci 30:217–228.

Demas J, Sagdullaev BT, Green E, Jaubert-Miazza L, McCall MA, Gregg RG, Wong RO, Guido W (2006) Failure to maintain eye-specific segregation in nob, a mutant with abnormally patterned retinal activity. Neuron 50:247-259.

Denk W, Strickler JH, Webb WW (1990) Two-photon laser scanning fluorescence microscopy. Science. 248:73-76.

Dhingra A, Vardi N (2012) "mGlu receptors in the retina" - WIREs membrane transport and signaling. Wiley Interdiscip Rev Membr Transp Signal 1:641-653.

Diamond JS (2017) Inhibitory interneurons in the retina: types, circuitry, and function. Annu Rev Vis Sci 3:1-24.

Djamgoz MB, Hankins MW, Hirano J, Archer SN (1997) Neurobiology of retinal dopamine in relation to degenerative states of the tissue. Vision Res 37:3509-3529.

Dodson PD, Dreyer JK, Jennings KA, Syed EC, Wade-Martins R, Cragg SJ, Bolam JP, Magill PJ (2016) Representation of spontaneous movement by dopaminergic neurons is cell-type selective and disrupted in Parkinsonism. Proc Natl Acad Sci U S A 113:E2180-E2188.

Dräger UC, Hubel DH (1978) Studies of visual function and its decay in mice with hereditary retinal degeneration. J Comp Neurol 180:85-114.

Draguhn A, Traub RD, Schmitz D, Jefferys JG (1998) Electrical coupling underlies high-frequency oscillations in the hippocampus in vitro. Nature 394:189-192.

Du G, Zhuang P, Hallett M, Zhang YQ, Li JY, Li YJ (2018) Properties of oscillatory neuronal activity in the basal ganglia and thalamus in patients with Parkinson's disease. Transl Neurodegener 7:17.

Dumitrescu ON, Protti DA, Majumdar S, Zeilhofer HU, Wassle H (2006) Ionotropic glutamate receptors of amacrine cells of the mouse retina. Vis Neurosci 23:79-90.

Ellis EM, Gauvain G, Sivyer B, Murphy GJ (2016) Shared and distinct retinal input to the mouse superior colliculus and dorsal lateral geniculate nucleus. J Neurophysiol 116:602–610.

Erskine L, Herrera E (2014) Connecting the retina to the brain. ASN Neuro 6.

Euler T, Schubert T (2015) Multiple independent oscillatory networks in the degenerating retina. Front Cell Neurosci 9:444.

Euler T, Haverkamp S, Schubert T, Baden T (2014) Retinal bipolar cells: elementary building blocks of vision. Nat Rev Neurosci 15:507-519.

Euler T, Hausselt SE, Margolis DJ, Breuninger T, Castell X, Detwiler PB, Denk W (2009) Eyecup scope-optical recordings of light stimulus-evoked fluorescence signals in the retina. Pflugers Arch 457:1393-1414.

Feigenspan A, Babai N (2015) Functional properties of spontaneous excitatory currents and encoding of light/dark transitions in horizontal cells of the mouse retina. Eur J Neurosci 42:2615-2632.

Feigenspan A, Gustincich S, Bean BP, Raviola E (1998) Spontaneous activity of solitary dopaminergic cells of the retina. J Neurosci 18:6776-6789.

Feller MB, Wellis DP, Stellwagen D, Werblin FS, Shatz CJ (1996) Requirement for cholinergic synaptic transmission in the propagation of spontaneous retinal waves. Science 272:1182-1187.

Filion M, Tremblay L (1991) Abnormal spontaneous activity of globus pallidus neurons in monkeys with MPTP-induced parkinsonism. Brain Res 547:142-151.

Firl A, Ke JB, Zhang L, Fuerst PG, Singer JH, Feller MB (2015) Elucidating the role of AII amacrine cells in glutamatergic retinal waves. J Neurosci 35:1675-1686.

Firl A, Sack GS, Newman ZL, Tani H, Feller MB (2013) Extrasynaptic glutamate and inhibitory neurotransmission modulate ganglion cell participation during glutamatergic retinal waves. J Neurophysiol 109:1969-1978.

Firth SI, Wang CT, Feller MB (2005) Retinal waves: mechanisms and function in visual development. Cell Calcium 37:425-432.

Floresco SB, West AR, Ash B, Moore H, Grace AA (2003) Afferent modulation of dopamine neuron firing differentially regulates tonic and phasic dopamine transmission. Nat Neurosci 6:968-973.

Foik AT, Lean GA, Scholl LR, McLelland BT, Mathur A, Aramant RB, Seiler MJ, Lyon DC (2018) Detailed visual cortical responses generated by retinal sheet transplants in rats with severe retinal degeneration. J Neurosci 38:10709-10724.

Ford KJ, Félix AL, Feller MB (2012) Cellular mechanisms underlying spatiotemporal features of cholinergic retinal waves. J Neurosci 32:850-863.

Fox MD, Greicius M (2010) Clinical applications of resting state functional connectivity. Front Syst Neurosci 4:19.

Franke K, Berens P, Schubert T, Bethge M, Euler T, Baden T (2017) Inhibition decorrelates visual feature representations in the inner retina. Nature 542:439-444.

Gao B, Wang Y, Liu W, Chen Z, Zhou H, Yang J, Cohen Z, Zhu Y, Zang Y (2015) Spontaneous activity associated with delusions of Schizophrenia in the left medial superior frontal gyrus: a resting-state fMRI study. PLoS One 10:e0133766.

Garaschuk O, Hanse E, Konnerth A (1998) Developmental profile and synaptic origin of early network oscillations in the CA1 region of rat neonatal hippocampus. J Physiol 507:219-236.

Garaschuk O, Linn J, Eilers J, Konnerth A (2000) Large-scale oscillatory calcium waves in the immature cortex. Nat Neurosci 3:452-459.

Gargini C, Terzibasi E, Mazzoni F, Strettoi E (2007) Retinal organization in the retinal degeneration 10 (*rd10*) mutant mouse: a morphological and ERG study. J Comp Neurol 500:222-238.

Ghosh KK, Haverkamp S, Wässle H (2001) Glutamate receptors in the rod pathway of the mammalian retina. J Neurosci 21:8636-8647.

Gisabella B, Bolshakov VY, Benes FM (2005) Regulation of synaptic plasticity in a Schizophrenia model. Proc Natl Acad Sci U S A 102:13301-13306.

Gonon FG (1988) Nonlinear relationship between impulse flow and dopamine released by rat midbrain dopaminergic neurons as studied by in vivo electrochemistry. Neuroscience 24:19-28.

Goo YS, Ahn KN, Song YJ, Ahn SH, Han SK, Ryu SB, Kim KH (2011) Spontaneous oscillatory rhythm in retinal activities of two retinal degeneration (*rd1* and *rd10*) Mice. Korean J Physiol Pharmacol 15:415-422.

Gregg RG, Mukhopadhyay S, Candille SI, Ball SL, Pardue MT, McCall MA, Peachey NS (2003) Identification of the gene and the mutation responsible for the mouse nob phenotype. Invest Ophthalmol Vis Sci 44:378-384.

Gregg RG, Kamermans M, Klooster J, Lukasiewicz PD, Peachey NS, Vessey KA, McCall MA (2007) Nyctalopin expression in retinal bipolar cells restores visual function in a mouse model of complete X-linked congenital stationary night blindness. J Neurophysiol 98:3023-3033.

Grewe BF, Voigt FF, van 't Hoff M, Helmchen F (2011) Fast two-layer two-photon imaging of neuronal cell populations using an electrically tunable lens. Biomed opt express 2:2035-2046.

Grossniklaus HE, Geisert EE, Nickerson JM (2015) Introduction to the retina. Prog Mol Biol Transl Sci 134:383-396.

Gustincich S, Feigenspan A, Wu DK, Koopman LJ, Raviola E (1997) Control of dopamine release in the retina: a transgenic approach to neural networks. Neuron 18:723-736.

Haider B, Duque A, Hasenstaub AR, McCormick DA (2006) Neocortical network activity in vivo is generated through a dynamic balance of excitation and inhibition. J Neurosci 26:4535-4545.

Hampson EC, Vaney DI, Weiler R (1992) Dopaminergic modulation of gap junction permeability between amacrine cells in mammalian retina. J Neurosci 12:4911-4922.

Hanson MG, Milner LD, Landmesser LT (2008) Spontaneous rhythmic activity in early chick spinal cord influences distinct motor axon pathfinding decisions. Brain Res Brain Res Rev 57:77-85.

Haq W, Arango-Gonzalez B, Zrenner E, Euler T, Schubert T (2014) Synaptic remodeling generates synchronous oscillations in the degenerated outer mouse retina. Front Neural Circuits 8:108.

Hartveit E (1999) Reciprocal synaptic interactions between rod bipolar cells and amacrine cells in the rat retina. J Neurophysiol 81:2923-2936.

Harris-Warrick RM, Johnson BR (1987) Potassium channel blockade induces rhythmic activity in a conditional burster neuron. Brain Res 416:381-386.

Haselier C, Biswas S, Rosch S, Thumann G, Muller F, Walter P (2017) Correlations between specific patterns of spontaneous activity and stimulation efficiency in degenerated retina. PLoS One 12:e0190048.

Hastie T, Tibshirani R (1986) Institute of mathematical statistics is collaborating with JSTOR to digitize, preserve, and extend access to statistical science. Stat Sci 1:297-318.

Haverkamp S, Grünert U, Wässle H (2000) The cone pedicle, a complex synapse in the retina. Neuron 27:85-95.

Haverkamp S, Wässle H (2000) Immunocytochemical analysis of the mouse retina. J Comp Neurol 424:1–23.

Haverkamp S, Grünert U, Wässle H (2001) The synaptic architecture of AMPA receptors at the cone pedicle of the primate retina. J Neurosci 21:2488-2500.

Helmstaedter M, Briggman KL, Turaga SC, Jain V, Seung HS, Denk W (2013) Connectomic reconstruction of the inner plexiform layer in the mouse retina. Nature 500:168-174.

Hirasawa H, Contini M, Raviola E (2015) Extrasynaptic release of GABA and dopamine by retinal dopaminergic neurons. Philos Trans R Soc Lond B Biol Sci 370.

Hoon M, Okawa H, Della Santina L, Wong RO (2014) Functional architecture of the retina: development and disease. Prog Retin Eye Res 42:44-84.

Hou Y, Wu X, Hallett M, Chan P, Wu T (2014) Frequency-dependent neural activity in Parkinson's disease. Hum Brain Mapp 35:5815-5833.

Huang Y, Enzmann V, Ildstad ST (2011) Stem cell-based therapeutic applications in retinal degenerative diseases. Stem Cell Rev Rep 7:434-445.

Ivanova E, Yee CW, Sagdullaev BT (2015) Increased phosphorylation of Cx36 gap junctions in the AII amacrine cells of RD retina. Front Cell Neurosci 9:390.

Ivanova E, Yee CW, Baldoni RJr, Sagdullaev BT (2016a) Aberrant activity in retinal degeneration impairs central visual processing and relies on Cx36-containing gap junctions. Exp Eye Res 150:81-89.

Ivanova E, Yee CW, Sagdullaev BT (2016b) Disruption in dopaminergic innervation during photoreceptor degeneration. J Comp Neurol 524:1208-1221.

Jiang S, Luo C, Liu Z, Hou C, Wang P, Dong L, Zhong C, Lai Y, Xia Y, Yao D (2016) Altered local spontaneous brain activity in juvenile myoclonic epilepsy: a preliminary resting-state fMRI study. Neural Plast 2016:3547203.

Jones BW, Watt CB, Marc RE (2005) Retinal remodelling. Clin Exp Optom 88:282-291.

Jones BW, Kondo M, Terasaki H, Lin Y, McCall M, Marc RE (2012) Retinal remodeling. Jpn J Ophthalmol 56:289-306.

Kalloniatis M, Nivison-Smith L, Chua J, Acosta ML, Fletcher EL (2016) Using the rd1 mouse to understand functional and anatomical retinal remodelling and treatment implications in retinitis pigmentosa: A review. Exp Eye Res 150:106-121.

Kamermans M, Fahrenfort I (2004) Ephaptic interactions within a chemical synapse: hemichannel-mediated ephaptic inhibition in the retina. Curr Opin Neurobiol 14:531-541.

Kemmler R, Schultz K, Dedek K, Euler T, Schubert T (2014) Differential regulation of cone calcium signals by different horizontal cell feedback mechanisms in the mouse retina. J Neurosci 34: 11826-43.

Kerschensteiner D (2016) Glutamatergic Retinal Waves. Front Neural Circuits 10:38.

Kerschensteiner D, Morgan JL, Parker ED, Lewis RM, Wong RO (2009) Neurotransmission selectively regulates synapse formation in parallel circuits in vivo. Nature 460:1016-1020.

Kerschensteiner D, Wong RO (2008) A precisely timed asynchronous pattern of ON and OFF retinal ganglion cell activity during propagation of retinal waves. Neuron 58:851-858.

Kirkby LA, Sack GS, Firl A, Feller MB (2013) A role for correlated spontaneous activity in the assembly of neural circuits. Neuron 80:1129-1144.

Khazipov R, Sirota A, Leinekugel X, Holmes GL, Ben-Ari Y, Buzsáki G (2004) Early motor activity drives spindle bursts in the developing somatosensory cortex. Nature 432:758-761.

Koike C, Obara T, Uriu Y, Numata T, Sanuki R, Miyata K, Koyasu T, Ueno S, Funabiki K, Tani A, Ueda H, Kondo M, Mori Y, Tachibana M, Furukawa T (2010) TRPM1 is a component of the retinal ON bipolar cell transduction channel in the mGluR6 cascade. Proc Natl Acad Sci U S A 107:332-337.

Kothmann WW, Massey SC, O'Brien J (2009) Dopamine-stimulated dephosphorylation of connexin 36 mediates AII amacrine cell uncoupling. J Neurosci 29:14903-14911.

Kothmann WW, Trexler EB, Whitaker CM, Li W, Massey SC, O'Brien J (2012) Nonsynaptic NMDA receptors mediate activity-dependent plasticity of gap junctional coupling in the AII amacrine cell network. J Neurosci 32:6747-6759.

Koulen P, Brandstätter JH (2002) Pre- and postsynaptic sites of action of mGluR8a in the mammalian retina. Invest Ophthalmol Vis Sci 43:1933-1940.

Leaver AM, Renier L, Chevillet MA, Morgan S, Kim HJ, Rauschecker JP (2011) Dysregulation of limbic and auditory networks in tinnitus. Neuron 69:33-43.

Leinekugel X, Khazipov R, Cannon R, Hirase H, Ben-Ari Y, Buzsáki G (2002) Correlated bursts of activity in the neonatal hippocampus in vivo. Science 296:2049-2052.

Levy R, Hutchison WD, Lozano AM, Dostrovsky JO (2000) High-frequency synchronization of neuronal activity in the subthalamic nucleus of parkinsonian patients with limb tremor. J Neurosci 20:7766-7775.

Liberman MC (1978) Auditory-nerve response from cats raised in a low-noise chamber. J Acoust Soc Am 63:442-455.

Liu X, Hirano AA, Sun X, Brecha NC, Barnes S (2013) Calcium channels in rat horizontal cells regulate feedback inhibition of photoreceptors through an unconventional GABA- and pH-sensitive mechanism. J Physiol 591: 3309-3324.

Llinás RR (1988) The intrinsic electrophysiological properties of mammalian neurons: insights into central nervous system function. Science 242:1654-1664.

Lolley RN, Farber DB, Rayborn ME, Hollyfield JG (1977) Cyclic GMP accumulation causes degeneration of photoreceptor cells: simulation of an inherited disease. Science 196:664-666.

London A, Benhar I, Schwartz M (2013) The retina as a window to the brain-from eye research to CNS disorders. Nat Rev Neurol 9:44–53.

Lukasiewicz PD, Wilson JA, Lawrence JE (1997) AMPA-preferring receptors mediate excitatory synaptic inputs to retinal ganglion cells. J Neurophysiol 77:57-64.

Magnin M, Morel A, Jeanmonod D (2000) Single-unit analysis of the pallidum, thalamus and subthalamic nucleus in parkinsonian patients. Neuroscience 96:549-564.

Maier N, Nimmrich V, Draguhn A (2003) Cellular and network mechanisms underlying spontaneous sharp wave-ripple complexes in mouse hippocampal slices. J Physiol 550:873-887.

Mao BQ, Hamzei-Sichani F, Aronov D, Froemke RC, Yuste R (2001) Dynamics of spontaneous activity in neocortical slices. Neuron 32:883-898.

Marc RE, Jones BW, Watt CB, Strettoi E (2003) Neural remodeling in retinal degeneration. Prog Retin Eye Res 22:607-655.

Margineanu DG (2010) Epileptic hypersynchrony revisited. Neuroreport 21:963-967.

Margolis DJ, Detwiler PB (2007) Different mechanisms generate maintained activity in ON and OFF retinal ganglion cells. J Neurosci 27:5994-6005.

Margolis DJ, Detwiler PB (2011) Cellular origin of spontaneous ganglion cell spike activity in animal models of retinitis pigmentosa. J Ophthalmol 2011:6.

Margolis DJ, Newkirk G, Euler T, Detwiler PB (2008) Functional stability of retinal ganglion cells after degeneration-induced changes in synaptic input. J Neurosci 28:6526-6536.

Margolis DJ, Gartland AJ, Singer JH, Detwiler PB (2014) Network oscillations drive correlated spiking of ON and OFF ganglion cells in the *rd1* mouse model of retinal degeneration. PLoS One 9:e86253.

Martersteck EM, Hirokawa KE, Evarts M, Bernard A, Duan X, Li Y, et al. (2017) Diverse central projection patterns of retinal ganglion cells. Cell Rep 18:2058–2072.

Marvin JS, Borghuis BG, Tian L, Cichon J, Harnett MT, Akerboom J, Gordus A, Renninger SL, Chen TW, Bargmann CI, Orger MB, Schreiter ER, Demb JB, Gan WB, Hires SA, Looger LL (2013) An optimized fluorescent probe for visualizing glutamate neurotransmission. Nat Methods 10:162-170.

Mazzoni A, Broccard FD, Garcia-Perez E, Bonifazi P, Ruaro ME, Torre V (2007) On the dynamics of the spontaneous activity in neuronal networks. PLoS One 2:e439.

McLaughlin ME, Sandberg MA, Berson EL, Dryja TP (1993) Recessive mutations in the gene encoding the beta-subunit of rod phosphodiesterase in patients with retinitis pigmentosa. Nat Genet 4:130-134.

Meister M, Wong RO, Baylor DA, Shatz CJ (1991) Synchronous bursts of action potentials in ganglion cells of the developing mammalian retina. Science 252:939-943.

Menzler J, Zeck G (2011) Network oscillations in rod-degenerated mouse retinas. J Neurosci 31:2280-2291.

Menzler J, Channappa L, Zeck G (2014) Rhythmic ganglion cell activity in bleached and blind adult mouse retinas. PLoS One 9:e106047.

Middleton JW, Kiritani T, Pedersen C, Turner JG, Shepherd GM, Tzounopoulos T (2011) Mice with behavioral evidence of tinnitus exhibit dorsal cochlear nucleus hyperactivity because of decreased GABAergic inhibition. Proc Natl Acad Sci U S A 108:7601-7606.

Millington-Ward S, Chadderton N, O'Reilly M, Palfi A, Goldmann T, Kilty C, Humphries M, Wolfrum U, Bennett J, Humphries P, Kenna PF, Farrar GJ (2011) Suppression and replacement gene therapy for autosomal dominant disease in a murine model of dominant retinitis pigmentosa. Mol Ther 19:642-649.

Milner LD, Landmesser LT (1999) Cholinergic and GABAergic inputs drive patterned spontaneous motoneuron activity before target contact. J Neurosci 19:3007-3022.

Morgans CW, Zhang J, Jeffrey BG, Nelson SM, Burke NS, Duvoisin RM, Brown RL (2009) TRPM1 is required for the depolarizing light response in retinal ON-bipolar cells. Proc Natl Acad Sci U S A 106:19174-19178.

Mühlnickel W, Elbert T, Taub E, Flor H (1998) Reorganization of auditory cortex in tinnitus. Proc Natl Acad Sci U S A 95:10340-10343.

Nachman-Clewner M, St Jules R, Townes-Anderson E (1999) L-type calcium channels in the photoreceptor ribbon synapse: localization and role in plasticity. J Comp Neurol 415:1-16.

Newkirk GS, Hoon M, Wong RO, Detwiler PB (2013) Inhibitory inputs tune the light response properties of dopaminergic amacrine cells in mouse retina. J Neurophysiol 110:536-552.

Nini A, Feingold A, Slovin H, Bergman H (1995) Neurons in the globus pallidus do not show correlated activity in the normal monkey, but phase-locked oscillations appear in the MPTP model of parkinsonism. J Neurophysiol 74:1800–1805.

Noreña AJ, Eggermont JJ (2003) Changes in spontaneous neural activity immediately after an acoustic trauma: implications for neural correlates of tinnitus. Hearing Research 183:137-153.

Northoff G, Duncan NW (2016) How do abnormalities in the brain's spontaneous activity translate into symptoms in schizophrenia? From an overview of resting state activity findings to a proposed spatiotemporal psychopathology. Prog Neurobiol 145-146:26-45.

O'Malley DM, Sandell JH, Masland RH (1992) Co-release of acetylcholine and GABA by the starburst amacrine cells. J Neurosci 12:1394-1408.

Oswald V, Zerouali Y, Boulet-Craig A, Krajinovic M, Laverdiere C, Sinnett D, Jolicoeur P, Lippe S, Jerbi K, Robaey P (2017) Spontaneous brain oscillations as neural fingerprints of working memory capacities: a resting-state MEG study. Cortex 97:109-124.

Painter DR, Dwyer MF, Kamke MR, Mattingley JB (2018) Stimulus-driven cortical hyperexcitability in individuals with Charles Bonnet hallucinations. Curr Biol 28:3475-3480.

Palop JJ, Chin J, Roberson ED, Wang J, Thwin MT, Bien-Ly N, Yoo J, Ho KO, Yu GQ, Kreitzer A, Finkbeiner S, Noebels JL, Mucke L (2007) Aberrant excitatory neuronal activity and compensatory remodeling of inhibitory hippocampal circuits in mouse models of Alzheimer's disease. Neuron 55:697-711.

Panigrahi B, Martin KA, Li Y, Graves AR, Vollmer A, Olson L, Mensh BD, Karpova AY, Dudman JT (2015) Dopamine is required for the neural representation and control of movement vigor. Cell 162:1418-1430.

Penn Y, Segal M, Moses E (2016) Network synchronization in hippocampal neurons. Proc Natl Acad Sci U S A 113:3341-6.

Perez-Reyes E (2003) Molecular physiology of low-voltage-activated T-type calcium channels. Physiol Rev 83:117-61.

Perry VH, Oehler R, Cowey A (1984) Retinal ganglion-cells that project to the dorsal lateral geniculate-nucleus in the macaque monkey. Neuroscience 12:1101–1123.

Petit-Jacques J, Volgyi B, Rudy B, Bloomfield S (2005) Spontaneous oscillatory activity of starburst amacrine cells in the mouse retina. J Neurophysiol 94:1770-1780.

Phillips MJ, Otteson DC, Sherry DM (2010) Progression of neuronal and synaptic remodeling in the *rd10* mouse model of retinitis pigmentosa. J Comp Neurol 518:2071-2089.

Pittler SJ, Baehr W (1991) Identification of a nonsense mutation in the rod photoreceptor cGMP phosphodiesterase beta-subunit gene of the rd mouse. Proc Natl Acad Sci U S A 88:8322–8326.

Plata V, Duhne M, Pérez-Ortega J, Barroso-Flores J, Galarraga E, Bargas J (2013) Direct evaluation of L-DOPA actions on neuronal activity of Parkinsonian tissue *in vitro*. BioMed Res Int 2013:519184.

Poria D, Dhingra NK (2015) Spontaneous oscillatory activity in *rd1* mouse retina is transferred from ON pathway to OFF pathway via glycinergic synapse. J Neurophysiol 113:420-425.

Power MJ, Rogerson LE, Schubert T, Berens P, Euler T, Paquet-Durand F (2019) Systematic spatio-temporal mapping reveals divergent cell death pathways in three mouse models of heriditary retinal degeneration. J Comp Neurol doi:10.1002/cne.24807.

Pu M, Xu L, Zhang H (2006) Visual response properties of retinal ganglion cells in the royal college of surgeons dystrophic rat. Invest Ophthalmol Vis Sci 47:3579-3585.

Puller C, Ivanova E, Euler T, Haverkamp S, Schubert T (2013) OFF bipolar cells express distinct types of dendritic glutamate receptors in the mouse retina. Neuroscience 243:136-148.

Puthussery T, Gayet-Primo J, Pandey S, Duvoisin RM, Taylor WR (2009) Differential loss and preservation of glutamate receptor function in bipolar cells in the *rd10* mouse model of retinitis pigmentosa. Eur J Neurosci 29:1533-1542.

Quraishi S, Gayet J, Morgans CW, Duvoisin RM (2007) Distribution of group-III metabotropic glutamate receptors in the retina. J Comp Neurol 501:931-943.

Raichle ME, Mintun MA (2006) Brain work and brain imaging. Annu Rev Neurosci 29:449-476.

Raichle ME, MacLeod AM, Snyder AZ, Powers WJ, Gusnard DA, Shulman GL (2001) A default mode of brain function. Proc Natl Acad Sci U S A 98:676-682.

Rajan R, Irvine DR, Wise LZ, Heil P (1993) Effect of unilateral partial cochlear lesions in adult cats on the representation of lesioned and unlesioned cochleas in primary auditory cortex. J Comp Neurol 338:17-49.

Raz A, Vaadia E, Bergman H (2000) Firing patterns and correlations of spontaneous discharge of pallidal neurons in the normal and the tremulous 1-methyl-4-phenyl-1, 2, 3, 6-tetrahydropyridine vervet model of parkinsonism. J Neurosci 20:8559–8571.

Rice DS, Curran T (2000) Disabled-1 is expressed in type AII amacrine cells in the mouse retina. J Comp Neurol 424:327-338.

Rizzo JF, Wyatt J, Loewenstein J, Kelly S, Shire D (2003) Methods and perceptual thresholds for short-term electrical stimulation of human retina with microelectrode arrays. Invest Ophthalmol Vis Sci 44:5355-5361.

Ross FM, Gwyn P, Spanswick D, Davies SN (2000) Carbenoxolone depresses spontaneous epileptiform activity in the CA1 region of rat hippocampal slices. Neuroscience 100:789-796.

Rousseeuw PJ (1987) Silhouettes: a graphical aid to the interpretation and validation of cluster analysis. J Comput Appl Math 20:53-65.

Rothschild G, Eban E, Frank LM (2017) A cortical-hippocampal-cortical loop of information processing during memory consolidation. Nat Neurosci 20:251-259.

Sandberg MA, Weigel-DiFranco C, Dryja TP, Berson EL (1995) Clinical expression correlates with location of rhodopsin mutation in dominant retinitis pigmentosa. Invest Ophthalmol Vis Sci 36:1934-1942.

Scholl HP, Strauss RW, Singh MS, Dalkara D, Roska B, Picaud S, Sahel JA (2016) Emerging therapies for inherited retinal degeneration. Sci Transl Med 8:368rv366.

Schubert T, Weiler R, Feigenspan A (2006) Intracellular calcium is regulated by different pathways in horizontal cells of the mouse retina. J Neurophysiol 96:1278-1292.

Sekirnjak C, Jepson LH, Hottowy P, Sher A, Dabrowski W, Litke AM, Chichilnisky EJ (2011) Changes in physiological properties of rat ganglion cells during retinal degeneration. J Neurophysiol 105:2560-2571.

Shen Y, Liu XL, Yang XL (2006) N-Methyl-D-Aspartate Receptors in the Retina. Mol Neurobiol 34:163-179.

Singh MS, Charbel Issa P, Butler R, Martin C, Lipinski DM, Sekaran S, Barnard AR, MacLaren RE (2013) Reversal of end-stage retinal degeneration and restoration of visual function by photoreceptor transplantation. Proc Natl Acad Sci U S A 110:1101-1106.

Soto F, Ma X, Cecil JL, Vo BQ, Culican SM, Kerschensteiner D (2012) Spontaneous activity promotes synapse formation in a cell-type-dependent manner in the developing retina. J Neurosci 32:5426-5439.

Stasheff SF (2008) Emergence of sustained spontaneous hyperactivity and temporary preservation of OFF responses in ganglion cells of the retinal degeneration (*rd1*) mouse. J Neurophysiol 99:1408-1421.

Stasheff SF (2018) Clinical impact of spontaneous hyperactivity in degenerating retinas: significance for diagnosis, symptoms, and treatment. Front Cell Neurosci 12:298.

Stasheff SF, Shankar M, Andrews MP (2011) Developmental time course distinguishes changes in spontaneous and light-evoked retinal ganglion cell activity in *rd1* and *rd10* mice. J Neurophysiol 105:3002-3009.

Steriade M, Contreras D, Curró Dossi R, Nuñez A (1993) The slow (< 1 Hz) oscillation in reticular thalamic and thalamocortical neurons: scenario of sleep rhythm generation in interacting thalamic and neocortical networks. J Neurosci 13:3284-3299.

Sterling P, Matthews G (2005) Structure and function of ribbon synapses. Trends Neurosci 28:20-29.

Strettoi E, Raviola E, Dacheux RF (1992) Synaptic connections of the narrow-field, bistratified rod amacrine cell (AII) in the rabbit retina. J Comp Neurol 325:152-168.

Strettoi E, Porciatti V, Falsini B, Pignatelli V, Rossi C (2002) Morphological and functional abnormalities in the inner retina of the rd/rd mouse. J Neurosci 22:5492-5504.

Ströh S, Sonntag S, Janssen-Bienhold U, Schultz K, Cimiotti K, Weiler R, Willecke K, Dedek K (2013) Cell-specific cre recombinase expression allows selective ablation of glutamate receptors from mouse horizontal cells. PLoS ONE 8:e83076.

Sun JJ, Luhmann HJ (2007) Spatio-temporal dynamics of oscillatory network activity in the neonatal mouse cerebral cortex. Eur J Neurosci 26:1995-2004.

Takahashi N, Sasaki T, Matsumoto W, Matsuki N, Ikegaya Y (2010). Circuit topology for synchronizing neurons in spontaneously active networks. Proc Natl Acad Sci U S A 107:10244-10249.

Takeuchi H, Horie S, Moritoh S, Matsushima H, Hori T, Kimori Y, Kitano K, Tsubo Y, Tachibana M, Koike C (2018) Different Activity Patterns in Retinal Ganglion Cells of TRPM1 and mGluR6 Knockout Mice. Biomed Res Int 2018:2963232.

Torborg CL, Feller MB (2005) Spontaneous patterned retinal activity and the refinement of retinal projections. Prog Neurobiol 76:213-235.

Tóth K, Hofer KT, Kandracs A, Entz L, Bago A, Eross L, Jordan Z, Nagy G, Solyom A, Fabo D, Ulbert I, Wittner L (2018) Hyperexcitability of the network contributes to synchronization processes in the human epileptic neocortex. J Physiol 596:317-342.

Toychiev AH, Yee CW, Sagdullaev BT (2013) Correlated spontaneous activity persists in adult retina and is suppressed by inhibitory inputs. PLoS One 8:e77658.

Trenholm S, Awatramani GB (2015) Origins of spontaneous activity in the degenerating retina. Front Cell Neurosci 9:277.

Trenholm S, Borowska J, Zhang J, Hoggarth A, Johnson K, Barnes S, Lewis TJ, Awatramani GB (2012) Intrinsic oscillatory activity arising within the electrically coupled AII amacrine-ON cone bipolar cell network is driven by voltage-gated Na^+ channels. J Physiol 590:2501-2517.

Tsukamoto Y, Omi N (2017). Classification of mouse retinal bipolar cells: type-specific connectivity with special reference to rod-driven AII amacrine pathways. Front Neuroanat 11:92.

Veruki ML, Zhou Y, Castilho A, Morgans CW, Hartveit E (2019) Extrasynaptic NMDA receptors on rod pathway amacrine cells: molecular composition, activation, and signaling. J Neurosci 39:627-650.

Voigt T, Wässle H (1987) Dopaminergic innervation of A II amacrine cells in mammalian retina. J Neurosci 7:4115-4128.

Wang DY, Chan WM, Tam PO, Baum L, Lam DS, Chong KK, Fan BJ, Pang CP (2005) Gene mutations in retinitis pigmentosa and their clinical implications. Clin Chim Acta 351:5-16.

Wang J, Johnson LA, Jensen AL, Baker KB, Molnar GF, Johnson MD, Vitek JL (2017) Network-wide oscillations in the parkinsonian state: alterations in neuronal activities occur in the premotor cortex in parkinsonian nonhuman primates. J Neurophysiol 117:2242-2249.

Wang K, Jiang T, Yu C, Tian L, Li J, Liu Y, Zhou Y, Xu L, Song M, Li K (2008) Spontaneous activity associated with primary visual cortex: a resting-state FMRI study. Cereb Cortex 18:697-704.

Wang Y, Chen K, Chan LLH (2018a) Responsive neural activities in the primary visual cortex of retina-degenerated rats. Neuroscience 383:84-97.

Wang Y, Zhao X, Xu S, Yu L, Wang L, Song M, Yang L, Wang X (2015) Using regional homogeneity to reveal altered spontaneous activity in patients with mild cognitive impairment. Biomed Res Int 2015:807093.

Wang Z, Jia X, Chen H, Feng T, Wang H (2018b) Abnormal spontaneous brain activity in early Parkinson's Disease with mild cognitive impairment: a resting-state fMRI study. Front Physiol 9:1093.

Wässle H, Puller C, Muller F, Haverkamp S (2009) Cone contacts, mosaics, and territories of bipolar cells in the mouse retina. J Neurosci 29:106-117.

Watt AJ, Cuntz H, Mori M, Nusser Z, Sjöström PJ, Häusser M (2009) Traveling waves in developing cerebellar cortex mediated by asymmetrical Purkinje cell connectivity. Nat Neurosci 12:463-473.

Wei Y, Krishnan GP, Komarov M, Bazhenov M (2018) Differential roles of sleep spindles and sleep slow oscillations in memory consolidation. PLoS Comput Biol 14:e1006322.

Weiland JD, Walston ST, Humayun MS (2016) Electrical stimulation of the retina to produce artificial vision. Annu Rev Vis Sci 2:273-294.

Wilks TA, Harvey AR, Rodger J (2013) Seeing with two eyes: integration of binocular retinal projections in the brain. In: Functional brain mapping and the endeavor to understand the working brain (Signorelli F, Chirchiglia D, ed) pp227-250. Croatia: In Tech.

Winkelman BHJ, Howlett MH, Holzel M-B, Joling C, Fransen KH, Pangeni G, Kamermans S, Sakuta H, Noda M, Simonsz HJ, McCall MA, De Zeeuw CI, Kamermans M (2019).

Winnubst J, Cheyne JE, Niculescu D, Lohmann C (2015) Spontaneous activity drives local synaptic plasticity in vivo. Neuron 87:399-410.

Witkovsky P, Gabriel R, Krizaj D (2008) Anatomical and neurochemical characterization of dopaminergic interplexiform processes in mouse and rat retinas. J Comp Neurol 510:158-174.

Wong RO (1999) Retina waves and visual system development. Annu Rev Neurosci 22:29–47.

Wong WT, Myhr KL, Miller ED, Wong RO (2000) Developmental changes in the neurotransmitter regulation of correlated spontaneous retinal activity. J Neurosci 20:351–360.

Wood SN, Pya N, Säfken B (2016) Smoothing parameter and model selection for general smooth models. J Am Stat Assoc 111:1548-1563.

Xiang J, Jia X, Li H, Qin J, Liang P, Li K (2016) Altered spontaneous brain activity in cortical and subcortical regions in Parkinson's Disease. Parkinsons Dis 2016:5246021.

Xie J, Wang GJ, Yow L, Humayun MS, Weiland JD, Cela CJ, Jadvar H, Lazzi G, Drami-Gavazi E, Tsang SH (2012) Preservation of retinotopic map in retinal degeneration. Exp Eye Res 98:88-96.

Xu HP, Furman M, Mineur YS, Chen H, King SL, Zenisek D, Zhou ZJ, Butts DA, Tian N, Picciotto MR, Crair MC (2011) An instructive role for patterned spontaneous retinal activity in mouse visual map development. Neuron 70:1115-1127.

Xu Y, Zhuo C, Qin W, Zhu J, Yu C (2015) Altered spontaneous brain activity in Schizophrenia: a meta-analysis and a large-sample study. Biomed Res Int 2015:204628.

Yang XL (2004) Characterization of receptors for glutamate and GABA in retinal neurons. Prog Neurobiol 73:127-150.

Ye JH, Goo YS (2007) The slow wave component of retinal activity in rd/rd mice recorded with a multi-electrode array. Physiol Meas 28:1079-1088.

Yee CW, Toychiev AH, Sagdullaev BT (2012) Network deficiency exacerbates impairment in a mouse model of retinal degeneration. Front Syst Neurosci 6:8.

Yee CW, Toychiev AH, Ivanova E, Sagdullaev BT (2014) Aberrant synaptic input to retinal ganglion cells varies with morphology in a mouse model of retinal degeneration. J Comp Neurol 522:4085-4099.

Yu WQ, Grzywacz NM, Lee EJ, Field GD (2017) Cell type-specific changes in retinal ganglion cell function induced by rod death and cone reorganization in rats. J Neurophysiol 118:434-454.

Zeck G (2016) Aberrant activity in degenerated retinas revealed by electrical imaging. Front Cell Neurosci 10:25.

Zhang C, McCall MA (2012) Receptor targets of amacrine cells. Vis Neurosci 29:11-29.

Zhang DQ, Zhou TR, McMahon DG (2007) Functional heterogeneity of retinal dopaminergic neurons underlying their multiple roles in vision. J Neurosci 27:692-699.

Zhang J, Ackman JB, Xu HP, Crair MC (2012) Visual map development depends on the temporal pattern of binocular activity in mice. Nat Neurosci 15:298-307.

Zhao Z, Klindt D, Chagas AM, Szatko KP, Rogerson L, Protti D, Behrens C, Dalkara D, Schubert T, Bethge M, Franke K, Berens P, Ecker A, Euler T (2019) The temporal structure of the inner retina at a single glance. bioRxiv 743047. doi.org/10.1101/ 743047.

Zhou Y, Tencerova B, Hartveit E, Veruki ML (2016) Functional NMDA receptors are expressed by both AII and A17 amacrine cells in the rod pathway of the mammalian retina. J Neurophysiol 115:389-403.

Zhou Y, Wang K, Liu Y, Song M, Song SW, Jiang T (2010) Spontaneous brain activity observed with functional magnetic resonance imaging as a potential biomarker in neuropsychiatric disorders. Cogn Neurodyn 4:275-294.

Zrenner E (2013) Fighting blindness with microelectronics. Sci Transl Med 5.

Zrenner E, Bartz-Schmidt KU, Benav H, Besch D, Bruckmann A, Gabel VP, Gekeler F, Greppmaier U, Harscher A, Kibbel S, Koch J, Kusnyerik A, Peters T, Stingl K, Sachs H, Stett A, Szurman P, Wilhelm B, Wilke R (2011) Subretinal electronic chips allow blind patients to read letters and combine them to words. Proc Biol Sci 278:1489-1497.

12. Contributions

Srivastava P*, Rogerson, LE*, Dalkara D, Berens P, Euler T, Schubert T **(Manuscript in preparation).** Bipolar cells mediate interaction between spontaneously active networks in the degenerated *rd10* retina.

*Authors contributed equally.

This study represents the main work of this thesis which I performed during my PhD. Here, using two-photon imaging of the population of neurons at the somatic and synaptic levels we show that the spontaneously active networks in the outer and inner degenerated *rd10* retina interact with other. Furthermore, we show that the interaction between the networks along the vertical pathway is mediated largely by the BCs.

For this study, I performed all the experiments (intravitreal injections, two-photon Ca^{2+} and glutamate imaging), pre-processing and initial analysis of the data. Statistical analysis of the data and respective statistical plots were generated by Luke Edward Rogerson (with input from my side). In addition, I also prepared figures and wrote the first draft of the manuscript with the help and suggestions from Dr. Timm Schubert, Prof. Dr. Thomas Euler, Prof. Dr. Philipp Berens, and Luke Edward Rogerson. Currently, we are working on editing the manuscript to the final version.

13. Acknowledgments

I would like to express my thanks to all the people who engaged their knowledge, effort and time in completion of my PhD thesis:

Dr. Timm Schubert, thank you for giving me the opportunity to work on this exciting project and for always being available for your guidance, support, valuable suggestions, and constructive feedback. Thank you for always encouraging me to present my work in different conferences and meetings, for motivating me to learn new things and for teaching me to do things with perfection.

Prof. Dr. Thomas Euler, thank you for welcoming me in your group, for giving me all the opportunities, valuable insights and guidance all throughout these years and for encouraging me to go to different conferences. Thank you for always being approachable for your advice and support.

switchBoard network, thank you, **Dr. Timm Schubert** and **Prof. Dr. Thomas Euler** for giving me the opportunity and great experience to be a part of this wonderful network that not only helped me in building a nice network with the scientists in the field but also to develop various interdisciplinary skills. Thank you for always encouraging me to engage in outreach activities. I would also like to thank all the members of this network for sharing their knowledge and ideas, and especially to **Prof Dr. Margaret Veruki**, **Prof. Dr. Espen Harveit** and **Prof. Dr. Alexandra Koschak** for allowing me to visit their lab and learn their expertise during my secondments. And a big thanks to all the Early Stage Researchers in this network for all the knowledge we shared and fun we had during these years.

Prof. Dr. Bernd Wissinger and **Prof. Dr. Aristides Arrenberg**, thank you for being a part of my advisory board and for constructive feedback.

Prof. Dr. Philipp Berens, thank you for your suggestions and contributions to this project.

Luke Edward Rogerson, thank you for all your inputs and insights on this project. Thank you for your effort, time and contributions for the statistical analysis of the data in this project.

Gordon Eske, thank you for the technical help and for taking care of the animals.

Valeska Botzenhardt, thank you for all the help and assistance you provided me during these years from the first day including my smooth settling down in Tübingen.

Euler lab members, thank you very much for welcoming me into the group and for creating a nice atmosphere in the lab. Thank you for all your helpful discussions, feedbacks and technical help. I would also like to thank Camille Chapot for introducing me to the two-photon setups and experimental procedures in the lab. Thank you, Michael Power for your help and time to revise and correct grammatical errors in the thesis as a native English speaker. And, thank you, Anna Vlasits for your suggestion to use UBP-310 in the glutamate imaging experiments.

Finally, I would like to extend my thanks to,

My parents and family, thank you for your love, support, and encouragement.

Gaurav Prakash Shrivastava, thank you brother, for always inspiring me and guiding me throughout this journey.

Parvej Alam, thank you so much for always being there for sharing all the emotions during my achievements and failures and for standing by my side during my best and toughest times.

Parul Srivastava, **Richa Awasthi,** and **Kalpana Gupta** thank you not only for your guidance, love, and support throughout this journey but also for making it more fun and enjoyable.